Halogen geochemistry of footwall breccia and associated units of the main mass of the Sudbury Igneous Complex, Ontario

by

Robert Craig Stewart

A Thesis Submitted to Saint Mary's University, Halifax,
Nova Scotia in Partial Fulfillment of the Requirements for
the Degree of Master of Science in Applied Science

April, 2011, Halifax, Nova Scotia

Approved:	Dr. Jacob Hanley Supervisor Department of Geology
Approved:	Dr. J. Brendan Murphy External Examiner Department of Earth Sciences St. Francis Xavier University
Approved:	Dr. Doreen Ames, Adjunct Professor, Geological Survey of Canada Supervisory Committee Member Department of Geology
Approved:	Dr. Marc Lamoureux Supervisory Committee Member Department of Chemistry
Approved:	Dr. Jeremy Lundholm Program Coordinator
Approved:	Dr. Kevin Vessey Dean of Graduate Studies & Research
Date:	April 7, 2011

Your file Votre référence
ISBN: 978-0-494-79648-1
Our file Notre référence
ISBN: 978-0-494-79648-1

Abstract

Halogen geochemistry of footwall breccia and associated units of the main mass, Sudbury Igneous Complex, Ontario

by Robert Craig Stewart

The potential for the halogen elements (F, Cl, Br, I) to be used as geochemical indicators for contact-style Ni-Cu-PGE mineralization along the lower contact of the Sudbury Igneous Complex (SIC) has been investigated. Specifically, halogen anomalies present within and around footwall breccia "plumes" as well as surrounding lithologies have been examined to determine how bulk and soluble halogens are related to mineralization. Two environments (one barren of mineralization, and the other hosting significant sulphide ore deposits) containing these structures were compared. There are no significant differences in bulk major and trace element geochemistry of rocks between these environments; however there were differences in halogen geochemistry. Two dominant fluid sources were recognized as having contributed to the water-soluble halogen budget of the samples: a high Cl^-/Br^- fluid phase of probably magmatic origin, originating from the SIC, and a low Cl^-/Br^- fluid phase derived from fluid release during dehydration of hydrous minerals in footwall rocks or from infiltration of saline groundwaters.

April 7, 2011

Acknowledgements

I would like to thank Dr. Jacob Hanley for his guidance and support throughout this project as primary supervisor and Dr. Doreen Ames at the Geological Survey of Canada (GSC) whose involvement was critical to the formation and success of the project. Funding for this project was provided by the Government of Canada Research Affiliates Program (RAP) and the Targeted Geoscience Initiative (TGI-3) program. I would like to thank Judy Vaive for developing a new method for bulk halogen analyses, Dr. Simon Jackson for assisting with LAICP-MS analyses, and Dr. Andrew MacRae for assistance with Wellplot software. I would also like to acknowledge QuadraFNX Mining Ltd. and Wallbridge Mining Ltd. for their support and access to drill core. I would like to thank Drs. M. M. Lamoureux (Saint Mary's University) and Brenden Murphy (St. Francis Xavier University) for their support as committee members.

Table of Contents

List of Figures

List of Tables

Chapter 1 – Introduction

1.1 Thesis Structure

This study was separated into two main parts. The first (Chp. 2) deals with the bulk geochemistry and structure of footwall breccia plumes and associated lithologies of the Sudbury Igneous Complex, and the second (Chp. 3) investigates the mineral chemistry of halogen-bearing phases in these rock types. The thesis has been written with the intention of publishing these two sections as papers in Economic Geology. As such, there is some repetition of key figures (e.g., maps, petrography) and some text between the two chapters constituting the two stand-alone articles. An introduction (Chp. 1) summarizes briefly the distribution and behaviour of halogens in magmatic-hydrothermal systems. Much of its content was built by combining introductory sections from Chps. 2 and 3. At the time of submission to Economic Geology, the content of this introduction will be redistributed back to the standalone introductions for each paper. A concluding chapter (Chp. 4), briefly reviews the key findings, their applications to exploration, and suggests possible future work.

1.2 Introduction

1.2.1 Purpose of study and motivation

The nature, behavior, and distribution of the halogen elements in the complex magmatic-hydrothermal environment of the Sudbury basin and in other mafic-ultramafic ore-forming systems is poorly understood. In the last 20 years, our understanding of quantitative geochemistry have advanced to allow for high precision analyses of the stable halogen elements to very low detection limits, leading to an improved understanding of their behavior in various geochemical reservoirs in nature. The halogen elements (group 17 on the periodic table) are characterized as missing one electron from their outer orbital. Their relative reactivity, electronegativity, and electron affinities decrease from F to I. Along with H_2O, S, and CO_2, the stable halogen-group elements (F, Cl, Br, I) constitute common volatile species in magmatic-hydrothermal systems. They are soluble in fluids, may be incorporated structurally into a variety of minerals in such systems, and their relatively conservative behavior during many geological processes (e.g., boiling, evaporation) allows them to be used to trace the origin and evolution of fluids involved in the formation of igneous rocks, and associated magmatic-hydrothermal ore deposits and alteration (Kovalenko, 1977; Flynn and Burnham, 1978; Webster et al., 1989; Keppler and Wyllie, 1991; Symonds et al., 1994; Peiffert et al., 1996; Aiuppa et al., 2009 and authors therein).

These characteristics of the halogens are of particular interest in mafic-ultramafic environments as it has been suggested that halogen-rich fluids have played a key role in the development of their sulphide ore deposits (Cu-Ni-platinum-group elements) (e.g.,

Boudreau et al., 1986; Farrow, 1994; Farrow et al., 1994; Jago et al., 1994; Luder et al., 2002; Hanley et al., 2004; and authors therein). This study aims to understand the behaviour of these elements in the complex magmatic-hydrothermal environment of the Sudbury Structure in Ontario, Canada, with the intention of developing exploration criteria for Ni-Cu-platinum group element (PGE) ore-hosting felsic and mafic systems at Sudbury and elsewhere.

This study focuses on F, Cl, Br, and I, and omits At due to a near complete lack of understanding of its basic behavior in geological systems, the inability to detect it using conventional geological analytical techniques owing to its marked scarcity as the rarest naturally occurring element, and its instability on geological time scales as a radioactive element with a very short half-life. The scope of this study is very broad, and as such is separated into two sections. The first paper is an extensive study of the bulk (whole rock) distribution of the halogens, with a focus on the geochemistry of the footwall breccia in the Sudbury Structure, a rock that acts as the primary host phase for contact-style magmatic sulphide deposits. The second paper is a preliminary investigation focusing on the mineral chemistry of halogen-bearing phases in those rocks. The overall objective of this work is to provide increased knowledge about the distribution of halogens in the Sudbury environment, and to describe geochemical criteria that may be applied to routine exploration for contact-style deposits, which will be defined in an upcoming section.

1.2.2 Halogens in the mantle

Newsom (1995) estimated that F and Cl are present in concentrations in primitive mantle ranging from ~10-40 ppm, while Br and I abundances range from ~40-450 ppb (with I being the least abundant halogen). These results were compared to published CI carbonaceous chondrite abundances that are up to ~100 times lower. This indicates that significant loss of halogens from the mantle occurred in Earth's early history, probably through magmatic degassing and the formation of stable crust containing minerals and circulating fluids into which the halogens have partitioned. This statement agrees well with the results of Wanke et al. (1984), who determined that typical average crustal values for halogens are much higher than mantle values, as follows: F = 525 ppm, Cl = 1900 ppm, Br = 7 ppm, and I = 1.5 ppm (based on analyses of thousands of different crustal rock types). Halogen abundances in mantle minerals were examined by Smith (1981) and Smith et al. (1981). They reported values typically less than 50 ppm for each of the primary mantle minerals (olivine, orthopyroxene, clinopyroxene, and garnet); these halogen values have been used to approximate the overall halogen budget for the mantle. However, trace phases in the mantle such as apatite (see Table 1.1.) and micas may carry substantially higher concentrations, even though their overall abundances would not contribute significantly to the halogen endowment of the mantle. Several authors (Smith, 1981; Smith et al., 1981; Larson et al., 2003; Aiuppa et al., 2009) have noted that these results must be interpreted with caution as they rely on not only the combination of several mantle data sets, but also that the abundances of each mineral in the mantle is still unknown. Though many of these values were published over 25 years ago, Aiuppa et al.

(2009) reported that the majority of published data after Smith (1981) and Smith et al. (1981) on the mantle halogen mineralogy are consistent with their findings. These publications estimated that F is 5-10x more abundant that Cl, and 10^3 to 10^4 times more abundant than Br. These reported values are similar to the estimated halogen budget (Wanke et al., 1984; Newsom, 1995) in the mantle, except that Cl may be slightly enriched (Wanke et al., 1984; Newsom, 1995).

Mineral/host rock	F	Cl	Source
phlogopite/kimberlite	0.43 wt. %	0.08 wt. %	Smith et al., 1981
amphibole/kimberlite	0.5 - 1.0 wt. %	30 - 300 ppm	Smith et al., 1981
apatite/mantle xenolith	0.4 - 1.4 wt. %	0.01 - 1.0 wt. %	Smith et al., 1981
apatite/carbonatite	2.0 - 3.7 wt. %	~100 - 1000s ppm	Smith et al., 1981
amphibole/mantle xenolith	0.12 +- 0.03 wt. %	0.02 +- 0.01 wt. %	Matson et al., 1984
biotite/syenite	0.22 - 3.3 wt. %	0.1 - 0.56 wt. %	Markl and Piazlo, 1998
scapolite/syenite	0 - 0.7 wt. %	0.3 - 1.01 wt. %	Markl and Piazlo, 2000
phlogopite/mantle xenolith	0.16 - 0.29 wt. %	0.3 - 0.9 wt. %	Ionov et al, 2006
apatite/mantle xenolith	0.52 - 1.51 wt. %	0.63 - 2.72 wt. %	Ionov et al, 2007

Table 1.1. Representative analyses of F and Cl in igneous minerals, illustrating the range in halogen abundance encountered in naturally occurring phenocrysts from the crust and mantle.

1.2.3 The halogens in ore-forming magmas and hydrothermal fluids

Halogens, as well as S, H_2O, and CO_2, are common volatiles in magmas. Their abundances, distribution and behavior in various magmatic reservoirs are determined primarily through analyses of bulk rocks, phenocrysts, volcanic matrix glasses, and silicate melt inclusions (Aiuppa et al., 2009 and references therein).

Fluorine and Cl are usually present in much greater abundances (up to ~0.5 wt% typically; rarely up to several wt. %) in silicate melts compared to Br and I (usually less

than ~250 ppm; Carroll and Holloway, 1994). Fluorine concentrations in magmas show great variation depending on tectonic setting and the type of igneous rocks crystallized. The lowest concentrations occur in basaltic rocks, whereas felsic magmas may contain very high concentrations. The greatest abundances of F are found in severely altered felsic continental magmatic rocks. However, F is incompatible in most minerals relative to fluids in the majority of magmatic environments so the nature of this enrichment in altered rocks is unclear (Carroll and Webster, 1994; Kiprianov, 2006; Kiprianov and Karpukhina, 2006; Webster and Thomas, 2006; Dolejs and Baker, 2007). Fluorine has the ability to lower solidus and liquidus temperatures of melts (Manning, 1981), alter phase equilibria (Dolejs and Baker, 2004; 2007), modify solubilities of Cl and H_2O in melts (Holtz et al., 1993; Webster and DeVivo, 2002), lower melt viscosity (Giordano et al., 2004; 2008) and increase cation diffusivities (Carroll and Holloway, 1994).

Since Cl, Br, and I have larger ionic radii, they do not dissolve into melts as easily as F (i.e., do not substitute as readily for bridging oxygen), resulting in less significant changes in phase relations and magma properties (Aiuppa et al., 2009). Chlorine is similar to F in that its dissolved abundance in magmas depends on tectonic setting and melt composition. For example, in ocean rift and island arc environments, Cl concentrations in magmas average ~ 800 ppm. Analyses of high silica, continental rhyolites show high abundances of Cl (up to 3000 ppm), while melt inclusions found in these systems contain as much as 7500 ppm Cl. The highest concentrations of magmatic Cl (up to 1.2 wt. %) occurs in intermediate to high silica peralkaline magmas. However, in contrast to F,

significant Cl can be lost during degassing associated with magma crystallization, and consequently, magma properties can change due to loss of Cl (Aiuppa et al., 2009).

Though there are many published data on F and Cl in rock-forming magmatic systems, there is little known about the abundance of Br and I in magmas. Bromine and iodine appear to be more abundant in volcanic glasses than in crystalline igneous rocks (Aiuppa et al, 2009 and references therein). For example, Br concentrations are typically less than 1 ppm in basalts, but have been reported to range up to ~300 ppm in concentration in some volcanic basaltic glasses; iodine concentrations are also typically less than 1 ppm in basalts but may reach concentrations up to 110 ppm in basaltic glass (Wedepohl, 1974). This confirms the highly incompatible nature of Br and I, and their tendency to readily partition into residual silicate liquid during magmatic fractionation. The large ionic radii of Br and I makes them the least mineral-compatible of the halogen elements, preventing them from readily replacing the OH^- group in hydrosilicate minerals.

Positive correlations between Cl and Br are observed in magmatic systems (Sugiura, 1968; Yoshida et al., 1971; Berndt and Seyfried, 1990). Correns (1956) noted that Br and I concentrations in minerals are similar and do not show enrichment or depletion varying with any other major geochemical parameters. Therefore, variations in bulk rock Br and I are probably caused by variations in the abundance of fluid inclusions. It is possible for Br and I to be present in minerals in very small amounts. Most data for Br and I in common rock-forming minerals were presented by early studies so the accuracy of analyses is questionable, but Von Fellenberg and Lunde (1926, 1927) and Kogarko and

Gulyayeva (1965) determined a range of ~70-1200 ppb in hydrosilicate minerals (e.g. – hornblende, phlogopite, biotite, etc.), with even less present in feldspars and olivine. Yoshida et al. (1971) showed that there is little variation in I content in different rock types, and that, unlike Br, I abundance does not correlate with the abundance of other halogens.

The halogens play a significant role in degassing processes, impact volcanic eruption styles, and influence the partitioning behavior of metals in magmatic-hydrothermal systems. Since Cl exsolves as part of a magmatic volatile phase, high salinity fluid phases in which the activity of H_2O is significantly lowered (e.g., Shinohara et al., 1989, Webster, 1992; Aranovich and Newton, 1996; Botcharinkov et al., 2004; Aiuppa et al., 2009 and authors therein). Even small concentrations of Cl, typical of silicate magmas (i.e., 100s to 1000s of ppm) in hydrous and anhydrous melts, are enough to allow exsolution of high salinity fluid phases, independent of the amount of coexisting vapour in the magma. Concentrations of Cl in saline magmatic fluids greatly exceed F, and these exsolving fluids can transport and precipitate a variety of trace elements carried in the form of Cl^- complexes. Generally, ore metals can be carried in such fluids at very high concentrations if conditions are appropriate (e.g., pH, fO_2), but the types of metals present in solution are dependent on the melt composition from which the metal-bearing fluids exsolve. Metals that have a complexing affinity for Cl^- include Li, Rb, Cs, Sn, W, Mo, Cu, Au, Ag, Pt, Hg, Pb, Zn, and Be (e.g., Kovalenko, 1977; Flynn and Burnham, 1978; Webster et al., 1989; Keppler and Wyllie, 1991; Peiffert et al., 1996; Bai and Kooster van Groos, 1999; Yardley, 2005; Duc-Tin et al., 2007). Metals can also be transported in low

salinity vapour as halogen complexes (Symonds et al., 1990; Symonds et al., 1992; Churakov et al., 2000; Heinrich, 2007). More recent studies have focused on the fractionation of these processes between dilute Cl-bearing aqueous vapours and coexisting saline liquids (formed during boiling of magmatic fluids), showing that metals such as Cu, Fe, Ag, and Zn partition strongly into Cl-bearing saline liquids (Williams et al., 1995; Simon et al., 2005; Williams-Jones and Heinrich, 2005). Where S is present, the observed behaviour differs remarkably than in Cl-only solutions; Cu and other specific metals such as Au will partition in favour of S and Cl-bearing vapours rather than coexisting saline liquids (Simon et al., 2005; Williams-Jones and Heinrich, 2005; Nagaseki and Hayashi, 2008).

While the studies listed above concluded that the majority of the listed metals are carried as Cl^- complexes, it is important to point out that some elements (e.g., W, Sn, Li, Al, Ca, Nb, Ta, REE) may be transported in peralkaline silicate melts, and associated hydrothermal liquid or vapour phases as dissolved F^- species (e.g., Mineyev, 1963; Flynn and Burnham, 1978; Kerrich and Fryer, 1979; Taylor and Fryer, 1980; Lindsey, 1982; Aksyuk, 2000; Pavlovich et al., 2010; Agangi et al., 2010). Less is known about the relative importance of F^- in the development of magmatic-hydrothermal ore deposits compared to Cl^-, but its role in the development of, for example, skarns, carbonatites, rare element pegmatites and volcanic-associated U deposits is probably significant.

In contrast to Cl and F, it has been shown recently through experimental work that Br and I do not significantly influence ore metal partitioning, and regardless, their

concentrations in typical geological fluids are unlikely to be high enough to be relevant (e.g., Veksler et al., 2005).

Chapter 2 - Whole rock geochemistry

2.1 Abstract

The potential for the halogen elements (F, Cl, Br, I) to be used as geochemical indicators for contact-style Ni-Cu-PGE mineralization along the lower contact of the Sudbury Igneous Complex (SIC) has been investigated. Specifically, halogen anomalies present within and around footwall breccia ridges or "plumes" as well as surrounding lithologies have been examined to determine how bulk and soluble halogens are related to mineralization. Footwall breccia plumes are elongated ridge-like structures that penetrated into the SIC while in a partially melted state, and can host economic grade Ni-Cu-PGE mineralization at their base. Two environments (one barren of mineralization, and the other containing significant sulphide ore deposits) containing these structures were compared. There are no significant differences in bulk major and trace element geochemistry between these environments; however there were some differences in halogen geochemistry that may serve as important exploration criteria for differentiating between barren and mineralized embayments. There is an enrichment in I in the mineralized plumes, caused by the leaching of I from brecciated sulphides at the base of the plume. Hydrothermal fluids transported the I to shallower depths within and adjacent to the plumes. Additionally, two dominant fluid sources were recognized as having contributed to the water-soluble halogen budget of the samples: a high Cl^-/Br^- fluid phase

of probably magmatic origin, originating from the SIC, and a low Cl^-/Br^- fluid phase derived from fluid release during dehydration of hydrous minerals in footwall rocks or from infiltration of saline groundwaters from the footwall during plume incursion. Barren plumes tend to be more enriched in the high Cl^-/Br^- component whereas mineralized footwall breccias are characterized by anomalously low Cl^-/Br^- ratios indicating interaction of thick packages of footwall breccia with the SIC.

2.2 Introduction

In igneous systems, the volatile halogen elements may constitute important anionic species. Whereas Cl, Br, and I will tend to partition into exsolving fluid phases or residual melt fractions during magmatic differentiation, F partitions into crystallizing minerals (e.g., apatite, biotite, amphibole). There have been several publications describing this general behavior in rock-forming systems (Lieberman, 1966; Johns and Huang, 1967; Sugiura, 1968; Yoshida et al., 1971; Shinohara et al., 1989; Webster, 1992; Aranovich and Newton, 1996; Jambon et al., 1990; Muramatsu and Wedepohl, 1998; Botcharinkov et al., 2004; Aiuppa et al., 2009 and authors therein). Evaluation of halogen abundances, ratios and the sites of their residence in crystalline rocks allows them to be used to trace the origin and evolution of fluids and melts involved in the formation of igneous rocks, and associated magmatic-hydrothermal ore deposits and alteration assemblages (e.g., Kovalenko, 1977; Flynn and Burnham, 1978; Webster et al., 1989; Keppler and Wyllie, 1991; Symonds et al., 1994; Peiffert et al., 1996; Aiuppa et al., 2009 and authors therein).

Knowledge of the general behavior of the halogens from studies such as those above, whether field- or experimental-based, were based primarily on felsic systems, and there has been little work done in characterizing halogen behavior in mafic-ultramafic systems. At the Sudbury Igneous Complex (SIC), a differentiated mafic complex in Ontario, Canada, recent studies of magmatic Ni-Cu-platinum group element (PGE) deposits have shown that the halogen abundances may be used as footwall mineralization proximity indicators (Hanley et al., 2004; McCormick et al., 2002) and that halogen ratios (e.g., Cl/Br, Br/I) may be used to trace the origin of hydrothermal fluids preserved in the rocks as fluids inclusions (Farrow, 1994; Jago et al., 1994; Farrow et al., 1994; Hanley et al., 2010;). However, the systematics of halogen occurrence has only been investigated surrounding ore bodies within country rocks below embayments along the margin of the Sudbury structure. Their distribution and origin is not known within the igneous units of the SIC, and along its contact with the country rocks. The present study focuses on the whole rock geochemistry of the SIC, main mass and country rocks in the vicinity of this contact, and a rock type known as footwall, or "late granite" breccia. This heterolithic breccia formed by partial melting of the country rocks and is an important host to contact-style magmatic sulphide mineralization. The study (i) compares major and trace element chemistry (including the halogens) of SIC units and footwall breccia in mineralized and barren embayments along the north range of the SIC to determine if the presence of mineralization or different host rock lithologies can be linked to variations in halogen abundance and distribution, (ii) identifies the most useful whole-rock geochemical indicators for mineralization vectoring, and (iii) discusses the likely sources for the

halogens within the studied lithologies. The studied areas comprise three drill core intervals along the northern margin of the SIC: two from a mineralized zone of footwall breccias near the Levack mine, and one from a barren to weakly mineralized interval near Sugarloaf Island, Windy Lake.

2.3 Geological setting

2.3.1 General geology of Sudbury region

The Sudbury structure ('SS'; Figure 2.1.1) is located in the southern region of the Canadian Shield. It is defined as containing: a) Archean and Proterozoic brecciated footwall rocks underlying the SIC b) the Whitewater Group (Onaping, Onwatin, and Chelmsford formations, and c) the SIC itself (Dressler, 1984). The complex stratigraphy of the Sudbury region is the result of large scale magmatic and tectonic events related to meteorite impact and associated impact-synchronous to post-impact deformational processes. It is widely accepted that the SS is a result of an astrobleme impact event at ~1.85 Ga (Dietz, 1960; Card et al., 1984; Naldrett et al., 1984; Grieve et al., 1991; Mungall et al., 2004; Ames et al., 2008) and that the SIC represents a crystallized impact melt sheet (Krogh, 1984; Golightly, 1994). This hypothesis is supported by a variety of physical evidence including the presence of rocks formed at ultrahigh strain rates (pseudotachylite; also known as "Sudbury Breccia"), and a variety of structural and mineralogical evidence for shock metamorphism (Peredery and Morrison, 1984). The SIC contains igneous units that represent the products of differentiation and crystallization of an impact melt sheet. Along the north range of the SIC, these are (from bottom to top):

the sublayer and associated quartz dioritic offset dykes, mafic norite, felsic norites, quartz gabbro, and granophyre (Coats and Snajdr, 1984; Lightfoot et al., 1997). The north range of the SIC is underlain by Archean-age gneissic rocks (the Levack Gneiss Complex) and granitoids (Card et al., 1984; Dressler, 1984). The sublayer is located above the footwall and footwall breccias and below the norite layer. It occurs as flat sheet-like lens. (Dressler, 1984). The sublayer can be divided into two units. The earlier of these two units consists of medium- to fine-grained gabbroic-noritic rocks containing more mafic to ultramafic fragments (exotic xenoliths, possibly from the lower crust; Dressler, 1984; Mungall et al., 2004). The younger unit is comprised of medium-grained gabbroic-quartz dioritic rocks. The fragments in the younger unit consist of gabbroic and mafic metavolcanic footwall rocks as well as some fragments of the older sublayer unit (Pattison, 1979; Dressler, 1984). The younger phase of the sublayer postdates the main mass norite unit. Both units of the sublayer, notably the quartz dioritic variety, can contain significant amounts of magmatic sulphides and are a major host for deposits. The quartz diorite tends to carry high sulphide tenor where it is inclusion-rich.

Along the contact between the sublayer and the Archean country rocks, a discontinuous unit known as footwall or "late granite" breccia occurs (Greenman, 1970). It is a heterolithic breccia comprised of fragments of country rocks, restite (from partial melting), and exotic fragments hosted in a variably textured igneous matrix. The footwall breccia forms lens-like accumulations along this contact but also forms discrete discordant ridge-shaped structures that extend up from the contact where they have intruded the SIC main mass.

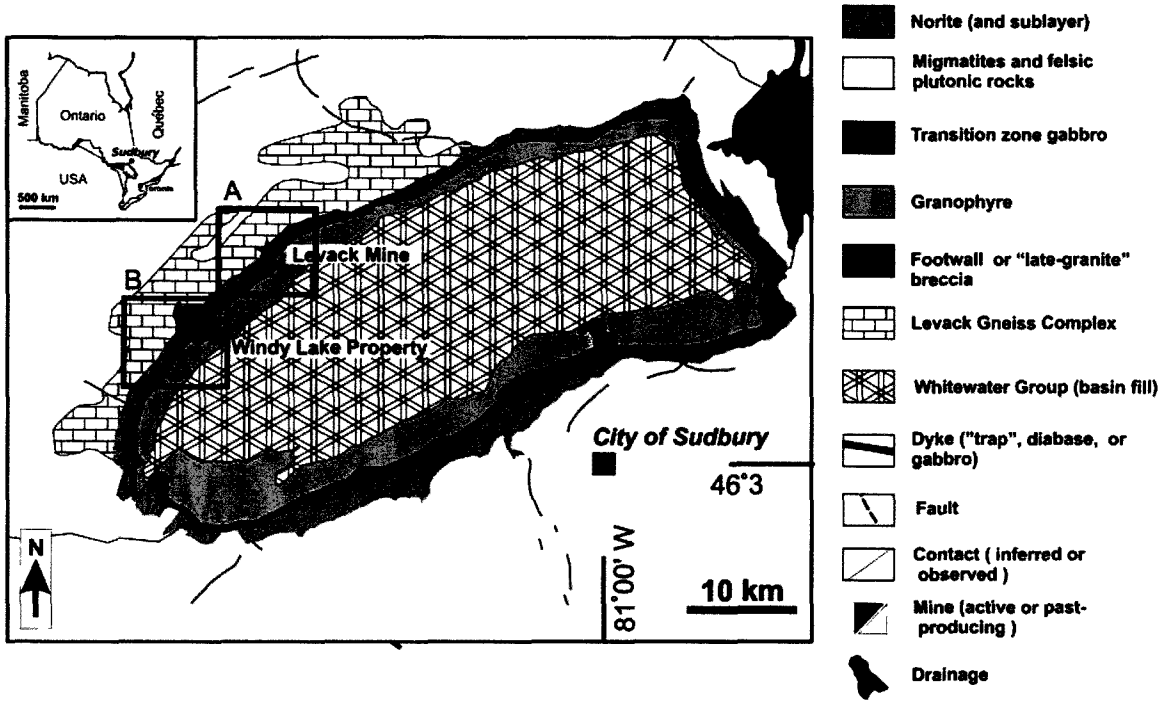

Figure 2.1.1 Regional map figure of Sudbury Structure. Area A (boxed in) contains the mineralized embayment, and the locations of the studied diamond drill holes FNX6103 and FNX6061 at the Levack Mine. Area B contains the barren environment, and diamond drill WWL-022 at the Windy Lake Property.

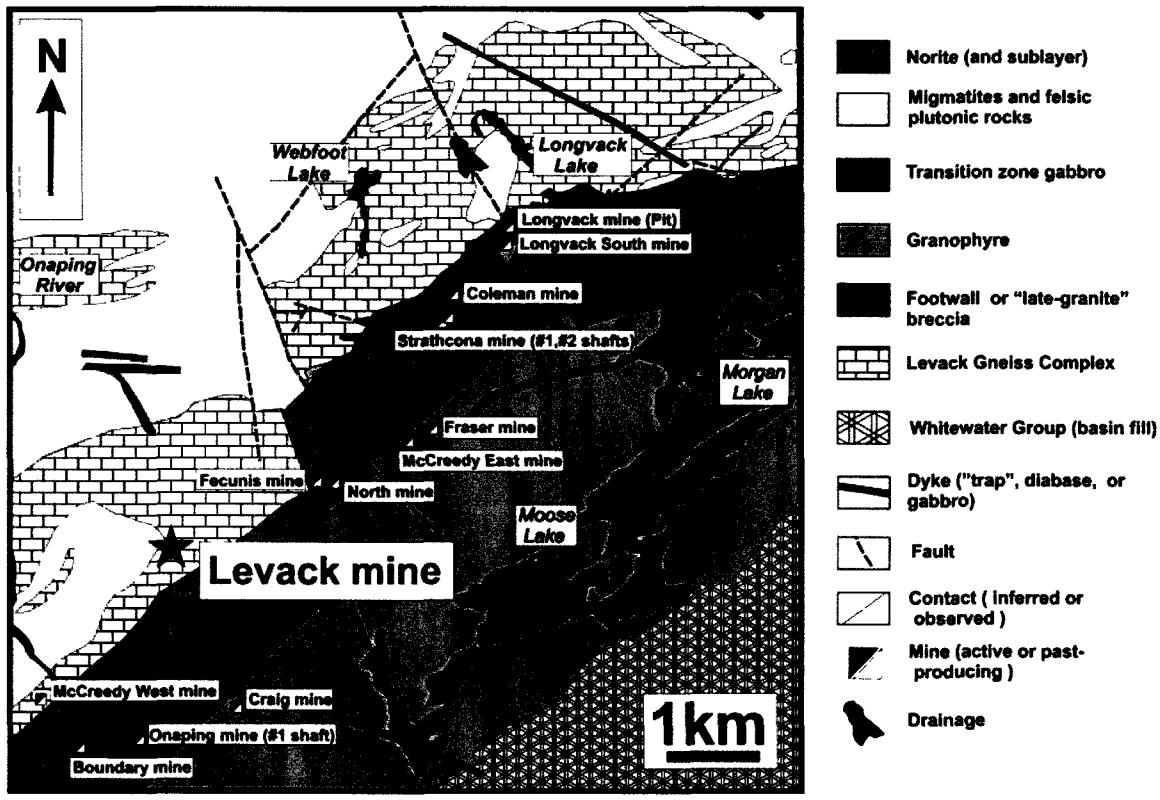

Figure 2.1.2. Map of Levack mining cluster (Area A on regional map) showing the location of mine from which diamond drill holes FNX6103 and FNX6061 were completed (Levack mine).

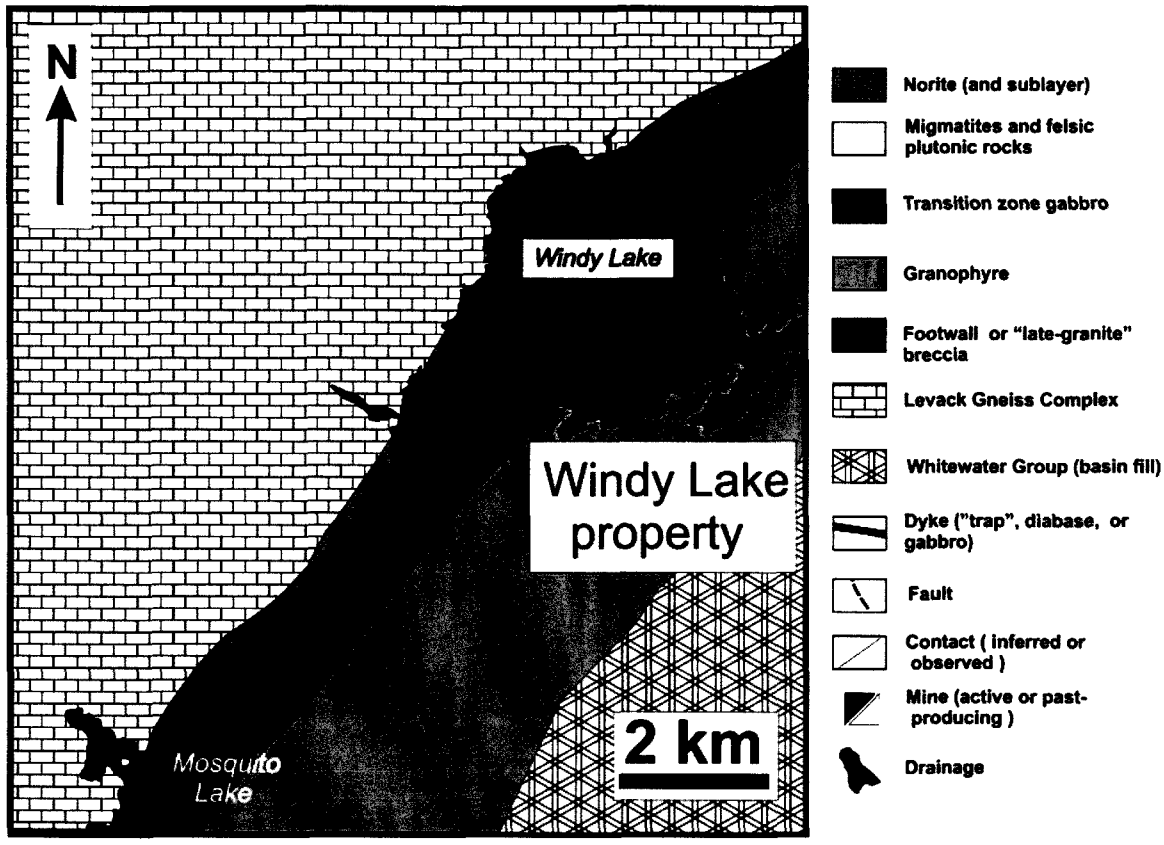

Figure 2.1.3. Map of Windy Lake exploration area showing the Windy Lake property on Sugarloaf Island (Area B on regional map) where diamond drill hole WWL-022 was located.

2.3.2 Ore deposit types of the Sudbury environment

Three primary magmatic sulphide ore deposit types associated with the SS including (Morrison et al., 1994; Lightfoot and Farrow, 2002):

1. contact-type deposits, occurring at or near the basal contact of the SIC with the Proterozoic and Archean basement, with a Ni/Cu ratio ~ 1
2. offset deposits hosted by SIC materials (e.g. – inclusion-rich quartz diorite) that intrude into the Archean basement rocks, with variable Ni/Cu ratios and often high PGE contents
3. footwall-type deposits occurring as stringers, disseminations, and sheet-like veins in the basement, up to 2 km outside of the SIC, with Ni/Cu ratios << 1

The contact-type deposits along the north range are hosted in the FWBX and are found along the contact between the base of the SIC (the sublayer) and the country rocks (Levack Gneiss complex and are comprised of massive, blebby, and disseminated sulphides (pyrrhotite > pentlandite > chalcopyrite) occurring in the matrix of the FWBX. Inclusions of country rock are present in the FWBX (primarily gneissic inclusions; Lightfoot et al., 1997). Contact deposits are most abundant and voluminous in embayments along the SIC contact, which are structurally complex depressions (possibly slump features) along the meteorite crater walls (Morrison et al., 1994). Magmatic sulphides occur as blocks and fragments in developed FWBX plume structures above the

normal stratigraphic contact region; these plumes will be discussed in a future section. Normally, in mineralized zones containing massive sulphide, Ni abundances are lowest closest to the sublayer and increase with increasing proximity towards the footwall. The Ni abundances in massive sulphides are highest in the transition zone between the FWBX and the country rocks. There are no consistencies in Ni/Cu ratios in contact-style deposits, although they tend to have Ni/Cu that are high compared to footwall-style deposits that are comprised of chalcopyrite-cubanite (see below; Morrison et al., 1994).

Like the FWBX, the thickness and morphology of the sublayer (other than offset dykes) is controlled partly by the depth of embayments in the footwall along the SIC contact. Mineralization hosted in the sublayer varies from disseminated to massive. Offset dyke deposits occur in radial and concentric offset structures and are typically hosted in an inclusion-bearing phase of quartz diorite (Lightfoot et al., 1997). These deposits constitute a very significant proportion of mineralization in the SS, compared to other styles (Ames and Farrow, 2007).

Ore deposits in the footwall are classified as footwall-style deposits. These deposits can take many different forms (stringers, veins, disseminated sulphides, offsets, etc.) and contain sulphides (chalcopyrite-cubanite-dominant) that are highly fractionated with Ni/Cu ratios much less than 1. There is a distinct metal zonation pattern with Ni/Cu ratios, platinum-group element (PGE) grades, and Au grades increasing away from the SIC. Through examination of the spatial association between footwall- and contact-style deposits, as well as their mineralogy and base/precious metal chemistry, it was concluded that fractionated sulphides originating from the contact region migrated into the footwall

(Morrison et al., 1994). Footwall-type deposits and offset dyke deposits both intrude the surrounding wallrocks. However, whereas the offset-type deposits are hosted in igneous material originating from the SIC (Lightfoot et al., 1997) that cross-cuts the stratigraphic layers of the footwall, the footwall-type deposits are hosted in impact-derived brecciated rocks in the footwall (pseudotachylite; Sudbury Breccia; Coats and Snajdr, 1984). Brecciated footwall rocks tend to be mineralized if (i) they are in close contact with ores hosted in embayments (i.e., zones of Sudbury breccia in close proximity to contact-style ores); (ii) show evidence of extreme thermal recrystallization (determined through petrography and mineralogy) caused by contact metamorphism, and (iii) show extensive hydrous alteration due to circulation of hydrothermal fluids focused in the embayments.

All of the data obtained regarding the SIC and the different types of deposits lead to the common conclusion that the SS and its deposit endowment was created during a single, continuous period of ore generation associated with the sulphide saturation and differentiation of the SIC melt sheet (Morrison et al., 1994). In general, the SS is the product of a diverse and protracted geological history that is globally unique.

2.4 Local Geology

2.4.1 Morphology and distribution of the footwall breccia

Footwall breccia occurs in concordant zones at the base of the SIC and in discordant zones that intrude the main mass of the SIC (Coats and Snydr, 1984; this study). Semi-conformable zones of footwall breccia extend along the base of the SIC, are typically 250-300 m wide and are comprised of the host rocks to the bulk of the north range

contact-style magmatic Ni-Cu sulphide ore bodies. Discordant zones of footwall breccia comprise a series of east-west trending, parallel, linear ridges ("plumes") spaced 150-200 m apart. The ridges extend along strike typically for 275 to 550 m along the basal SIC contact and intrude up into the sublayer, norite and transition zone gabbro phases of the main mass of the SIC (Figure 2.2.1-2.2.2). As they disrupt some contact-style mineralization (see area circled in Figure 2.2.2), understanding the distribution and characteristics of these ridges is valuable for exploration purposes. Drill core observations showed that the footwall breccia transported (i) clasts and large blocks of felsic and mafic gneiss from the footwall up to the level of the sublayer, and noritic units of the SIC, (ii) fragments of mafic norite up to the level of the felsic norite, and (iii) brecciated fragments (i.e., solidified) of massive pyrrhotite-pentlandite-bearing contact-style sulphides up to the level of the mafic norite.

The ridges have a thickening at their base which trends into massive (concordant) footwall breccia along the footwall contact. A three dimensional analysis of a ~1.2 x 0.8 km segment of the SIC margin (Figure 2.2.1) reveals five ridges intruding the SIC at variably high angles (75-90°) relative to the SIC contact and semiconcordant footwall breccia. A primary plume maintains a relatively constant shape horizontally (along strike with the SIC contact) and maintains consistent height and thickness over the majority of the cross sections observed. Secondary plumes are defined as those ridge structures that show significant variations in thickness horizontally, and do not show consistent height and thickness where they penetrate upwards into the SIC. This environment contains two

"primary" and three "secondary" plume bodies. Primary plumes are labelled "B" and "C", while the secondary plumes are labelled "A", "D", and "E" (Figure 2.2.1). Plume A is located closest to the present surface while plumes D and E were intersected in drill core at considerable depths.

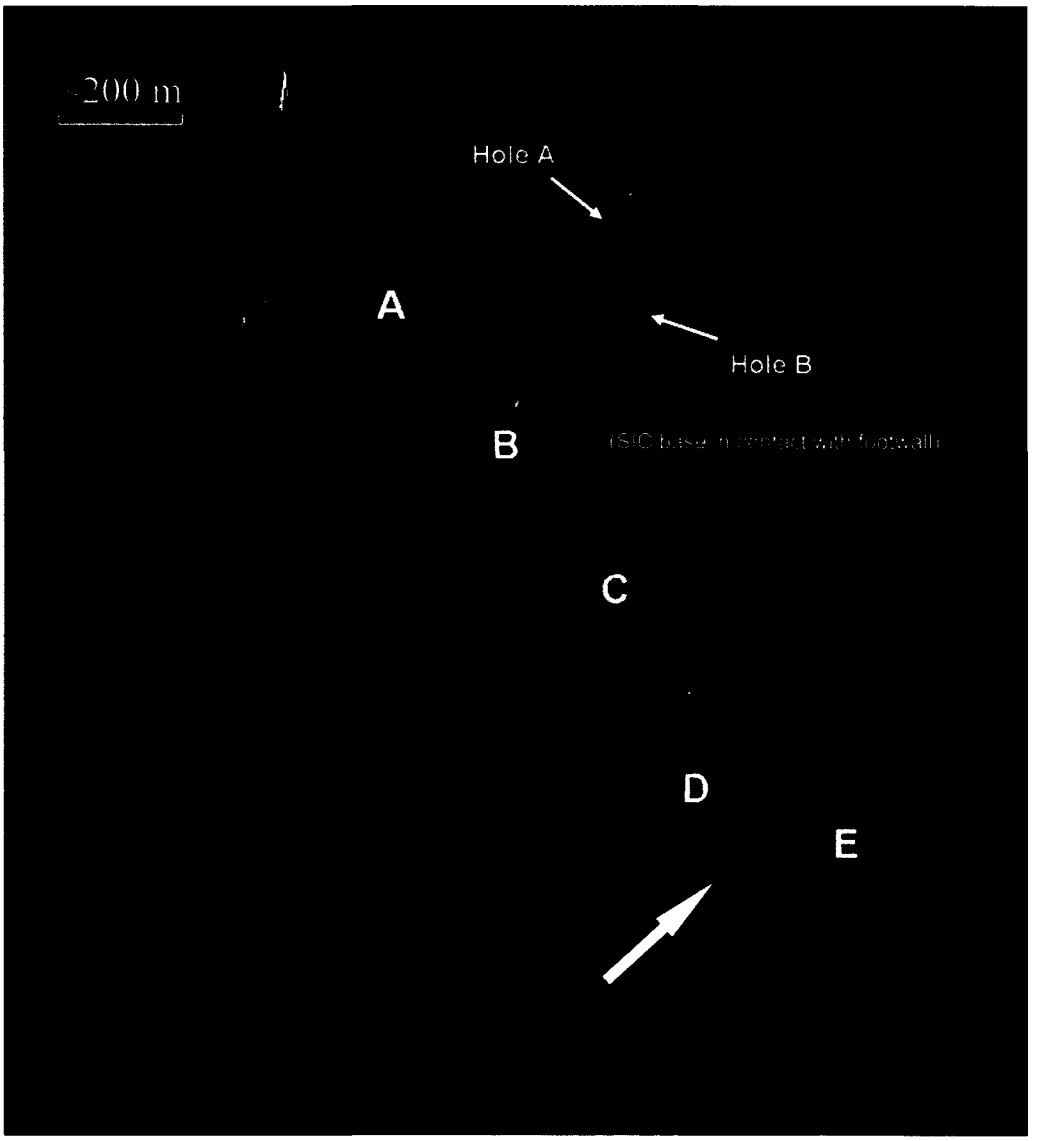

Figure 2.2.1: Block diagram showing 3-D representation of the SIC contact region along a ~1.2 x 0.8 km area of the north range footwall. The diagram was built by combining a series of 45 cross sections (vertical sections) spaced ~15 m apart. All features are interpolated from drill core data. Lithologies: blue = Sudbury breccia (in the footwall); brown = Levack Gneiss (footwall) basement; yellow = footwall breccia; green = diabase dikes; purple = areas free of footwall breccia where the sublayer of the SIC (base of SIC) is in direct contact with the basement rocks. Five plume ridges are present in this section, labelled A-E. Plumes B and C are classified as primary plumes while A, D and E are secondary plumes. Arrow marks a vertically extensive plume structure that appears to how separations horizontally (parallel to SIC contact) due to missing data between cross sections, however in reality it forms a continuous elongated ridge of footwall breccia.

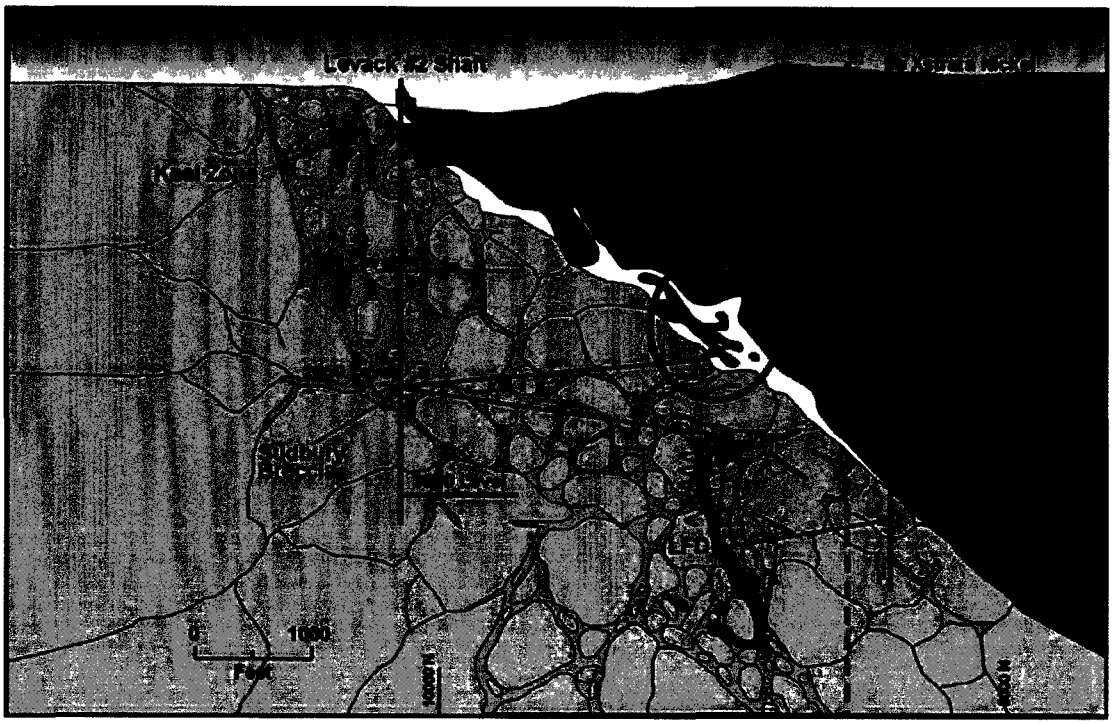

Figure 2.2.2. Schematic cross section of footwall in the North Range, Sudbury, showing the SIC, footwall breccia, Sudbury breccia, and basement gneiss. A footwall breccia plume ridge is circled which contains contact-style sulphide mineralization.

The shape, size, and dip of these ridge structures are summarized in Table 2.1. These data were obtained by careful scaled measurements made on vertical sections showing projected diamond drill hole log information. The main continuous plume C extends for 550 m (horizontally along the strike of the SIC contact) and intrudes up to ~90 m into the SIC from its contact with concordant footwall breccia its base. For comparison, ridge B is semi-continuous for 335 m along strike, but intrudes to a similar height of ~85 m. Characteristic plume morphologies range from single, thin and well-defined structures without sill-like apophyses, to irregular with numerous apophyses at their top. This multi-headed phenomenon does not occur in the secondary plumes observed in the study area. Multiple ridges may originate from the same basal (concordant) footwall breccia lens within a single embayment.

Importantly, comparison of plume size and morphology in mineralized and barren environments shows that abundance of, and the largest and most vertically extensive plumes are associated with mineralized embayments.

Table 2.1: Approximate dimensions and spatial calculations for plume ridge structures. Measurements were obtained using mine vertical sections. Dimensions: Y^{I} = width at base of plume; Y^{II} = width in throat of plume; Y^{III} = width at top of plume; Z^{I} = height from top of the concordant footwall breccia unit to tip of plume; Z^{II} = height from sublayer base to tip of plume; Z^{III} = height from mafic norite/felsic norite contact to tip of plume; total length = strike length of plume; bearing = angle of plume tip/centre of footwall breccia concordant contact measured from a vertical plane perpendicular to the ground.

Plume	A	B	C	D	E
width 1(Y^{I}m)	106.1	86.1	79.4	53.6	82.0
width (Y^{II}m)	45.9	28.6	28.2	22.1	38.7
width 3 (Y^{III}m)	13.6	7.3	8.0	11.1	9.9
height 1 (Z^{I}m)	101.1	85.3	88.7	71.8	83.7
height 2 (Z^{II}m)	65.5	36.0	58.8	41.7	73.8
height 3 (Z^{III}m)	13.0	17.4	42.4	26.7	43.5
total length (m)	182.9	350.5	548.6	182.9	182.9
~area (m^2)	17607.7	12033.5	11530.6	6330.1	11273.6
bearing (°)	14	23	29	31	16

2.4.2 Petrographic characteristics of the studied lithologies

The footwall breccia is a granitic rock that shows a wide range of textures, varying from a heterolithic breccia containing a fine-grained igneous matrix and clasts of variably digested footwall gneiss (and restitic clasts) to more equigranular, clast-free, plastically deformed equivalents of the footwall gneiss. In some cases, rocks logged as footwall breccia appear identical to the Levack Gneiss in hand sample. This observation suggests that large blocks of Levack Gneiss were mobilized during partial melting/footwall breccia formation and rise up to shallower stratigraphic levels in the plumes but do not melt completely or only experience some thermal metamorphism. Therefore, footwall materials cannot be heated too far above their solidus temperature during interaction with the SIC. The heterolithic breccia variety contains felsic clasts composed of quartz, albitic plagioclase, and alkali feldspar are visible and mafic clasts with amphibolitic compositions are also present in a fine-grained, granular, grey matrix (Figure 2.3a). These clasts are residual rounded fragments from the partially and dynamically melted Levack Gneiss. Equigranular footwall breccia varieties (leucocratic and melanocratic) are related to the proportions of felsic and mafic minerals from the original (parental) gneisses (Figure2.3d). Secondary alteration veins and patches of granophyric intergrowth related to cooling of the footwall breccia and post-crystallization hydrothermal alteration occur (Figure 2.3b and c). The granophyric matrix material is also common in the host SIC lithologies and may be a late stage residue from the footwall breccia as it recrystallizes in the plumes. Figure 2.3e shows a mafic clast rich footwall breccia sample with a fine grained, grey igneous matrix infilling the spaces between the clasts. For comparison,

Figure 2.3f shows the Levack Gneiss several hundred metres below the SIC contact. Its textural similarities to the footwall breccia suggest that many samples logged as breccia are actually large pods of weakly altered and thermally metamorphosed gneiss that were emplaced with partial melt during plume formation, as described above. Evidence for fluids released from the footwall breccia into adjacent SIC rock types is shown in Figure 2.3g-h in which normal felsic norite and a coarse-textured pegmatitic equivalent are compared.

Three main textural changes in the footwall breccia that may be related to the extent of partial melting of the original gneiss from which they were sourced are shown (Figure 2.4). In relatively fresh Levack Gneiss or weakly developed footwall breccia, many of the original characteristics of the gneiss are visible including large, subhedral to euhedral polycrystalline quartz aggregates containing triple junctions and well defined matrix domains containing large oikocrysts of plagioclase containing tabular albite crystals (Figure 2.4a). As melting proceeded, domains of quartz aggregates and feldspar rich matrix became poorly defined, quartz and albite grains became anhedral as they melted and recrystallized to form large complexely intergrown masses, and grain boundaries developed sawtooth like morphologies (Figure 2.4b) similar to stylolites in chemical sedimentary rocks. Grain boundary migration continued as melting advanced and quartz and albite grains develop highly irregular grain boundaries. Sieve texture indicates resorption of feldspars (Figure 2.4c-d). Partial melt that collected in the matrix of the footwall breccia as it forms recrystallized to a graphic-textured intergrowth (granophyre; Figure 2.4e), accompanied by the growth and recrystallization of halogen-bearing

silicates (fibrous actinolite, Figure 2.4f; and lathy biotite, Figure 2.4g). In the surrounding SIC rock types (norite, gabbro, sublayer) fresh igneous textures are generally preserved but are coarsened locally and show evidence of replacement of primary pyroxene by biotite (Figure 2.4i) and infiltration of granophyric liquid (Figure 2.4j).

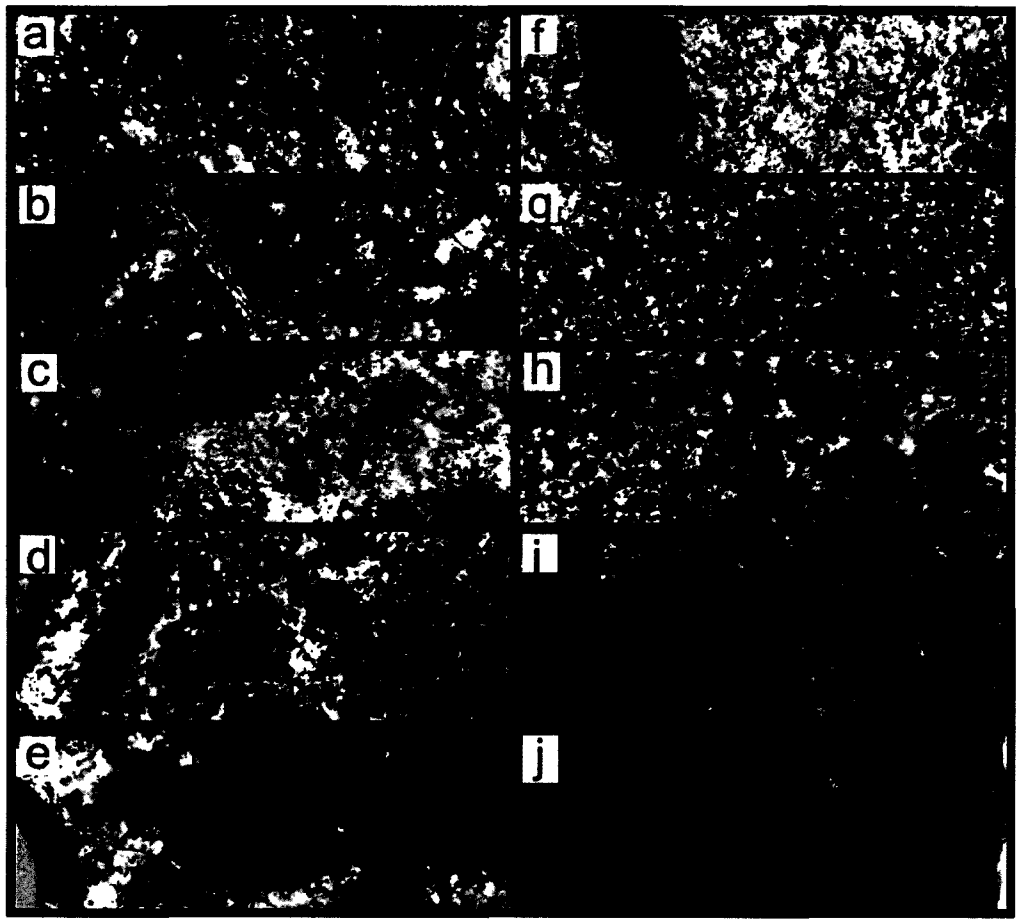

Figure 2.3. Petrographic characteristics of studied lithologies in hand sample. (a-d) Footwall breccias showing a range of textures resulting from a combination of varying clast compositions (from melted protoliths) and degree of melting. In fully developed footwall breccia (a), a variety of restitic and relict clasts from melted gneissic rocks occur in a grey, fine-grained, granular to granophyric granitic matrix. Lesser developed breccias (b-d) show microtextural evidence of partial melting but macroscopically preserve characteristics of the primary footwall gneiss with variable mafic content resulting from variations in the in original proportions of mafic and felsic bands in the protolith gneisses. Image (a-c) show more leucocratic varieties of footwall breccia whereas image (d) shows a melanocratic variety. Image (c) shows a large patch of quartz-alkali feldspar granophyric intergrowth within the breccia matrix. Note in image (d) the lack of any discernable "brecciated" textures. (e) Leucocratic footwall breccia matrix hosting several large mafic restitic clasts. (f) Typical Levack Gneiss from the region near the contact with the SIC showing pink hematitic-K-feldspar alteration, mafic clasts (from the original gneiss, not from partial melting). (g) Felsic norite (fine-grained). (h) Felsic norite (coarse-grained pegmatitic variety from immediately adjacent to footwall breccia.(i) Mafic norite. (j) Sublayer containing abundant pyroxenitic inclusions in a noritic matrix.

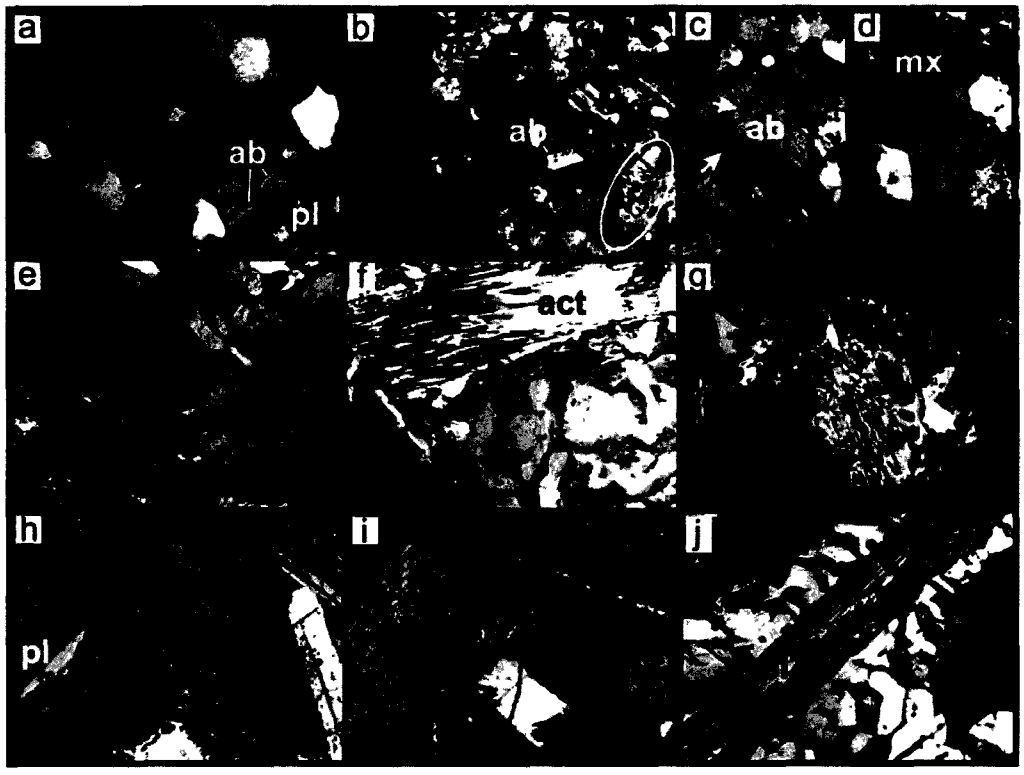

Figure 2.4. Petrographic characteristics of studied lithologies in thin section. All images have a height of field of 500 mm. (a) thermally metamorphosed but unmelted Levack Gneiss from adjacent to the SIC contact along an embayment. Note the occurrence of polycrystalline quartz (qtz) forming a patch or "eye" with relatively smooth grain boundaries and abundant trip junctions, and a matrix containing euhedral (tabular) albitic alkali feldspar (ab) included in plagioclase (pl). Matrix and quartz patches form discrete domains within the gneiss. (b) Footwall breccia showing partially melted footwall gneiss. As melting progressed, quartz (qtz) grain boundary migration occurred resulting in anhedral "sawtooth" or stylolite-like grain surfaces (area outlined in white oval), and the euhedral character of matrix feldspars (ab) became greatly diminished. (c-d) Fully developed footwall breccia showing extensively melted footwall rock. In (c) sieve texture in remnant feldspars is well developed (arrows), resulting from resorption, and in (d) domains of remnant quartz and matrix are still visible, the matrix (mx) has a granular appearance and relict quartz grains have a highly irregular grain shape. (e) granophyric matrix within footwall breccia, occurring as a mm-size vuggy infilling within the matrix. (f) Lathy, acicular amphibole (var. actinolite; mx) surrounding in granophyric matrix from a footwall breccia sample. (g) Platy biotite (bt) within the matrix of a footwall breccia sample; circular dark areas are LA-ICPMS pits. (h-i) Typical noritic and sublayer rock types showing the occurrence of ophitic plagioclase (pl) - orthopyroxene (opx) intergrowth with secondary (or late magmatic) replacement of orthopyroxene by biotite (bt). Image (j) shows a resorbed plagioclase lath surrounding in granophyric matrix potentially introduced as a partial melt from the adjacent footwall breccia plume.

2.5 Sampling and analytical methodology

Representative samples of the rock types within the SIC and contact region were obtained in mineralized and unmineralized environments from 3 drillholes along the north range of the SIC in the Levack and Windy Lake areas (figures 2.1.2 and 2.1.3). In total, ~140 samples were collected for petrographic evaluation and geochemical analyses.

Bulk rocks (~5 grams powder) were analyzed for major and trace elements (other than the halogens) by X-ray fluorescence spectrometry with a detection limit of 0.01 wt. %. at the Geoscience Laboratories (Ontario Ministry of Northern Development, Mines and Forestry, Sudbury) and ICP-MS analyses were completed at the Geological Survey of Canada in Ottawa, Ontario. Bulk rock halogens were analyzed by ICP-MS at Geological Survey of Canada, modifying a technique developed and described in detail by Hall et al., 1986 to allow for the analysis for bromine and iodine in addition to fluorine and chlorine. For sample preparation, a pyrolysis combustion tube furnace was heated to 1070°C. Each 100 mg rock sample was mixed with 200 mg of V_2O_5 in a precleaned Ni boat. The boat was inserted into the combustion oven, and oxygen (humidified by a 60°C water filter) was passed over the sample. The gases evolved during sample combustion were bubbled through 10 mL of a basic (0.005M NaOH) solution to capture the released halogens. In order to stabilize iodide in solution, 50 μL of a 0.5 vol. % Na_2SO_3 solution was added to a 5 mL aliquot of the collection solution (final solution is ~50ppm $NaSO_3$). The stabilized solution was analysed by ICP-MS for both Br and I and the concentration determined in solution was calculated back to the original dry sample weight and reported as either ppm or ppb. The remaining 5 mL of sample was used for analysis of F and Cl by ion

chromatography (I and Br concentrations are too low in solution to be able to analyse and provide accurate result). The analysis was done on a 50 μL aliquot of sample using a Dionex DX-600 IC with hydroxide eluant generation using an AS18 guard and analytical column. A gradient separation was carried out from 12 to 52 mM KOH to ensure complete resolution of the F peak from the water dip. The peaks were calibrated by area and compared to aqueous standards. The concentrations were again corrected back to the original dry weight.

Soluble halogens, leachable from 40 powdered rock samples at room temperature, were analyzed using colorimetric determination at Saint Mary's University, and by ion chromatography at Geoscience Laboratories (Sudbury). For each analysis, 5 grams of sample was crushed and powdered with extreme caution to prevent contamination. Each powdered sample was then flushed with 20ml of deionized water, stirred, and left to settle. The resulting solution was then transported using a pipette to a beaker so the solution can be run through a nano filter to remove any remaining sediments. This process is the repeated once again with 20 ml and finally 10 ml of deionized water. The 50ml of filtered solution was then stored in a Nalgene sample container. 10 ml of solution is placed in a glass beaker with 2 ml of zirconyl acid SPADNS reagent and 0.5 ml sodium solution. The beaker is then shaken and analyzed using a LaMotte Smart 2 Colorimeter under the "041 – Fluoride" protocol. A blank of pure deionized water is used as a reference, and samples of tap water with certified analyses for F were used to check the accuracy of the F determinations on unknowns.

2.6 Results

2.6.1 Bulk rock geochemistry (excluding halogens)

Major and trace element geochemical analysis of 145 samples were obtained, including footwall breccia (92), felsic norite (13), mafic norite (8), sublayer (15), Levack gneiss (12), quartz gabbro (3), and aplite (2) lithologies in the barren and mineralized environments (Table 2.2, 2.3, and appendicies A1-A13) to determine if any significant differences and correlations exist that may aid exploration and provide insight into geochemical interaction between the footwall breccia and the SIC.

Major element compositional variations in the footwall breccia, such as SiO_2 (~59-61.5 wt. %), are relatively minor and likely the result of slight variations in mafic and felsic mineral abundance in the matrix, variations in the the composition and abundance of footwall clasts in the footwall breccia analyzed, and the secondary effects of post-solidus hydrothermal alteration. Overall, there are no systematic differences in major element abundances for any rock types between the barren and mineralized environments. However some slight variations in the chemistry of the felsic norite are worth noting here. The felsic norite shows a small decrease (variation of ~2.0 wt. %) in Fe_2O_3 with increased depth in the barren environment. A more significant decrease in CaO (variation of ~5.5 wt. %) with depth was also recognized.

Trace element geochemistry for all lithologies is remarkably similar with minor and non-systematic variations in between barren and mineralized environments. There is significant variation in Cu, Ni and Cr between the mineralized and barren environments in all lithologies. However, the enrichments in Cu and Ni, for example, are not

characteristic of the mineralized samples. For example, Cu is enriched in footwall breccia, felsic norite, and basement gneiss from the mineralized environment, while depleted in mafic norite and sublayer norite from the same environment. Abundances of Ni also shows significant but non-predictive variation. Mineralized footwall breccia, felsic norite, basement gneiss, and to a lesser degree, sublayer norite, are enriched in Ni while mafic norite is depleted.

Systematic trace element variations include a slight overall enrichment in LREE in footwall breccias in the barren environment, possibly attributable to increased abundance of LREE-enriched apatite or other REE bearing phases. Variations in REE abundance

		footwall breccia				norite			
		b	n = 32	m	n = 7	b	n = 7	m	n = 2
Element	Detection Limit	average	1 σ =	average	1 σ =	average	1 σ =	average	1 σ =
SiO_2 (wt. %)	0.01	59.01	4.36	61.51	4.84	55.90	6.11	59.33	0.25
TiO2	0.01	0.43	0.17	0.50	0.23	0.78	0.89	0.38	0.10
Al_2O_3	0.01	15.79	2.37	15.98	1.51	14.99	2.88	13.47	3.26
Fe_2O_3	0.01	6.57	3.10	6.14	2.75	8.07	3.87	8.55	1.58
MnO	0.01	0.09	0.04	0.10	0.05	0.12	0.06	0.14	0.03
MgO	0.01	4.56	2.59	3.32	2.13	6.22	2.25	8.05	2.37
CaO	0.01	5.74	1.60	5.80	1.37	6.16	3.66	5.31	1.09
Na_2O	0.01	4.63	1.56	4.55	0.83	3.50	1.51	2.75	0.55
K_2O	0.01	1.05	0.37	1.10	0.46	1.49	0.69	1.15	0.16
P_2O_5	0.01	0.22	0.13	0.15	0.06	0.16	0.06	0.12	0.01
LOI	0.05	1.84	0.79	0.89	0.35	2.43	0.80	0.68	0.01
Total		99.93	0.38	100.03	0.37	99.81	0.63	99.91	0.39

		sublayer				basement gneiss			
		b	n = 3	m	n = 4	b	n = 2	m	n = 5
Element	Detection Limit	average	1 σ =	average	1 σ =	average	1 σ =	average	1 σ =
SiO_2 (wt. %)	0.01	49.65	1.12	50.99	6.94	67.40	1.25	62.99	25.14
TiO2	0.01	0.64	0.14	0.32	0.13	0.35	0.10	0.51	0.19
Al_2O_3	0.01	9.81	1.83	9.97	6.84	15.76	1.04	15.29	5.92
Fe_2O_3	0.01	14.21	1.27	13.83	7.84	3.71	0.74	5.41	2.11
MnO	0.01	0.21	0.00	0.16	0.05	0.06	0.01	0.08	0.03
MgO	0.01	11.67	1.63	12.88	6.73	1.43	0.10	3.50	2.32
CaO	0.01	9.02	0.97	6.87	1.55	4.12	0.35	5.47	2.11
Na_2O	0.01	1.43	0.38	2.21	2.01	5.14	0.74	4.42	1.88
K_2O	0.01	0.57	0.05	0.71	0.58	1.44	0.04	1.26	0.53
P_2O_5	0.01	0.18	0.04	0.11	0.06	0.15	0.00	0.21	0.11
LOI	0.05	1.96	0.36	1.32	0.82	0.92	0.25	0.86	0.35
Total		99.34	0.32	99.38	0.68	100.44	0.44	100.01	38.58

Table 2.2: Average analyses for bulk rock major elements from representative lithologies in barren (b) and mineralized (m) environments. Abbreviations: FWB = footwall breccia, MNOR = mafic norite, FNOR = felsic norite, SL = sublayer norite, GN = basement gneiss.

were not observed between environments in the mafic and felsic norites. Rubidium is also noticeably lower in the mineralized environment (i.e., by a half order of magnitude in average abundance).

Figure 2.5 shows normalized abundance patterns for all analyzed lithologies in each environment. The patterns illustrate the marked similarity in overall trace element abundances between lithologies and environments. Variations in the absolute abundance of all trace elements are most recognizable in the data for the footwall breccias, however, it should be noted that these variations are in part more noticeable due to the number of analyses reported for that rock type. Nonetheless, variations in absolute abundances in the footwall breccias, footwall gneisses and sublayer lithologies can vary by up to an order of magnitude. These variations, although systematic, probably reflect different mafic-felsic clast and matrix proportions (in the case of the footwall breccias), variable proportions of mafic and felsic gneissic components (in the case of the footwall gneiss samples), and variable degrees of contamination by footwall gneiss (in the case of the sublayer). Subtle but consistent depletions in Nb, Ta, Ti, Co, Cr and Ni are recognized in all lithologies.

Element (ppm)	Detection Limit	footwall breccia				mafic norite			felsic norite			sublayer				basement gneiss			
		b	n = 32	m	n = 7	b	n = 2	m	b	n = 6	m	b	n = 3	m	n = 4	b	n = 2	m	n = 5
		average	1 σ =	average	1 σ =	average	1 σ =	average	average	1 σ =	average	average	1 σ =	average	1 σ =	average	1 σ =	average	1 σ =
Ba	0.8	520	208	574	214	134	6	435	440	95	380	229	61	419	169	505	135	697	287
Be	0.04	1.01	0.26	0.76	0.21	1.02	0.60	0.69	0.91	0.17	0.54	0.84	0.22	0.65	0.31	1.11	0.16	0.92	0.11
Cd	0.013	0.10	0.12	0.23	0.28	0.31	0.08	0.12	0.57	0.84	0.09	0.34	0.17	0.22	0.07	0.07	0.01	0.12	0.07
Ce	0.12	47.9	21.2	37.4	18.5	54.0	34.4	45.6	40.9	8.5	34.0	48.4	10.2	30.6	16.0	34.7	5.5	52.8	34.3
Co	0.13	38.9	34.4	43.1	58.5	147.4	0.0	55.7	42.1	28.0	31.3	104.4	39.7	74.5	56.2	8.7	1.1	19.7	10.5
Cr	3	275	157	645	1139	429	158	1162	229	30	491	957	276	649	433	142	14	229	168
Cs	0.013	0.48	0.52	0.27	0.19	0.74	0.03	0.63	0.82	0.76	0.41	1.17	0.18	0.45	0.41	0.19	0.03	0.34	0.28
Cu	1.4	207	396	1013	2004	2270	1479	211	31	22	85	2408	2851	464	273	39	27	94	98
Dy	0.009	2.21	0.96	1.93	1.04	3.09	1.72	2.27	1.95	0.53	1.32	3.47	0.80	2.34	1.26	1.53	0.18	1.94	1.03
Er	0.007	1.13	0.48	0.99	0.55	1.38	0.63	1.31	1.08	0.32	0.68	1.72	0.33	1.22	0.68	0.77	0.07	0.91	0.40
Eu	0.0031	1.27	0.39	1.10	0.38	1.67	1.02	0.85	1.14	0.11	1.04	1.33	0.06	0.99	0.23	0.90	0.13	1.34	0 58
Ga	0.04	19.0	3.7	17.6	4.4	11.8	3.6	12.7	16.6	2.8	17.0	13.4	0.8	16.2	7.4	19.9	0.3	19.1	1.0
Gd	0.009	3.13	1.48	2.49	1.27	4.36	2.62	2.86	2.49	0.52	1.81	4.54	0.95	2.99	1.52	2.08	0.21	3.09	2.12
Hf	0.14	2.2	0.5	2.4	0.6	4.0	2.9	2.9	2.2	0.5	2.2	1.8	0.3	1.8	1.0	2.7	1.4	3.2	1.1
Ho	0.0025	0.41	0.17	0.36	0.20	0.54	0.28	0.44	0.37	0.11	0.24	0.64	0.14	0.44	0.24	0.28	0.03	0.34	0.17
In	0.0018	0.04	0.01	0.05	0.04	0.13	0.03	0.05	0.03	0.01	0.03	0.08	0.02	0.04	0.01	0.03	0.00	0.03	0.01
K	6	8716	3540	9013	4643	2728	481	12769	13569	3783	9475	5236	375	7244	4719	12916	204	11305	1933
La	0.04	22.8	8.9	18.7	8.3	23.6	15.2	22.3	20.0	4.3	17.3	21.2	5.6	14.5	7.8	18.2	3.5	25.9	14.6
Li	0.4	10	4	6	2	12	2	9	21	11	8	9	2	8	4	5	2	8	2
Lu	0.002	0.14	0.06	0.12	0.07	0.16	0.06	0.19	0.15	0.05	0.09	0.22	0.03	0.16	0.09	0.10	0.00	0.11	0.04
Mn	6	664	293	716	426	1295	541	1121	712	135	789	1403	52	1055	276	386	11	540	192
Mo	1	4	1	4	1	3	0	3	4	1	4	2	0	3	1	5	2	3	1
Na	25	30344	11422	28112	11598	4293	1978	15476	24259	5335	22654	8831	2012	20433	11652	35055	1334	31280	5015
Nb	0.028	3.3	1.2	3.2	1.5	18.8	17.5	3.5	3.6	1.3	2.4	3.4	1.2	2.7	2.2	3.7	0.9	3.6	1.5
Nd	0.06	24.0	11.7	17.2	9.4	28.8	18.0	20.8	18.4	3.3	14.9	27.6	4.8	16.5	7.8	15.0	0.5	25.2	18.8
Ni	1	185	278	1097	2431	4347	3587	212	31	8	114	618	239	761	663	18	5	75	76
P	5	949	522	583	310	709	509	589	583	161	520	813	194	707	240	671	54	966	610
Pb	0.6	11	24	10	4	6	0	9	8	5	6	6	1	10	5	8	0	13	11
Pr	0.014	6.00	2.80	4.46	2.35	7.09	4.49	5.46	4.86	0.97	3.99	6.50	1.15	3.94	1.93	3.96	0.35	6.45	4.57
Rb	0.23	21	11	16	8	16	1	28	37	10	17	21	1	18	19	23	1	25	15
Sb	0.04	0.1	0.1	0.1	0.0	0.1	0.0	0.1	0.3	0.2	0.1	0.1	0.0	0.1	0.0	0.1	0.0	0.1	0.0
Sc	1.1	14	10	14	8	22	2	23	15	2	12	36	7	26	12	7	1	12	6
Sm	0.012	4.32	2.17	3.18	1.72	5.56	3.36	3.69	3.28	0.62	2.45	5.71	1.10	3.48	1.70	2.69	0.21	4.43	3.34
Sr	0.6	560	214	585	288	261	153	278	388	191	660	277	84	560	406	441	184	634	137
Ta	0.023	0.2	0.1	0.2	0.1	1.7	1.6	0.2	0.2	0.1	0.1	0.2	0.1	0.2	0.1	0.1	0.0	0.2	0.1
Tb	0.0023	0.41	0.18	0.34	0.18	0.58	0.34	0.39	0.34	0.08	0.24	0.61	0.14	0.41	0.22	0.28	0.03	0.37	0.23
Th	0.018	1.26	1.52	1.73	1.52	2.00	1.39	2.77	3.00	2.06	1.19	2.45	1.13	1.74	2.23	0.48	0.12	2.20	2.94
Ti	7	2665	1022	2872	1361	10268	8801	2932	2532	330	1716	3853	849	2456	1288	2164	649	3181	834
Tm	0.0019	0.16	0.07	0.14	0.08	0.18	0.08	0.19	0.16	0.05	0.10	0.24	0.05	0.17	0.10	0.11	0.01	0.12	0.05
U	0.011	0.19	0.11	0.26	0.16	0.26	0.14	0.52	0.53	0.41	0.16	0.59	0.45	0.45	0.62	0.20	0.03	0.37	0.33
V	0.8	88	42	102	53	217	130	141	103	20	68	183	31	121	46	48	7	93	38
Y	0.05	11.0	4.8	9.5	5.2	13.9	6.8	11.5	10.1	2.8	6.2	17.0	3.7	11.6	6.5	7.7	0.8	9.1	4.3
Yb	0.009	0.99	0.43	0.86	0.47	1.11	0.42	1.25	1.01	0.30	0.62	1.50	0.26	1.06	0.62	0.66	0.04	0.77	0.31
Zn	3	63	25	73	41	91	5	97	195	225	77	107	23	80	12	50	7	69	33
Zr	1	85	23	102	32	147	107	98	80	15	82	66	16	65	35	106	51	136	38

Table 2.3: Average analyses for bulk rock trace elements from representative lighologiesin barren and mineralized environments. Mineralized mafic norite and felsic norite data are missing 1 sigma calculations due to sampling limitations. Abbreviations: b = barren; m = mineralized.

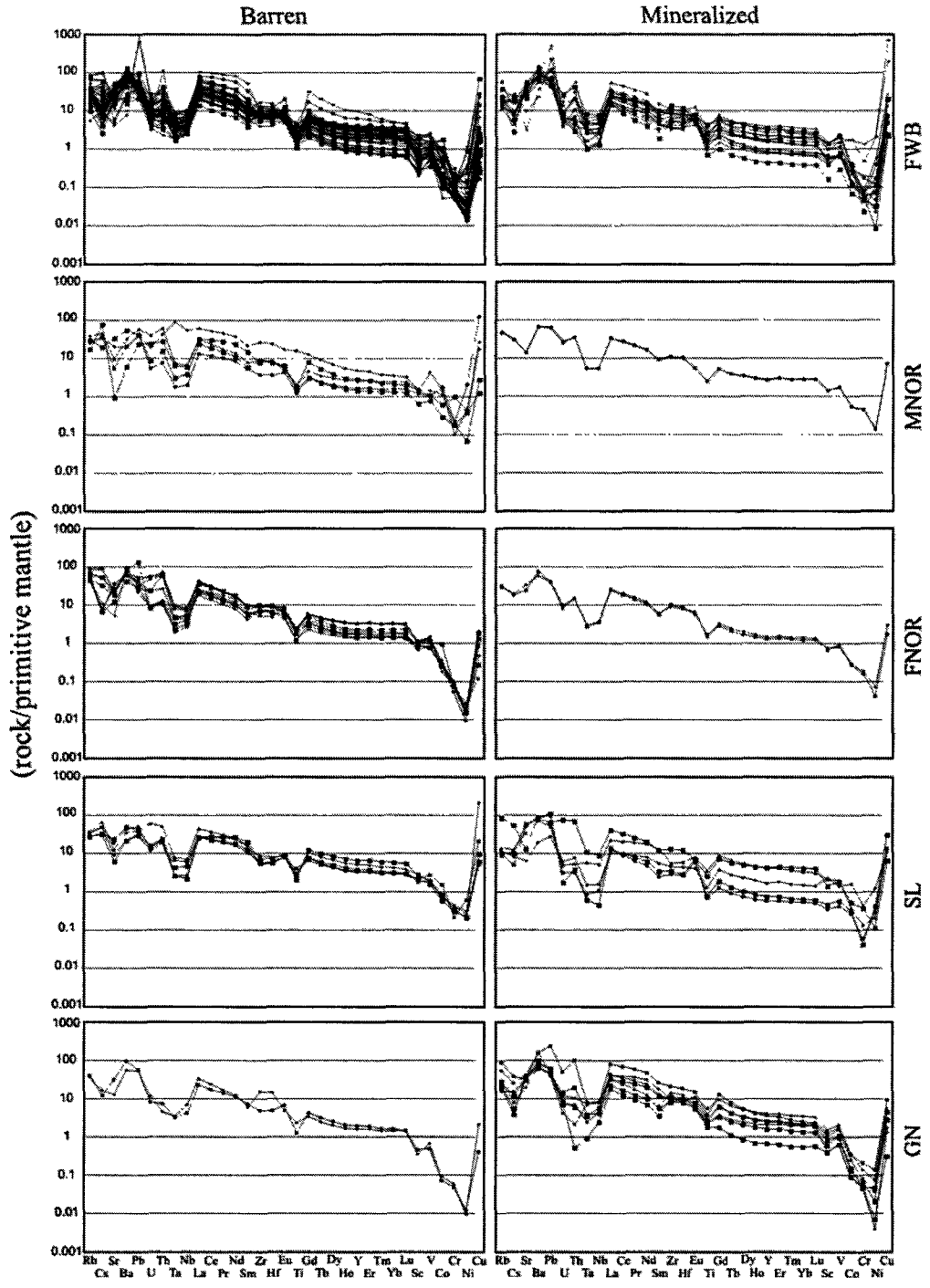

Figure 2.5: Normative abundance diagrams for barren and mineralized environments, separated by lithology. Abbreviations: FWB = footwall breccia, MNOR = mafic norite, FNOR = felsic norite, GN = basement gneiss, and SL = sublayer.

2.6.2 Bulk rock geochemistry of the halogens

Table 2.4 summarizes the abundances and ratios of the halogen elements in lithologies from each environment. Tabulated full analyses of all samples can be found in the Appendices. Footwall breccias comprised the most abundantly analyzed lithology (n = 89). Several systematic differences in the halogen content of the contact lithologies were observed (Table 2.4) between the barren and mineralized environments. Average F abundances in footwall breccia are significantly higher in the barren environment, with a maximum value almost 3x that of the mineralized environment. Aside from a few outliers, average Cl and Br abundance are similar in both environments. Iodine, however, may be significantly more enriched in the mineralized environment, up to twice the abundance found in barren footwall breccia. There were fewer samples analyzed from mafic and felsic norite (2 from barren environment, 3 from mineralized environment). Therefore, average abundances of the halogens in this lithology are not as statistically significant as in the footwall breccia.

All four halogens are comparable in abundance between the two environments with statistically insignificant differences (Figure 2.6). In the basement gneiss, F and I abundances are substantially greater in the mineralized environment, but no significant differences were seen in relative Cl and Br abundances. The sublayer shows the greatest overall variability in halogen abundances, notably Cl and I which vary by up to an order of magnitude and which are up to 4x and 7x greater in mineralized sublayer samples than in the barren embayment.

A few variations in halogen abundance with depth were also noted. In the mineralized environment, Br becomes increasingly enriched with increasing depth. In the barren environment, Br becomes increasingly depleted with increasing depth. In the barren environment, I behaves erratically but becomes gradually depleted with increasing depth. Ratios of halogen elements were also examined. In one of the two studied drill holes from the mineralized environment, there is a gradual increase in Cl/Br with increasing depth in the entire hole; however Cl/Br in the plume (i.e., within footwall breccia) only shows a slight increase. This trend is not present in the second hole within the same embayment. In the barren environment, the Cl/Br ratio also increases with depth. A general increase in Br/I was noted with increasing depth in one of the two mineralized holes but this trend was not reproducible in the second hole or in the barren environment.

Significant variations in halogen abundance are present between different lithologies and from the mineralized to barren environments. Average halogen abundances in lithologies from each study area are also shown (Figure 2.6). While there is significant overlap between the two environments, a few differences are significant. All lithologies show similar F abundances, footwall breccia, mafic norite, and sublayer from the mineralized environment are slightly depleted in F compared to the barren environment. Average abundances of Cl, Br and I are not similar in most lithologies except for the sublayer which is consistently and significantly enriched in Cl, Br and I in the mineralized environment. The footwall breccia and basement gneiss in the mineralized environment are also notably enriched in I compared to barren rocks (with respect to increasing depth in the Sudbury stratigraphy). The depth transition from felsic norite to

the basement gneiss shows no systematic increases or decreases in halogen abundance with the exception of I and Br which increase in abundance relative to Cl with depth at and below the sublayer.

			F (ppm)				Cl (ppm)				Br (ppb)				I (ppb)			
Unit	Environment	n=	avg	1 σ	min	max	avg	1 σ	min	max	avg	1 σ	min	max	avg	1 σ	min	max
fwb	b	67	433	232	245	1657	393	156	158	829	1921	930	437	3996	64	32	20	177
	m	22	268	158	51	594	317	137	58	634	1748	939	217	3831	118	73	22	333
mnor	b	2	407	224	183	631	193	14	179	207	848	173	675	1020	92	4	88	96
	m	3	367	53	314	420	386	182	204	568	884	314	570	1198	83	39	44	122
fnor	b	11	344	216	48	599	474	240	133	788	2385	1146	852	4861	79	24	33	115
	m	2	362	20	342	382	372	11	361	382	1229	162	1067	1390	84	8	76	92
sl	b	9	283	50	223	351	203	15	182	229	552	134	301	693	35	10	21	49
	m	6	223	143	69	493	733	719	268	2166	1975	730	1213	2946	241	169	67	548
gn	b	3	364	19	345	383	359	119	240	478	1601	65	1536	1665	42	13	29	55
	m	8	526	348	207	1247	343	115	163	481	1980	948	637	3125	84	44	25	141

			Cl/Br				Cl/F				Br/I			
Unit	Environment	n=	avg	1 σ	min	max	avg	1 σ	min	max	avg	1 σ	min	max
fwb	b	67	238	102	108	620	1.00	0.40	0.20	1.82	33.6	12.4	11.3	57.5
	m	22	206	65	94	325	1.75	1.43	0.19	5.41	15.4	5.3	8.8	25.9
mnor	b	2	234	31	203	265	0.65	0.33	0.33	0.98	9.1	1.5	7.7	10.6
	m	3	416	58	358	474	1.00	0.35	0.65	1.35	11.4	1.6	9.8	13.0
fnor	b	11	202	68	104	313	2.10	1.34	0.60	4.80	33.9	19.4	9.4	69.8
	m	2	307	32	338	338	1.03	0.09	0.95	1.12	14.6	0.5	14.0	15.1
sl	b	9	222	65	156	287	1.01	0.38	0.63	1.39	18.0	4.2	14.1	25.9
	m	6	196	50	144	273	1.00	0.59	0.13	1.84	10.8	4.9	5.4	19.9
gn	b	3	400	140	303	678	0.74	0.13	0.56	0.91	41.6	11.3	30.3	53.0
	m	8	337	212	132	735	3.18	1.44	1.33	5.28	25.0	3.9	18.6	29.7

Table 2.4: Average bulk halogen abundance for various lithologies in Sudbury. Abbreviations: fwb = footwall breccia; mnor = mafic norite; fnor = felsic norite; sl = sublayer norite; gn = basement gneiss; b = barren; m = mineralized.

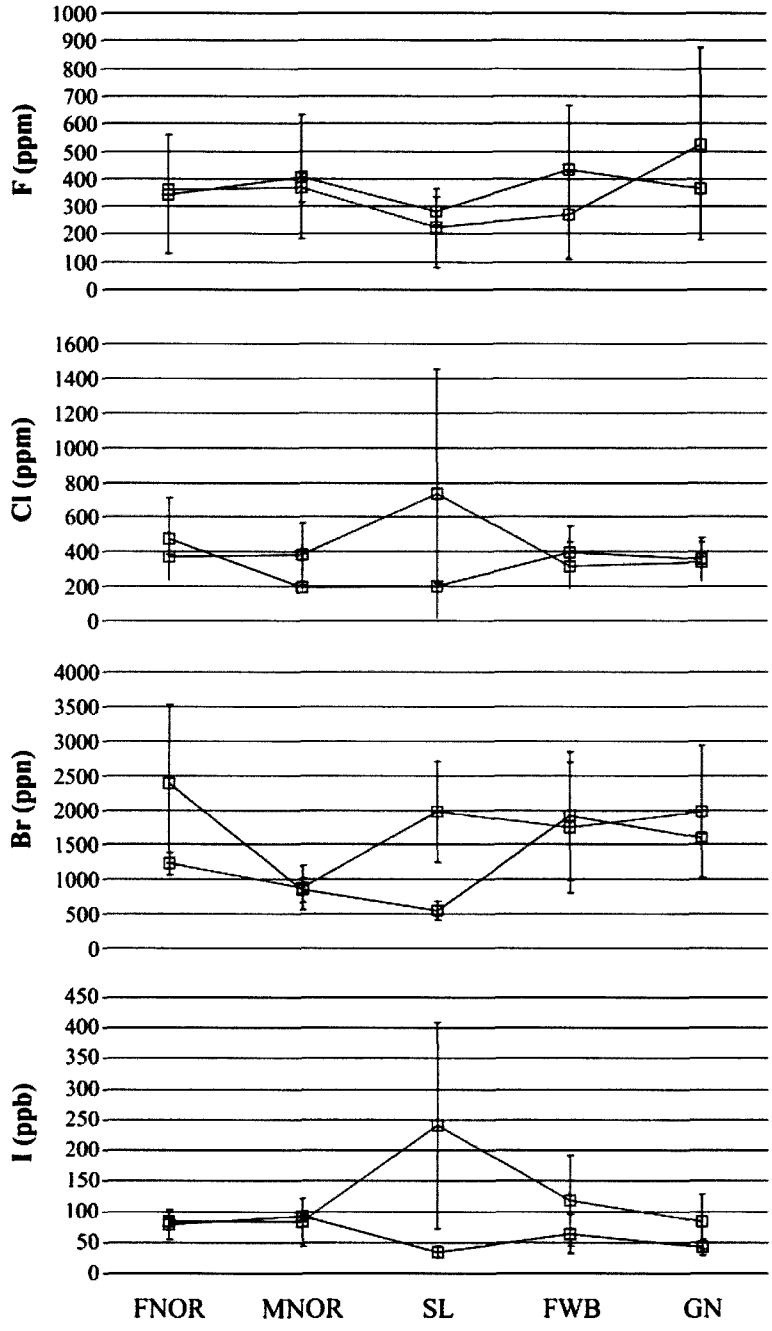

Figure 2.6. Average halogen abundance in each contact region vs. lithology. Lithologies are in approximate order of depth (shallow = felsic norite, deep = basement gneiss). Blue = barren environment; red = mineralized environment. Abbreviations: FWB = footwall breccia, MNOR = mafic norite, FNOR = felsic norite, SL = sublayer norite, GN = basement gneiss. Boxes show mean values and bars show 1 sigma variability on the average values.

Figures 2.7 and 2.8 show average halogen ratios in each lithology from the barren and mineralized embayments plotted against bulk Cl. In Figure 2.7, Cl/Br vs. Cl is summarized for both for both barren and mineralized environments. Though there were more samples analyzed from the barren suite, differences are noticeable between the two environments (Figure 2.7). The majority of footwall breccia samples from both environments plot in the same general region, however the barren plot show approximately 15% outlying samples containing anomalously high Cl/Br or anomalously high Cl. For example, sublayer norite samples generally contain a higher Cl/Br ratio in the barren zone and exhibit greater bulk Cl values in the mineralized environment. Felsic norite samples plotted similarly for both environments. Mafic norite was scattered between the two environments, however there are only two samples for the mineralized environment so the statistical representivity of the data set is questionable. Basement gneiss samples also plotted in similar regions between the two environments with the exception of one outlier sample from the mineralized suite.

Ratios of bulk Cl/Br (Figure 2.8) are similar in both environments in the sublayer, footwall breccia and basement gneiss lithologies, but the noritic units in the mineralized environment show much higher ratios. With the exception of the mafic norite, ratios of bulk Br/I (Figure 2.8) are greater in the barren environment in all lithologies, and show a subtle increase with depth in both embayments.

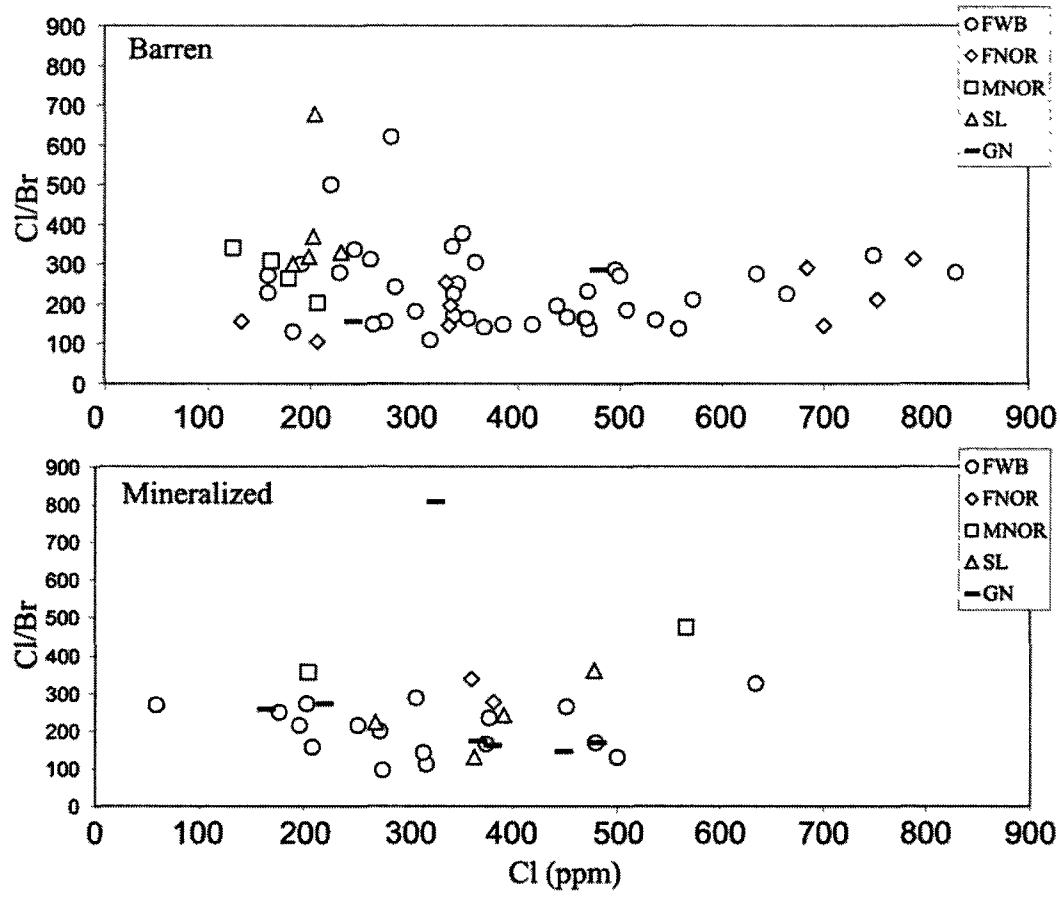

Figure 2.7. Cl/Br vs. Cl plots for barren and mineralized environments. Abbreviations: FWB = footwall breccia, MNOR = mafic norite, FNOR = felsic norite, SL = sublayer norite, GN = basement gneiss.

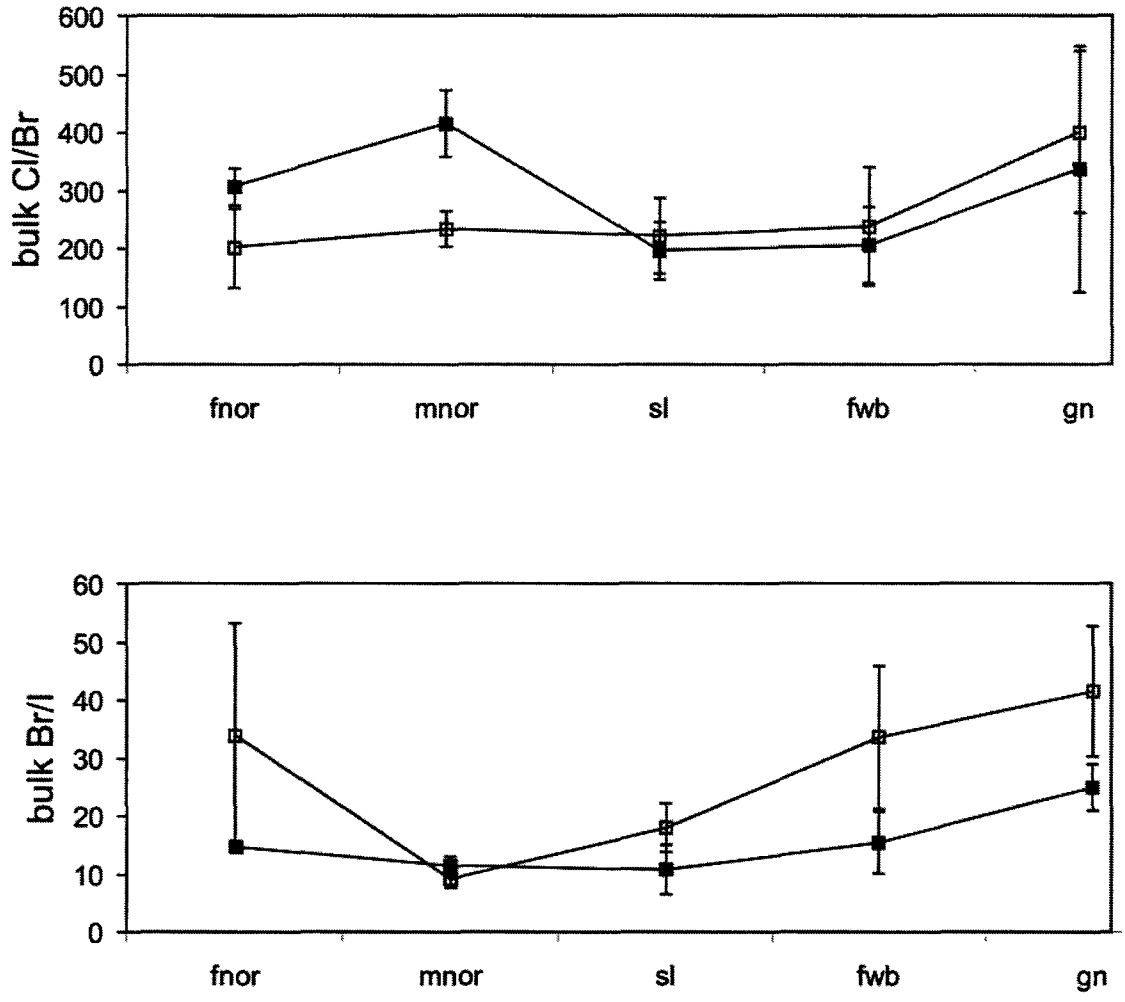

Figure 2.8. Cl/Br and Br/I vs. lithology. Blue = barren environment; red = mineralized environment. Abbreviations: FWB = footwall breccia, MNOR = mafic norite, FNOR = felsic norite, SL = sublayer norite, GN = basement gneiss. Boxes show mean values and bars show 1 sigma variability on the average values.

2.6.3 Soluble halogens and sulphate

Soluble halogens were analyzed to determine the percentage of bulk halogens that are soluble, and also to attempt to constrain fluid signatures in the two environments. Tables 2.5.1 and 2.5.2 summarize the halogen ion abundances in solutions prepared by leaching powdered samples of only footwall breccia, along with calculated values for halogen ratios in solution and the % (by mass) of each halogen that was soluble in water at 20°C, determined by comparing the soluble fraction with the bulk rock (soluble + insoluble) analyses. While F^- (by both ion chromatography and colorimeter) and Br^- abundances are similar in the footwall breccia from the two environments, Cl^- is significantly more enriched in the barren environment by a factor of up to 4, resulting in much higher Cl^-/Br^- ratios in barren samples. This result is interesting because it implies that variations in bulk rock Br must be related only to variations in the amount of Br in insoluble phases during alteration, or the abundances of those phases. Possible reasons for the higher Cl^-/Br^- in the barren embayment are discussed in a later section.

Comparison of the soluble fraction and bulk rock data (Table 2.5.1, 2.5.2) shows that the vast majority (>96%) of the F in the sampled lithologies was insoluble during alteration, a large proportion (and relatively consistent from sample to sample) of the bulk rock Cl and Br are soluble (up to 92% for Cl; up to 64% for Br). In other words, mineral-bound Cl and Br exert a much lesser control on bulk rock Cl and Br abundance than previously thought.

Interestingly, values of SO_4^{2-} in leachates are higher in the barren footwall breccia samples. This enrichment is either caused by the presence of trace amounts of sulphide

minerals in the sampled rocks (which would oxidize during pulverization and leaching) or is produced by the crystallization of sulphide minerals. More reducing conditions in embayments that would ultimately become mineralized would promote the stability of sulphide rather than sulphate; thus, an excess of sulphate would be expected in hydrothermal fluids associated with barren embayments where fO_2 was inherently higher. This fluid, if trapped in fluid inclusions, would lead to elevated abundances of SO_4^{2-} in leachates from those samples.

	Bulk Halogens				Leachate (ppm in solution)				% Soluble Halogens								
Sample	F (ppm)	Cl (ppm)	Br (ppm)	I (ppb)	F^-	Cl^-	Br^-	SO_4^{-2}	F	Cl	Br	Sol. Cl (ppm)	Sol. Br (ppm)	Sol. Cl/Br	Insol. Cl/Br	Insol. Cl (ppm)	Insol. Br (ppm)
CS10	488	495	1.718	71.0	0.27	31.65	0.09	1.69	0.56	63.9	50.5	316	0.87	365	210	179	0.85
CS12	550	353	2.172	78.0	0.26	32.43	0.14	1.79	0.47	91.9	63.9	324	1.39	234	37	29	0.78
CS15					0.20	26.86	0.10	135.15						265			
CS18	406	438	2.249	87.0	0.18	20.28	0.08	74.68	0.45	46.3	34.9	203	0.79	258	161	235	1.46
CS21	295	260	1.759	39.0	0.19	15.54	ND	153.60	0.63	59.8		155			59	105	1.76
CS24	794	183	1.406	27.0	0.21	10.63	ND	64.05	0.27	58.1		106			55	77	1.41
CS28					0.20	15.04	0.04	259.96						334			
CS32					0.28	46.62	0.14	1.31						328			
CS36					0.27	28.27	0.06	1.43						514			
CS41	1657	337	0.975	63.0	0.40	19.74	0.04	34.37	0.24	58.6	45.3	197	0.44	446	262	140	0.53
CS47	425	415	2.823	76.0	0.30	28.69	0.15	8.45	0.70	69.1	52.5	287	1.48	194	96	128	1.34
CS51	323	535	3.336	58.0	0.20	35.79	0.13	1.42	0.62	66.9	40.3	358	1.34	266	89	177	1.99
CS55					0.17	9.06	0.05	9.97						173			
CS59					0.16	9.03	0.05	0.51						197			
CS64	340	242	0.714	44.0	0.28	8.59	n.a.	1.97	0.81	35.5		86			219	156	0.71
CS67					0.28	8.24	n.a.	1.19									
CS71	394	368	2.630	47.0	0.34	27.29	0.15	6.43	0.86	74.2	57.8	273	1.52	180	86	95	1.11
CS74					0.42	51.52	0.21	0.34						241			
CS76	379	571	2.719	84.0	0.37	32.73	0.10	5.50	0.98	57.3	37.4	327	1.02	322	143	244	1.70
CS89	444	282	1.168	24.0	0.28	12.91	0.04	15.51	0.64	45.8	36.2	129	0.42	305	205	153	0.74
CS92					0.31	15.42	n.a.	1.72									
avg	541	373	1.972	58.2	0.27	23.16	0.10	37.19	0.60	60.6	46.5	230	1.03	289	135	143	1.20
1 sigma	359	116	0.782	20.9	0.07	12.25	0.05	66.10	0.21	14.0	9.7	92	0.40	92	72	60	0.46
min	295	183	0.714	24.0	0.16	8.24	0.04	0.34	0.24	35.5	34.9	86	0.42	173	37	29	0.53
max	1657	571	3.336	87.0	0.42	51.52	0.21	259.96	0.98	91.9	63.9	358	1.52	514	262	244	1.99

Table 2.5.1: Soluble halogen geochemistry of footwall breccia from the barren environment. Bulk rock halogen abundances were determined by an applied pyrolysis combustion method. Leachate data are reported as anions in solution leached into 50ml deionized water from 5g of sample. Soluble/insoluble calculations are based on these paramcters.

	Bulk Halogens				Leachate (ppm in solution)				% Soluble Halogens							
Sample	F (ppm)	Cl (ppm)	Br (ppm)	I (ppb)	F^-	Cl^-	Br^-	SO_4^{-2}	F	Cl	Br	Sol. Cl (ppm)	Sol. Br (ppm)	Sol. Cl/Br	Insol. Cl/Br	Insol. Cl (ppm)	Insol. Br (ppm)
CS102	214	251	1.174	95	0.21	9.21	0.05	0.68	0.98	36.69	38.59	92.1	0.45	203	220	159	0.72
CS106	88	196	0.909	71	0.17	9.56	n.a.	1.30	1.95	48.79		95.6	0.00		110	100	0.91
CS107	347	176	0.705	61	0.25	7.17	n.a.	1.03	0.72	40.74		71.7	0.00		148	104	0.71
CS108	104	202	0.744	57	0.16	7.57	0.04	1.03	1.53	37.45	60.48	75.7	0.45	168	430	126	0.29
CS113	442	634	1.952	125	0.24	13.09	0.10	2.40	0.54	20.65	50.42	130.9	0.98	133	520	503	0.97
CS115	594	500	3.831	163	0.25	19.30	0.17	1.34	0.41	38.60	43.30	193.0	1.66	116	141	307	2.17
CS118					0.27	29.34	0.20	0.89						150			
CS119	334	374	2.249	121	0.25	15.05	0.11	1.34	0.74	40.24	47.65	150.5	1.07	140	190	224	1.18
CS122	478	451	1.718	98	0.23	11.78	0.06	3.26	0.48	26.11	33.67	117.8	0.58	204	292	333	1.14
CS124	471	317	2.873	111	0.38	23.34	0.13	5.48	0.80	73.63	45.61	233.4	1.31	178	53	84	1.56
CS125	354	314	2.197	96	0.21	14.13	0.09	17.64	0.61	45.01	38.77	141.3	0.85	166	128	173	1.35
CS126					0.18	14.45	0.07	1.25						208			
CS127	303	58	0.217	22	0.32	3.10	n.a.	74.82	1.05	53.38		31.0	0.00		125	27	0.22
CS130	201	480	2.846	253	0.24	18.78	0.13	2.94	1.22	39.13	45.20	187.8	1.29	146	187	292	1.56
CS132	196	307	1.075	95	0.24	9.98	0.04	3.07	1.24	32.51	33.39	99.8	0.36	278	289	207	0.72
CS134					0.29	10.10	0.04	3.72						262			
CS135	145	273	1.362	113	0.26	12.10	ND	3.33	1.76	44.31		121.0	0.00		112	152	1.36
CS136	72	377	1.622	144	0.24	15.66	0.05	4.10	3.33	41.55	28.20	156.6	0.46	342	189	220	1.16
CS138					0.21	36.57	0.45	7.81						82			
avg	290	327	1.698	108	0.24	13.54	0.09	7.20	1.16	41.25	42.30	126.5	0.63	193	209	201	1.07
1 sigma	155	143	0.944	52	0.05	7.84	0.10	16.37	0.74	11.70	8.66	51.0	0.52	65	123	116	0.49
min	72	58	0.217	22	0.16	3.10	0.04	0.68	0.41	20.65	28.20	31.0	0.00	82	53	27	0.22
max	594	634	3.831	253	0.38	36.57	0.45	74.82	3.33	73.63	60.48	233.4	1.66	342	520	503	2.17

Table 2.5.2: Soluble halogen geochemistry of footwall breccia from the mineralized environment. Bulk rock halogen abundances were determined by an applied pyrolysis combustion method. Leachate data are reported as anions in solution leached into 50ml deionized water from 5g of sample. Soluble/insoluble calculations are based on these parameters.

2.7 Discussion

2.7.1 Comparison to other studies

Previous studies reported strong halogen geochemical anomalies in brecciated zones in footwall rocks (McCormick and McDonald, 1999; McCormick et al., 2002; Hanley and Mungall, 2003; Hanley et al., 2004). Enrichments in Cl and F within a few hundred metres of footwall-style sulphide ore bodies were first reported by Jago et al. (1994) in Sudbury breccia zones in the basement of the McCreedy deposit. They showed that enrichments are greatest in intensely mineralized zones where Fe-Mn-chloride and fluoride minerals, uncommon to magmatic sulphide environments, exist in spatial association with platinum-group element minerals, galena, sphalerite, stannite, cassiterite, tellurides, and bismuthinides. In those areas, Cl abundances may reach up to 4000 ppm (increasing towards mineralization), compared to background levels of ~200-300 ppm. Fluorine concentrations can reach 1200 ppm compared to values ~ 400 ppm in barren footwall rocks. Through SEM analysis, it was determined that there exists a strong correlation between the occurrence of alkali, halogen, and metal-rich precipitates in microfractures and halogen-rich interstitial phases in the footwall ore zones (e.g. – Cl-bearing grunerite, fluorite, etc.; Jago et al., 1994). These halogen-rich minerals are unlikely to have formed as products of assimilation and digestion of country rocks because they are not found in the country rocks themselves, characterized by hornfels to lower greenschist assemblages of pyroxene, hornblende, chlorine-poor actinolite, quartz, plagioclase, biotite and epidote (Coats and Snajdr, 1984; Jago et al., 1994; Hanley and Mungall, 2003). Rather, some researchers attribute the presence of Cl-rich phases in the

immediately vicinity of footwall sulphides to fluid/salt phases released during the crystallization of the sulphides themselves (Jago et al., 1994; Li, 1992; Farrow, 1994; Hanley et al., 2005). In some cases, unusually Cl-rich phases (e.g., lawrencite, an Fe-chloride) have been observed as phenocryst phases in sulphide minerals directly (Farrow, 1994) arguing that the sulphide melts that entered the footwall were enriched in halogens. However, despite indications that halogen enrichments in the host rocks could be tied to sulphide proximity, Jago et al., 1994 hypothesized that in regions where no halogen-rich solid (primary) phases were observed, halogen-rich precipitates could have been derived from saline fluids that were introduced to the system from the drilling process. Therefore, not all of the halogen endowment of a given rock may be tied to its original geological evolution. Additionally, Jago et al. (1994) determined that some alkali and halogen-rich solid phases that were initially in equilibrium with the surrounding fluids at the time of hydrothermal alteration were redistributed and are now hosted in microfractures/pore spaces. The bulk halogen content may result partly from primary enrichments (in minerals or trapped in inclusions), externally derived phases (introduced during sample preparation), and locally redistributed phases. Jago et al. (1994) suggested that analyzing for Cl would be more cost effective for exploration than for F, but no further work occurred to examine the nature of these enrichments in the footwall rocks at the time, possibly due to the ambiguity of halogen origins in the rocks. However, Wallbridge Mining Ltd. extensively explored the use of Cl as an exploration tool in the footwall.

Since the preliminary study in 1994, the use of halogens as an exploration tool to locate magmatic sulphide deposits in the Sudbury environment has been investigated in

more detail by a few authors (Hanley and Mungall, 2003; Hanley et al., 2004; McCormick and McDonald, 1999; McCormick et al., 2002). These authors have shown that hydrothermal alteration associated with the formation of contact and footwall-style deposits has modified the primary halogen abundances in basement rocks and in footwall breccia. Studies by Hanley and coworkers confirmed many of the observations made by Jago et al. (1994) and provided systematic evaluation of the nature of the Cl (and also Br) enrichments in footwall lithologies surrounding sulphide vein deposits.

Less detailed evaluations of halogen distribution are available for the footwall breccia and SIC, and the data available are limited to small bulk rock data sets that perhaps are not statistically representative (Hanley and Mungall, 2003; Hanley et al., 2010). Only the studies by McCormick and coworkers examined the halogen chemistry of footwall breccias and showed that there is an apparent increase in Cl/F whole-rock ratios with increasing proximity to contact-style mineralization that is related to increasing bulk rock Cl (in amphibole, biotite, phlogopite, and also apatite). Variations of F in the rocks were attributed to the abundance of apatite as well (McCormick et al., 2002). Halogen ratio variations correlate to alkali abundance in the footwall breccia. A variety of Cl-rich minerals (apatite, phlogopite, biotite, amphibole, ferropyrosmalite, scapolite; McCormick et al., 2002) are associated with mineralization within the footwall breccia, some of which are found in footwall breccia samples in this study (amphibole, phlogopite, apatite). These minerals comprise halos that can occur up to 5 m away from massive sulphides in the footwall breccia, and may contain up to 20 vol % hydrous mafic and Cl-rich minerals. In particular, chloropotassic hastingsite (Cl-rich amphibole) containing up to 4.0 wt. % Cl

and up to 2.7 wt. % K_2O. As well, Cl-rich biotite grains contain as much as 1.1 wt.% Cl were observed in the footwall breccia (McCormick et al., 2002). Less pronounced mineralogical and bulk geochemical anomalies were recognized with increasing distance, up to ~100 m distance from sulphides. They found that Cl and Na_2O abundances are greater in mineralized breccias than in unmineralized breccias, and K_2O abundance is higher in unmineralized breccias. All of these anomalous characteristics in mineralized footwall breccia were suggested by McCormick et al. (2002) to be evidence of a saline fluid that passed through the rocks, although the origin of that fluid was not speculated upon.

Although unusual Cl-rich phases were not observed in this study, McCormick et al. (2002) reported much higher (maximum) Cl values in for both barren and mineralized footwall breccia than in this study (566 and 840 ppm compared to 393 and 317 ppm, respectively). However, they reported similar F values (278 and 270 ppm compared to 433 and 268 ppm, respectively). Sublayer norite samples were also analyzed by McCormick et al. (2002), showing an enrichment in Cl between barren and mineralized (233 to 674 ppm, respectively) and a depletion in F (268 to 190 ppm, respectively). They reported a similar enrichment in Cl concentration (from 203 to 722 ppm) from barren to mineralized environments (McCormick et al., 2002). Sublayer norite samples from barren and mineralized environments yielded Cl values of as well as F values. Data from McCormick et al. (2002), suggests that Cl values in the footwall increase with proximity to mineralization, however data from this study indicate that Cl values decrease slightly. Differences in data between McCormick et al. (2002) and this study can be attributed to

sampling techniques. McCormick et al. (2002) sampled footwall breccia in contact with sulphides and sampling in this study involved footwall breccia from a mineralized environment that are not in direct contact with sulphide mineralization.

2.7.2 Comparison of barren and mineralized environments

Upon thorough examination of all bulk rock, trace, and halogen data, several differences were noted between the two environments. Interestingly, no differences in major element or trace element chemistry were noted in each lithology, with the exception of halogen abundances and halogen ratios. In fact, all studied lithologies are remarkably similar in terms of their trace element chemistry. This is suprising considering that the comparison made in the normative abundance diagrams (Figure 2.5) involves rock types representing pristine Archean gneisses (part of the target rocks at Sudbury), partially melted equivalents of those (footwall breccias) and mineralogical diverse units produced by the differentiation of an impact melt sheet. In particular, it is worth noting a slight depletion in Nb, Ta, Ti, Sc, Co, Cr, and Ni, in all units, indicating that the original arc magma source signature for the Archean and Proterozoic target rocks was geochemically preserved through impact, differentiation, and partial melting processes. Nonetheless, these ancient arc magmatic signatures are common to all units in both mineralized and barren embayments.

Variations in ore metals hosted in contact-style deposits are considerable in all lithologies, but the greatest enrichments in Ni and Cu are not tied to the samples from the mineralized embayment. In fact, some of the highest spot analyses of Cu and Ni come

from sublayer and mafic norite samples from the barren embayment. For footwall breccias, these enrichments and depletions are complicated by Ni, Cu and Cr concentrations being inherently higher in some footwall lithologies than others leading to enrichments in footwall breccia that are unrelated to the presence of magmatic sulphide deposits. These are important observations for the explorationist because they demonstrate that Ni and Cu abundances cannot be directly associated with a rock unit or embayments' potential to host sulphides. Local accumulations of Ni and Cu due to other processes such as hydrothermal fluid remobilization, the presence of unusually Ni- and Cr- rich silicate phases in the SIC, or sulphide saturation due to small scale contamination of the SIC with footwall materials introduced during plume formation. All of these features may be independent of the "fertility" of an embayment.

The extensive halogen data set allowed for the statistical significance of correlations to be examined between all major and trace elements. The best correlations and most useful X-Y scatter plots that contribute to understanding the distribution of the halogens or those showing significant correlations involve those with Na_2O and SiO_2 (Fig 2.9-2.16), whose concentrations may be influenced by secondary hydrothermal alteration (Na_2O) or are most sensitive to variations in the lithology of primary clasts hosted within the breccias were found to be discriminative.

Figure 2.9 shows an important positive correlation between Na_2O vs Br, with all plotted samples separated by both lithology and environment. Since the presence of Na in fluid inclusions cannot possibly influence bulk rock Na_2O abundances, this correlation is related to albitization with increasing Br. This process involves the exchange of Na^+ in

infiltrating fluids with Ca^{2+} in plagioclase, creating an Na-enriched plagioclase and releasing Ca^{2+} to the surrounding environment. This hydrothermal alteration generally occurs in low T environments (McCormick et al., 2002). As Br abundances in fluids are associated with albitization, this must indicate that the fluid responsible for albitization also caused Br enrichment via growth of a Br-bearing mineral phases, or entrapment of increasing proportions of a Br-enriched fluid. However, this process was common to both barren and mineralized embayments. Figure 2.10 shows Na_2O vs Cl, and again supports the idea of albitization related to not only Br enrichment but also Cl enrichment. This is likely caused either by an increase in the abundance of trapped fluids, or an increase in the Cl content of silicate minerals in the system. However, the increase in bulk rock Cl with increasing albitization is much more subtle than recognized for Br, suggesting that the infiltrating fluid responsible for albitization was characterized by a low Cl/Br ratio compared to the fresh rocks prior to albitization. In effect, this albitization caused a lowering of the Cl/Br ratio of the rocks, a process common to both barren and mineralized environments. This is supported by Figure 2.11 showing the relationship between Cl/Br ratio and Na_2O. Generally, higher Na_2O values are associated with lower Cl/Br ratios. Regardless of the exact reason for these relationships, the data support the simultaneous introduction of Na and low Cl/Br fluids into the footwall breccia and surrounding SIC rocks along the SIC north range margin at some stage. A correlation also exists between Br and I (Figure 2.12) in both barren and mineralized samples, suggesting that the sites of deposition (and the timing of formation of these sites of deposition) are the same. However, it is possible to distinguish these environments from one another since the

mineralized samples show slightly more enrichment in I compared to Br, resulting in lower Br/I ratios. Since the bulk rock Br contents of mineralized and barren samples are similar (Figure 2.9), differentiation of sample groups in Figure 2.12 must occur due to the higher I in mineralized samples. Bromine and I are the two halogen elements that prefer to be hosted in fluids (McCormick et al., 2002). Figure 2.13 shows a similar differentiation between barren and mineralized samples when Cl and I are compared. While not as strong, a correlation between Cl and I is also apparent in both groups, suggesting that Cl, Br and I are all present in common host sites in the rock. A linear trend along the X-axis shows a significant enrichment I in the mineralized samples with no change in Cl abundance. The majority of data points with anomalously high I values are from mineralized sublayer and footwall breccia samples.

When the abundances of Cl and Br are compared (Figure 2.14), no clear distinction can be made between barren and mineralized embayments with respect to Cl/Br ratios

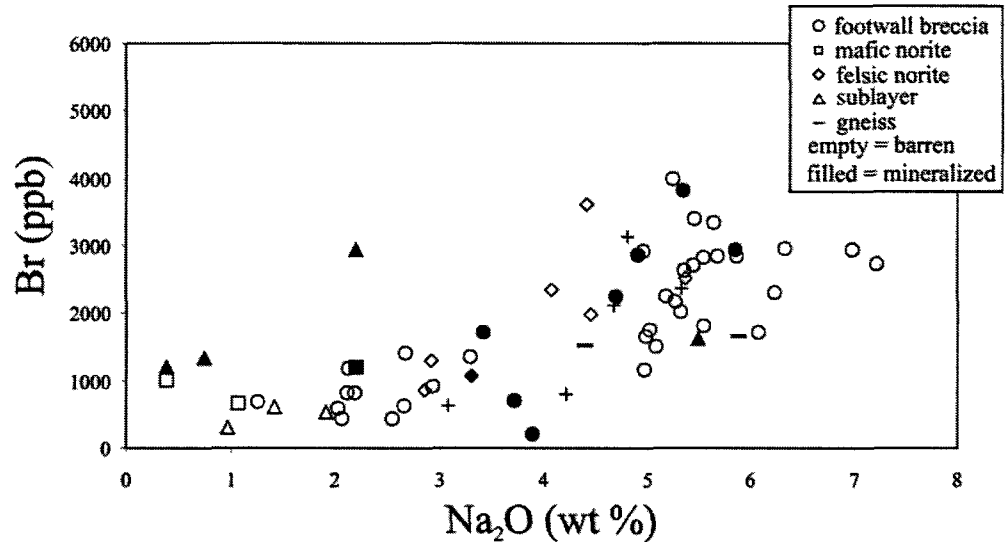

Figure 2.9. Bulk Na_2O vs Br. This Na_2O enrichment associated with increasing Br is similar to the correlation between Na_2O and Cl. The Na-enrichment is not related to an increased abundance of fluid inclusions as there would need to be many fluid inclusions present to raise Na_2O on a weight percent scale.

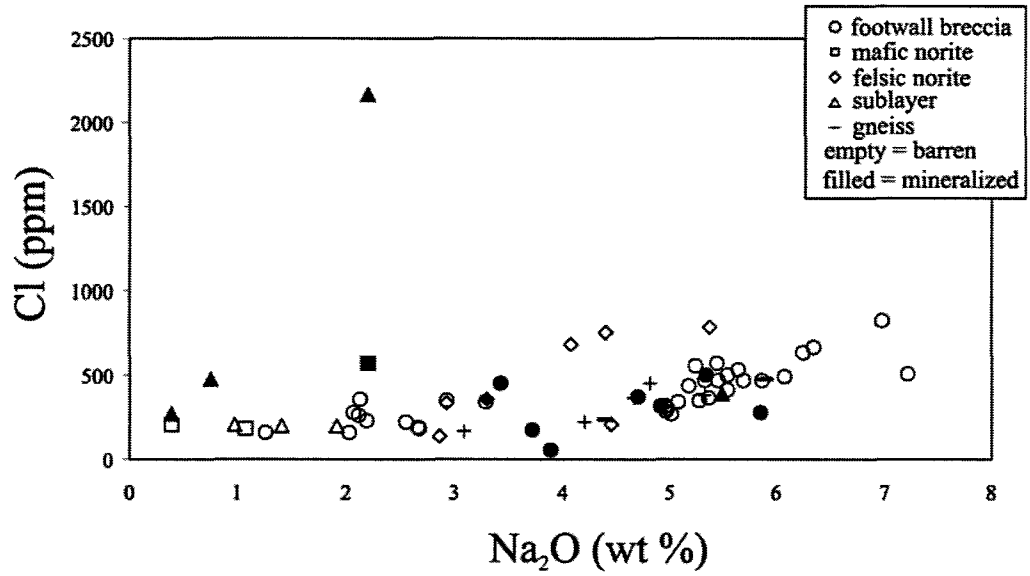

Figure 2.10. Bulk Na_2O vs Cl. Increase in Na_2O in barren samples is related to albitization of plagioclase associated with the influx of halogen-bearing fluids. These fluids probably originated in the footwall.

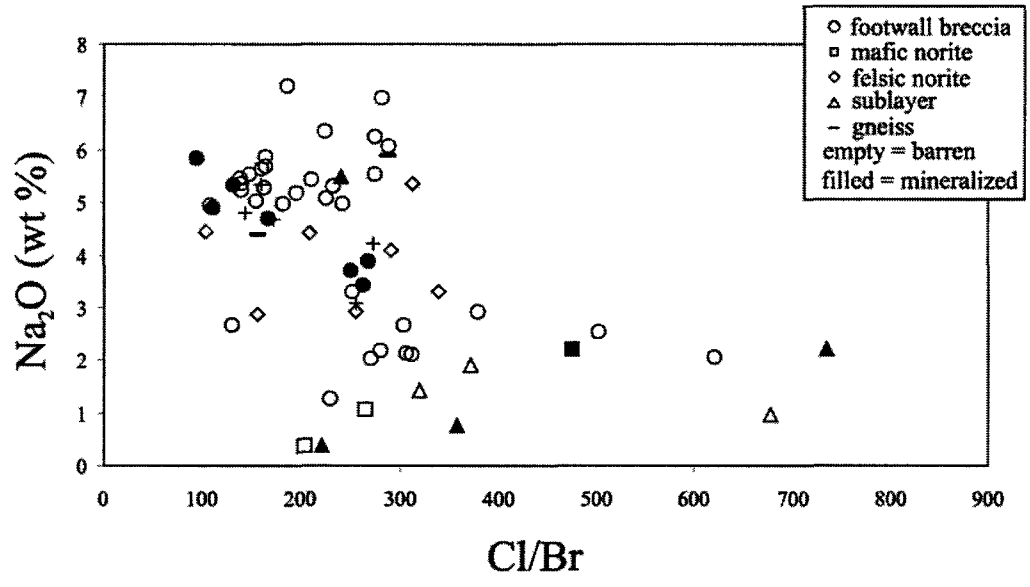

Figure 2.11. Bulk Cl/Br vs Na_2O. Bulk Cl/Br increases when Na_2O is lower. Therefore, albitization is related to a low Cl^-/Br^- fluid, most likely derived from footwall groundwaters.

because these have the same overlapping range in both sample groups. However, it is again clear from the correlation between Cl and Br in both sample groups shown in this diagram that the abundance of Cl and Br, like Br and I are controlled by the same sites in the rock (i.e., temporally coeval halogen mineral phases or a common mineral host, increasing amounts of a single trapped fluid phase relative to another). It is evident in Figure 2.1.4 that barren samples may have higher overall Cl enrichment compared to mineralized samples, with the highest Cl values being several hundred ppm more in footwall breccia and norite from the barren environment. Halogen ratio plots are useful in differentiating the two environments on a Cl/Br vs Br/I diagram (Figure 2.15). Also, samples from both environments show a comparable range in Cl/Br ratios but the mineralized samples show much higher (on average) I/Br ratios.

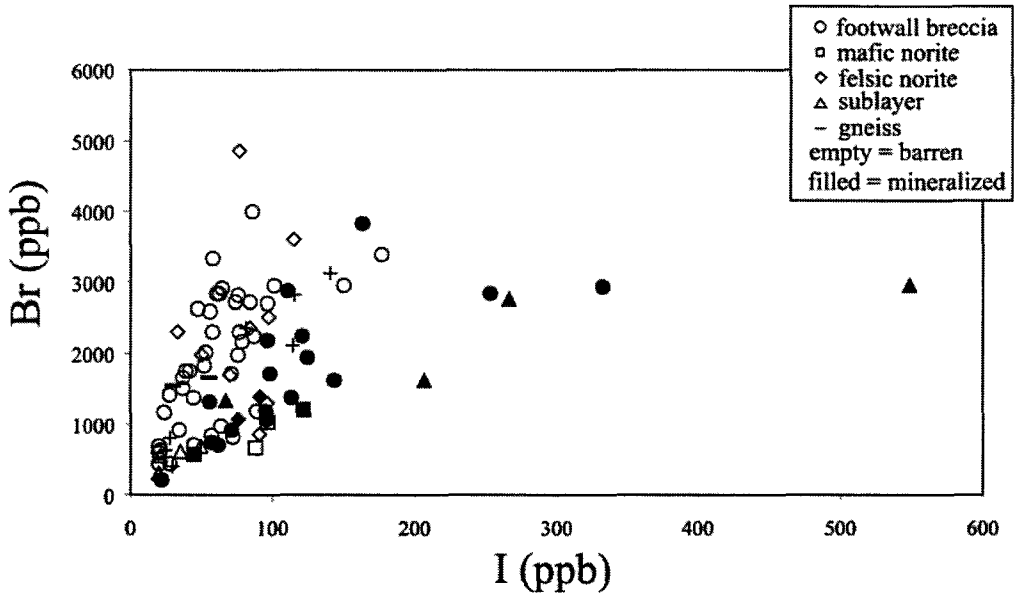

Figure 2.12. Bulk I vs. Br. Bulk I is higher in mineralized environment. Insoluble Br is higher in the barren environment. Soluble bromine does not differ between the two environments, indicating that there was a common deposition site and that the differences are not related to fluids. Iodine and at least some amount of Br therefore must be mineral bound.

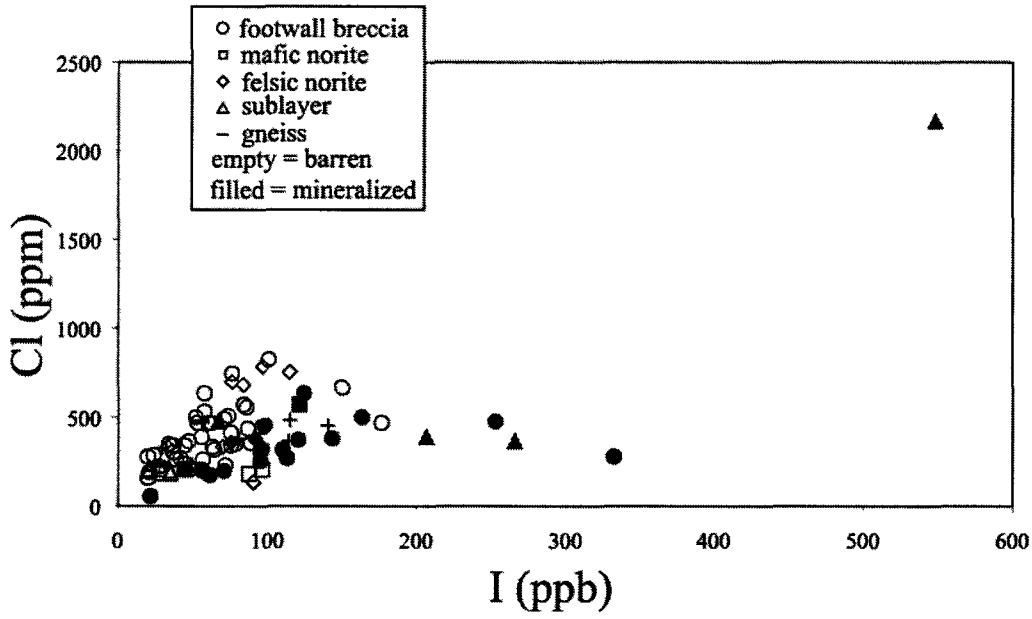

Figure 2.13. Bulk I vs. Cl. A weak correlation exists between these elements. However samples contining the greatest abundance of I are mineralized footwall breccia and sublayer norite.

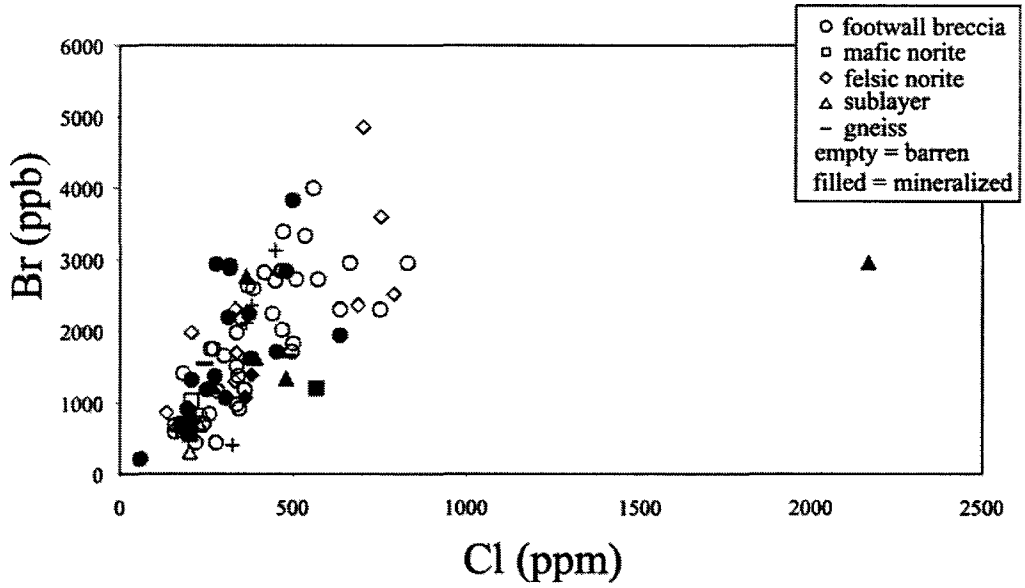

Figure 2.14. Bulk Cl vs bulk Br. A correlation exists between these elements, indicating that they are affected by a common site and controls.

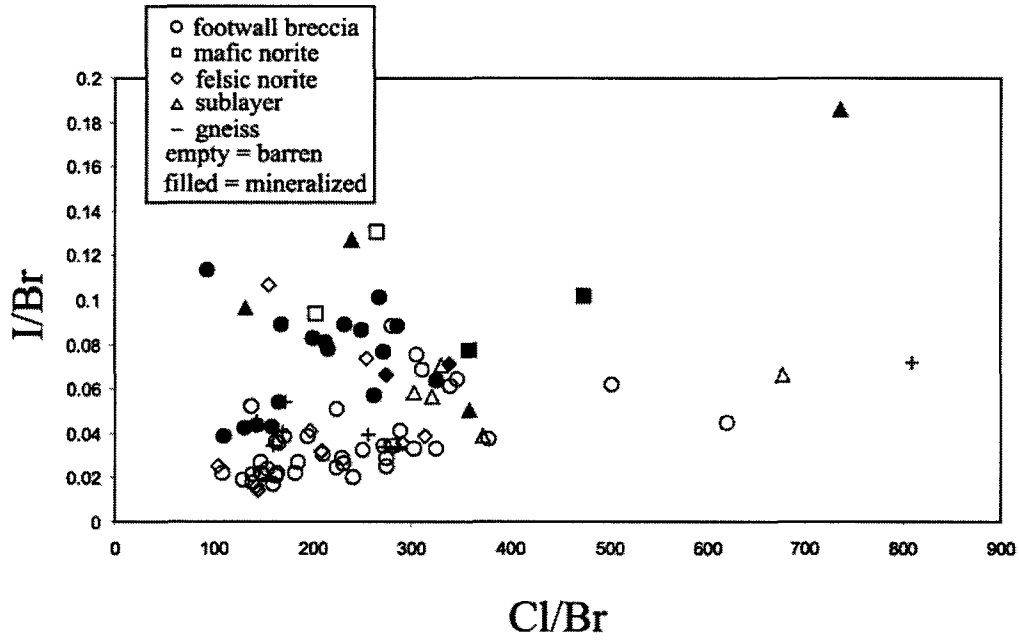

Figure 2.15. Bulk Cl/Br vs. I/Br. Mineralized samples scatter towards the top of the diagram due to higher I values (also seen in previous diagrams).

Generally, these correlation diagrams provide evidence that halogen abundances and ratios have been modified in the footwall breccia and adjacent SIC units due to processes unrelated and related to crystallization of sulphides, forming contact-style mineralization, and provide a means to discriminate mineralized from barren environments. However, the explorationist is cautioned that bulk analyses of halogens in bedrock can be deceiving and studies of bulk halogen abundance alone may be misleading. This is due to the unique nature of the three of the halogens (Cl, Br, and I) which can be concentrated into fluid phases as well as mineral phases. For example, Cl may be enriched minerals that grew during an entirely different hydrothermal event than one that introduced a low Cl/Br fluid into the rock later on, preserved as trapped fluid inclusions. If mineral soluble Cl and Br are not modified synchronously to the entrapment of new fluid inclusions, bulk rock analyses will reflect mixed abundances – that is, anomalous Cl from an earlier event and anomalous Br from a later event. The net result will be a rock that has a bulk Cl/Br ratio that may be no different than fresh equivalents of those rocks that have seen no modifications of primary halogen abundances at all, thereby preventing detection of hydrothermal events related to (for example) mineralization. Whereas Cl enrichments may be tied to mineral growth, Br and I may be preferentially more enriched in fluid phases and this differing behavior must be recognized.

The one advantage the explorationist has with the halogens is that, unlike most other trace elements, the abundance of Cl, Br and I are controlled by insoluble and readily soluble phases (fluids, salts), the latter of which can be easily leached from the rocks.

Soluble halogen data, in this study, appears to provide the most useful discrimination tool in differentiating the two environments. Figure 2.16 (Cl^- vs Br^-) again shows a clear discrimination between barren and mineralized footwall breccia samples. Note that the values are directly those from solution (from leachates) and have not been recalculated to reflect the actual amount of soluble Cl^- and Br^- in the rocks on a mass basis. The power of such leachate analysis is immediately apparent when Figure 2.16 is compared to that for bulk Cl and Br (Figure 2.14). In Figure 2.16, barren samples appear enriched in Cl^- relative to mineralized samples, and also show a distinctly higher Cl/Br ratio.

2.7.3 Factors controlling the distribution of halogens in the footwall breccia

The halogen elements may occur as either fluids/salts trapped in inclusions or in mineral phases (hydroxysilicates, apatite). A relatively minor amount of salts trapped along fractures in the rocks may have been introduced post-crystallization but analyses of bulk rocks samples in this study were restricted to those samples that came from coherent drill core samples lacking in fracture planes and secondary alteration veins. Since the amount of soluble F relative to bulk F is so small, F must reside in minerals (e.g., apatite). Significant proportions of the bulk rock Cl and Br are water-soluble (as Cl^- and Br^-) indicating their affinity to both soluble salts and trapped fluids that could be exposed by grinding/pulverizing the samples, and insoluble mineral phases (e.g., amphibole). The relative proportions of I that are soluble vs. insoluble are unknown but the large ionic size of I suggests that, like Br, it will tend to be more abundant as a water-soluble species (in inclusion fluids, trapped salts, etc.) On the other hand, analyses of the soluble fraction of

Br shows that significant amounts of Br are likely dissolved in insoluble mineral phases and, therefore, it is possible that I also occurs that way.

Correlations between Cl, Br and I demonstrate that the abundance of these elements are generally being controlled by common depositional sites in the rock. For example, if

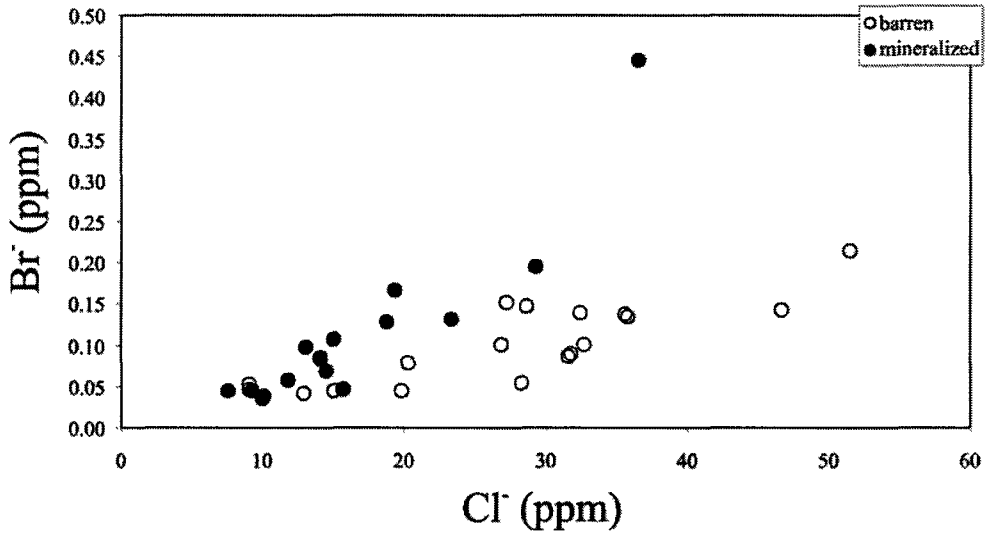

Figure 2.16. Cl^- vs Br^- plot for footwall breccia samples. Barren samples contain a higher Cl^-/Br^- ratio while mineralized samples contain a lower ratio. This relationship is not seen in Figure 2.14 and is obscured by the insoluble Cl and Br fractions.

fluid inclusions are present, their overall abundances control the amount of Cl, Br and I in the soluble fraction. However, several generations of fluids are likely present (Molnar and Watkinson, 2001). These were trapped at different times, in different abundances, and their contained fluids are probably all Cl, Br and I-bearing. Therefore, correlations demonstrate common controls on overall abundance but they do not necessarily allow differentiation of the specific contributions to halogen abundance made by different fluid generations passing through the rocks.

Figure 2.17 shows one such discrimination diagram, showing the relative abundances of F, Cl and Br. Considering all observations made about the relative sites of deposition in the rocks, and the proportions of insoluble vs. soluble halogen species, shifts in sample position in this diagram towards the F apex reflect increases in the abundance of F-bearing minerals (e.g., apatite), or decreases in the abundance of Cl- and Br-bearing minerals and fluid inclusions (or a decrease in their Cl and Br content). Shifts towards the Cl or Br apex are more difficult to interpret. Increases in bulk rock Cl abundance may reflect decreasing abundance of F bearing phases. They may also reflect increasing proportion of high Cl (but low Br) fluid inclusions trapped in the rock, or conversely, decreasing proportions of low Cl (but high Br) fluid inclusions. In other words, in samples that contain abundant high Cl/Br fluids trapped in inclusions, those samples may also contain other generations of low Cl/Br fluids but it is the higher Cl/Br fluids that must be more abundant. Likewise, since a large % of the bulk rock Cl and Br in the studied samples must be present in insoluble phases (such as hydroxysilicate minerals), changes in relative Cl and Br bulk rock abundances may be related to varying modal

abundances of Cl-rich, Br-poor minerals, or Br-rich, Cl-poor minerals, or both. The Cl/Br ratios of primary mineral assemblages may also be modified by successive hydrothermal events. In this example, it is apparent that anomalous bulk rock halogen abundances cannot be simply attributed to the influx of a halogen-rich fluid into a geological environment. A detailed mass balance of each site of deposit must be considered before such generalized statements can be made. However, the discrimination diagrams still allow a means for general comparison.

In Figure 2.17, no distinction can be made between barren and mineralized samples. They show overlap with respect to the overall ranges of all parameters. However, the variations shown can be related to processes described above. Notably, examination of the whole rock data for samples with the highest F abundances (relative to Cl and Br) show that they also contain very high P_2O_5, confirming that apatite or some other phosphate is controlling F abundance. The diagram also confirms that bulk Cl and Br analyses alone provide no effective means to discriminate mineralized from barren environments when plotted with F. Additionally, it is seen that as relative abundances of F decrease, samples become more enriched (relatively in Br). Preliminary petrographic analysis of the samples showed that the abundances of typical Cl-bearing phases such as amphibole are the same in barren and mineralized samples that show variable bulk halogen abundances. Therefore, the shift in relative Br abundance as F decreases (Figure 2.17), must reflect a real change in the Cl/Br ratio of halogen-bearing minerals, or an

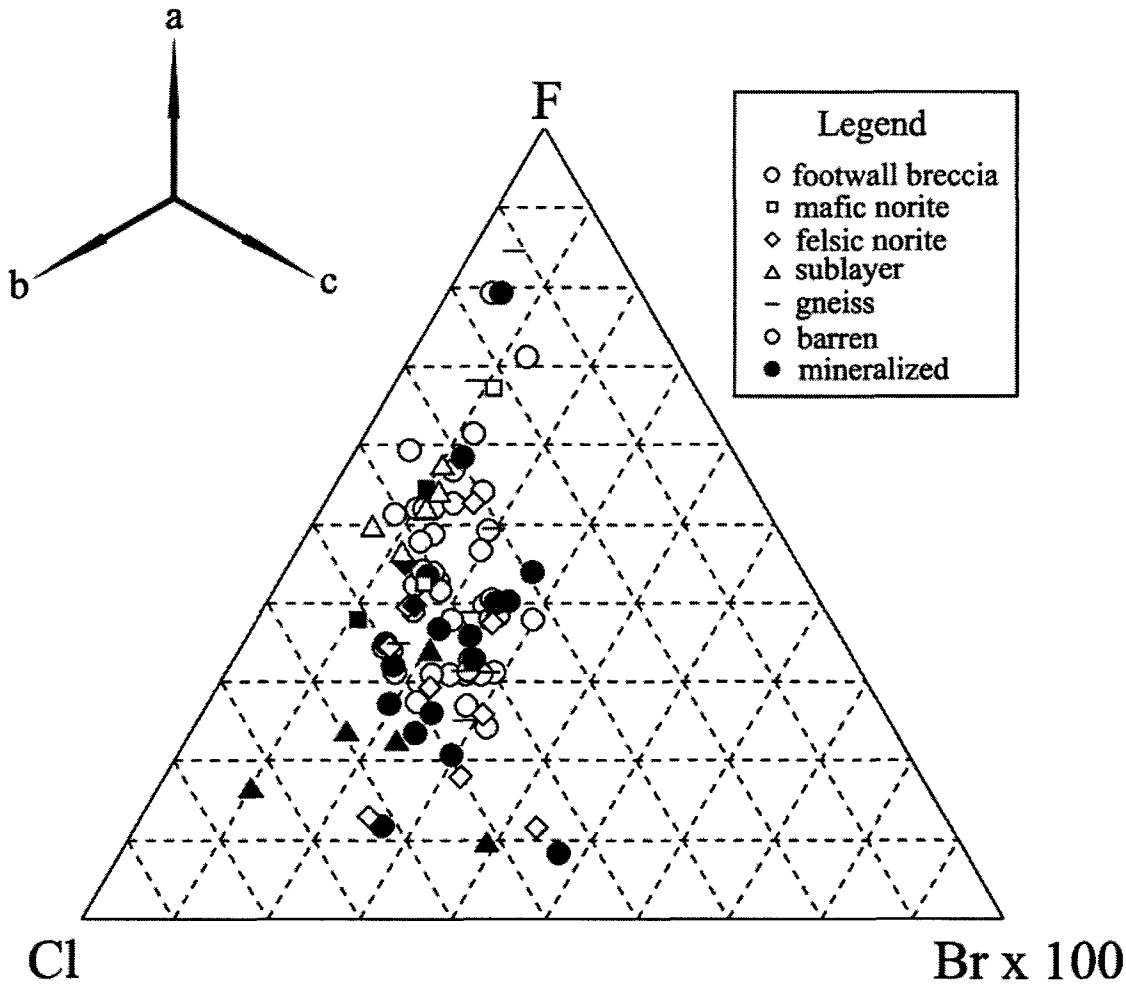

Figure 2.17. Ternary diagram of bulk rock F, Cl and Br. The diagram shows three possible trends (labelled a, b, and c). Trend a (fluorine enrichment) indicates higher volume % of apatite. Trend b (chlorine enrichment) indicates an increase in the volume % of amphibole, or a higher Cl:Br ratio in trapped within the rock or a greater proportion of trapped fluid with this higher Cl:Br ratio. Trend C (bromine enrichment) indicates a lower Cl:Br ratio in trapped fluids, or a greater amount of this low Cl:Br trapped fluid.

increase in the abundance of low Cl/Br fluids trapped in inclusions.

Figure 2.18 illustrates a more useful differentiation involving bulk rock abundances of Cl, Br and I. As in Figure 2.17, abundances of Br and I are plotted after using arbitrary multiplication factors of 100 and 5000 respectively, in order to scale the date and utilize the entire space of the ternary diagram. In this diagram, the combined characteristics of elevated I in mineralized samples and higher Cl/Br ratios in barren samples (due partly to higher soluble Cl^-/Br^- ratios in those barren rocks) provides an effective discrimination, one that could be readily applied to routine exploration. The observed I enrichment trend is particularly interesting because I has not been investigated previously at Sudbury or in any magmatic Ni-Cu sulphide deposit. The association between I and sulphide mineralization may indicate that sulphide minerals contain this halogen phase. Though traditionally not though of as chalcophile in nature, the halogens, in particular I, has been show to dissolve into sulphide melts and minerals (Fuge and Johnson, 1984; Mungall and Brenan, 2003). Fuge and Johnson (1984) showed that up to 75% of the bulk I contained in sulphide minerals may be structurally bound and insoluble in cold water. Mungall and Brenan (2003) characterized the abundance and behaviour of halogens in a sulphide melt phase coexisting with silicate melt. Their findings are generally in agreement with the observed correlation between unusually high concentrations of the halogen elements associated with some PGE-rich magmatic sulphide deposits such as those in the footwall of the SIC. They showed that halogens partition into sulphide melts and that I has the greatest affinity for sulphide (highest $D^{sulphide\text{-}silicate}$) and that partition coefficents for Cl and Br between sulphide and silicate melt are similar. Iodine prefers to be hosted in a

sulphide melt, however will be released during crystallization of sulphides. Therefore, if Cl and Br are dissolved initially in the sulphide melt/solid phase and then exsolve at a later stage as salt or fluid phases, this would not influence (i.e., not modify) the Cl/Br ratio of the system. However, exsolved fluid and salt phases from sulphides will be enriched in I relative to Cl and Br. If these salts or fluids are incorporated into infiltrating hydrothermal solutions, they have the potential to lead to large scale I enrichment of the host rocks to the sulphides. Vertically extensive I enrichments in the plume could only result from *large* amounts of sulphide present in the embayment at depth.

The influence of varying proportions of trapped fluids from different sources can be further exemplified in Figure 2.19 that shows the relative abundances of soluble halide ions F^-, Cl^- and Br^- plotted against one another. Footwall breccia was the only lithology analyzed for soluble halogens. In this diagram, a clear distinction can be made between the two environments because barren samples are enriched in Cl^-. This enrichment cannot be related to simply an increase in the abundance of trapped fluids in inclusions. Rather, it reflects an increased proportion high Cl^-/Br^- fluid inclusions relative to low Cl^-/Br^- fluid inclusions.

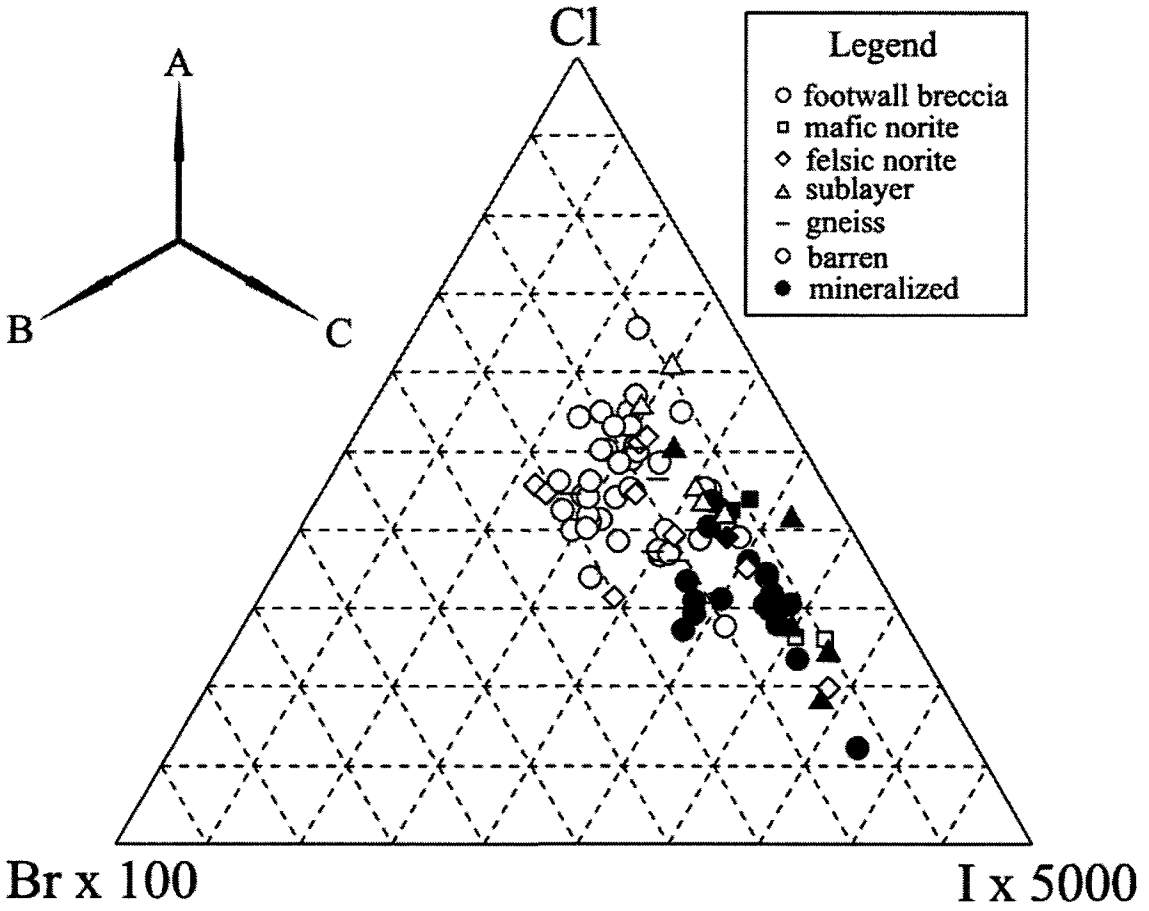

Figure 2.18. Ternary diagram of bulk rock Cl, Br, and I. The diagram displays three possible trends (labelled A, B, and C). Barren and mineralized samples are differentiated in this case. Trend A (chlorine enrichment) indicates an increase in the volume % of amphibole, or a higher Cl:Br ratio fluid trapped within the rock or a greater proportion of trapped fluid with this higher Cl:Br ratio. Trend B (bromine enrichment) indicates a lower Cl:Br ratio in trapped fluids, or a greater amount of this low Cl:Br trapped fluid. Trend C (iodine enrichment) indicates addition of I leached by footwall fluids passing through brecciated sulphides (see text for explanation).

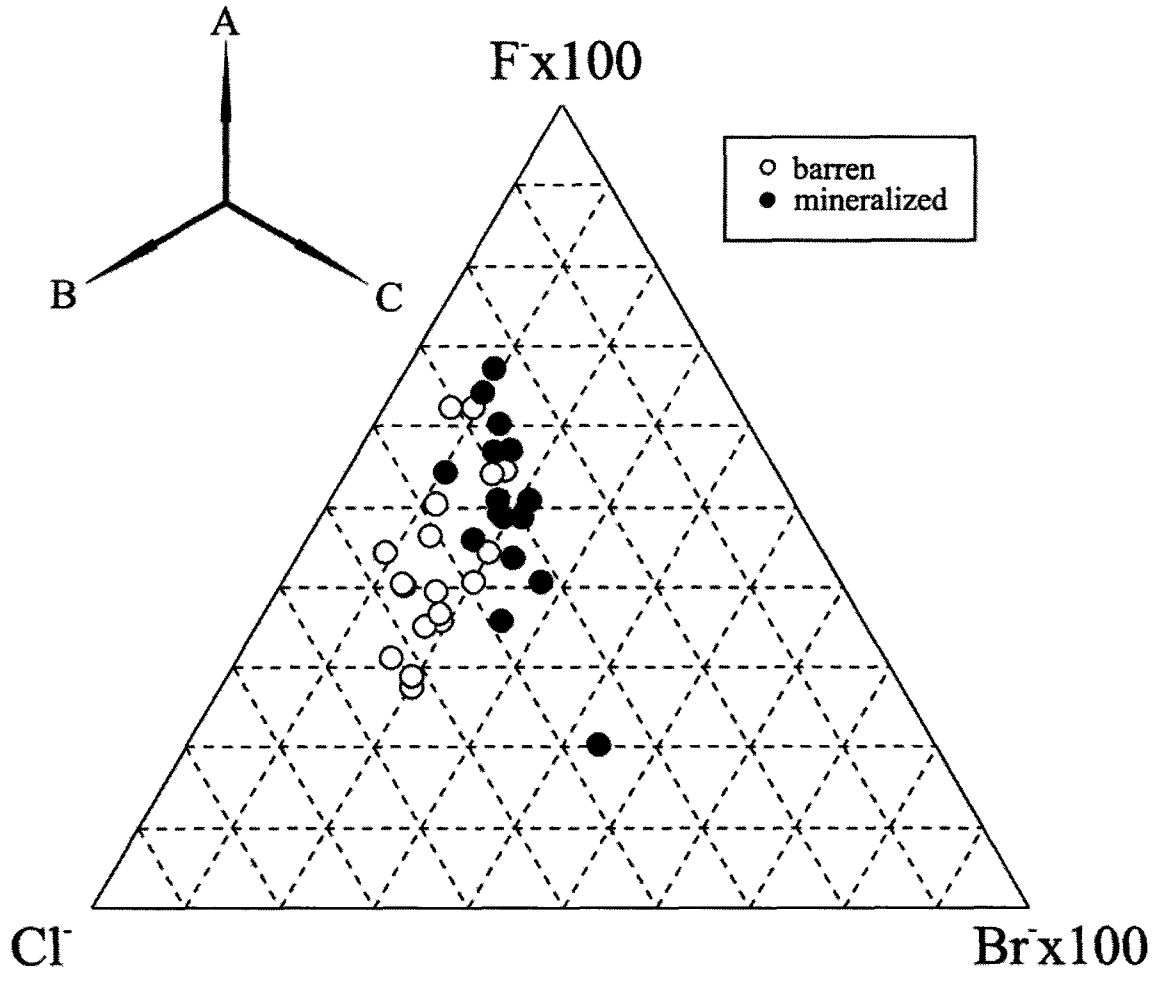

Figure 2.19. Ternary diagram of soluble halogens (F^-, Cl^-, and Br^-) in footwall breccia samples. The diagram shows three possible trends (labelled A, B, and C) and provides good differentiation of barren and mineralized samples. Trend A (F^--enrichment) indicates a consistent Cl^-/Br^- ratio but variations in trapped F^-. Trend B (Cl^--enrichment) indicates increasing proportion of trapped high Cl^-/Br^- ratio fluids (SIC-derived magmatic fluid). Trend C (Br^--enrichment) indicates lower overall Cl^-/Br^- ratios in trapped fluids (less of the SIC fluid relative to footwall fluid).

2.7.4 The origin of halogens in mineralized and barren embayments

Unless fluid:rock ratios are low during hydrothermal alteration, or boiling/evaporation/mixing occur, Cl^-/Br^- ratios are conservative in nature and can be used to determine fluid sources. Higher Cl^-/Br^- values were observed in the barren footwall breccia, and the variations in Cl^-/Br^- ratios observed from one environment to another (and within individual environments) must be the result of mixed soluble fractions derived from different sources, introduced into the rocks at different times. Since the priority for this study was to identify specific bulk geochemical criteria that could be used for exploration, it was beyond the scope of this work to conduct a detailed investigation of the different fluid generations present in primary and secondary inclusions (the bulk soluble halogen fraction) and discriminate between primary and secondary halogen enrichments in minerals that are homogeneous in appearance (lacking any zoning) and texturally complex. However, it is possible to identify the most likely reservoirs that contributed to the bulk of the halogen endowments in the rocks. A detailed review of the available literature in the context of the Sudbury impact environment identified five possible fluid sources that could have contributed to the halogen endowment of the footwall breccia samples:

1. *pre-impact Paleoproterozoic seawater* - The Sudbury region was covered in sea water during the impact event (Dressler, 1984; Ames, 1999). At ~1.85 Ga, this water would have had a Cl^-/Br^- ratio of > 600 (Foriel et al., 2004) and was

possibly incorporated into the melt sheet during impact, introduced substantial amounts of Cl, Br and I to the silicate magma.

2. *magmatic fluids* – These saline fluids have circulated through the main mass, contact and footwall environments and may have been responsible for remobilization of some ore metals. Though these fluids may themselves have been sourced from either pre-impact seawater or from groundwater, they were modified through magmatic processes (i.e., exsolution) and fluid-rock interaction during the crystallization of the SIC (Farrow, 1994; Farrow et al., 1994; Molnar and Watkinson, 2001; Campos-Alvarez et al., 2010; Hanley et al., 2011). Evidence for these magmatic-derived fluids comes from an extensive fluid inclusion database showing that the magmatic fluid endmember was an H_2O-NaCl fluid of high salinity (Farrow, 1994; Molnar and Watkinson, 2001; Pentak et al., 2008; Hanley et al., 2005; Hanley et al., 2010). The actual Cl^-/Br^- ratio of this magmatic fluid was estimated to be as high as ~1000 by Hanley et al., (2004).

3. *Canadian Shield groundwaters* – The chemistry of these deep groundwaters has been characterized by Frape and Fritz (1987). At great depth, they are close to halite saturation and contain on average: ~25000 mg/L Na, ~162000 mg/L Cl, and ~1250 mg/L Br (Cl^-/Br^- ~ 130). Less saline waters from shallower depths contain on average: ~7500 mg/L Na, 56000 mg/L Cl, and ~500 mg/L Br (Cl^-/Br^- ~ 110) These fluids currently occupy pore spaces/fractures in the gneiss country rocks

and formed by the slow leaching of country rocks by circulating water for the last ~2 Ga. These processes allow for halogens to accumulate from the fluids through chemical reaction with halogen-bearing minerals, and amalgamation of soluble halogens from the system (by leaching from fluid inclusions, salts precipitated along fractures, etc.)

4. *mantle and lower crust* – Mungall et al. (2004) showed that lower crust was digested during the formation of the melt sheet at the time of bolide impact, and earlier studies suggested mantle contributions. Primitive mantle and lower crust have bulk Cl/Br ratios in the ~300-350 range, but the composition of fluids associated with mantle contributions are probably best represented by the earliest fluid phases observed in porphyry systems ($Cl^-/Br^- > 400$; Nahnybida et al., 2009).

5. *metamorphic fluids*

   The dehydration of hydrous minerals both in the footwall rocks (by contact metamorphism) and during footwall breccia formation (by partial melting) would have released halogens (Cl, some F) as well as H_2O into the fluids. These fluids likely had Cl^-/Br^- ratios similar to groundwaters (< 200; Hanley et al., 2004).

Figure 2.20 shows the bulk Cl/Br and Cl^-/Br^- ratios of the studied rock types. Also plotted on this diagram are the same parameters for a variety of different reservoirs and related rock types including Sudbury breccias (distal and proximal to footwall ores;

Hanley et al., 2004), primitive mantle (McDonough and Sun, 1995), average upper continental crust (Wedepohl, 1995), Earth's core (McDonough, 1998), saline groundwater from the Sudbury footwall (Frape and Fritz, 1987), modern seawater and metal-depleted Archean seawater (Foriel et al., 2004), fluids in modern submarine hydrothermal systems (Luders et al., 2002), early potassic-stage fluids in Cu-Au porphyry systems (Nahnybida et al., 2009), and fresh mid ocean ridge basalt (Uitterdijk-Appel, 1997).

While the ranges in data for the studied lithologies are large, it is clear from this diagram that average Cl/Br in most lithologies are very similar to the saline groundwaters and associated basement gneiss. Other footwall rocks (Hanley et al., 2004) also show these characteristically low ratios. It is also evident from this diagram that Cl/Br and Cl^-/Br^- ratios in barren footwall breccia may extend to much higher values than in the mineralized embayment. This comparison reasserts that at least two types of fluids are trapped in the footwall breccia. One fluid likely originated from the footwall with a low Cl^-/Br^- ratio and is consistent with saline groundwater (or metamorphic fluid released by the thermal metamorphism and partial melting of those footwall rocks). The other fluid was of probable magmatic origin, derived from the SIC. It is interesting to note that most magmatic rocks/fluids (mantle, porphyry, MORB) are characterized by such high Cl/Br ratios. While halogens exsolved from the SIC could have been originally derived from seawater at the time of impact, ancient seawater had a much higher Cl/Br ratio than was observed in any of the samples studied here. It is also notable that studies on the influence of hydrothermal alteration on mafic rocks (Luders et al., 2002) show that Cl/Br ratios

decrease during alteration. This phenomenon might explain why the felsic norite in immediate contact with the discordant footwall breccias show such anomalously low Cl/Br ratios compared to fresh mafic norite and sublayer in the profiles.

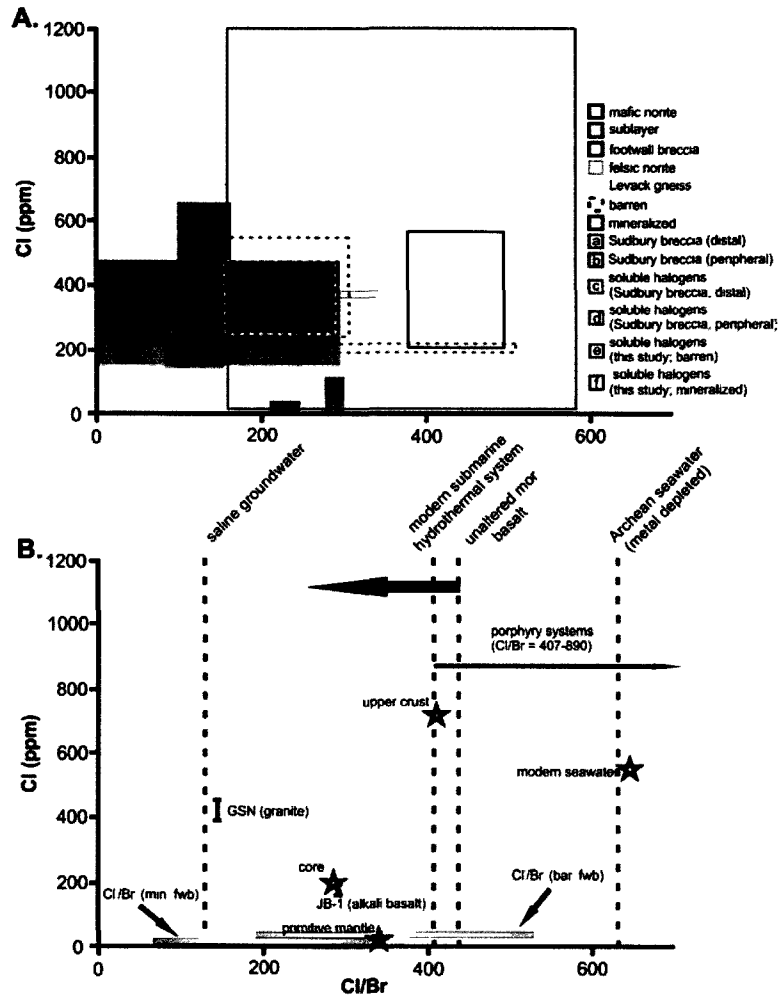

Figure 2.20. Cl/Br vs. Cl diagrams. Data for this study from both barren and mineralized samples from all lithologies are represented by the coloured rectangles on the diagram A. The centre of each rectangle is the Cl/Br and Cl average for the samples while the size of the box represents a one-sigma error in any direction. In figure B, the four vertical lines represent published Cl/Br ratios. Samples JB-1 and GSN represent the Cl/Br vs. Cl for reference standard granite and alkaline basalt samples plotted with one-sigma uncertainity for Cl. The range in soluble Cl^-/Br^- ratios for the footwall breccia is also shown for the barren (purple bar) and mineralized (red bar) environments. Porphyry systems data represents early stage fluid associated with potassic alteration in porphyry deposits, and it ranges from 407-890 Cl/Br. Sources: Sudbury breccia (distal and peripheral) = Hanley et al., 2004; JB-1 (alkaline basalt) and GSN (granite) = Shinonaga et al., 1994; primitive mantle = McDonough and Sun, 1995; upper continental crust = Wedepohl, 1995; core = McDonough, 1998; Sudbury groundwater = Frape and Fritz, 1987; modern seawater and metal-depleted Archean seawater = Foriel et al., 2004; modern submarine hydrothermal systems = Luders et al., 2002; porphyry systems = Nahnybida et al., 2009; fresh mid ocean ridge basalt = Uitterdijk-Appel, 1997.

2.7.5 Physical and chemical evolution of footwall breccia plumes

All indications from the plume structural data suggest that the ridges are intrusive features originating from the chemically- and mineralogically-identical concordant footwall breccia units immediately below the plumes at the base of the SIC. This hypothesis is supported by the observation that the majority of the plumes extend from the thickest areas of concordant footwall breccia within the deepest embayments, while the concordant footwall breccia unit between plumes is noticeably thinner. It is probable that these plumes formed synchronously with respect to the Sudbury impact event, during a time the melt sheet was still cooling and the environment as a whole was still in a partially molten state. The relative chronology of the stratigraphic units of the ridges postdates the stratification and most of the crystallization in the lower units of the SIC and contact-style Ni-Cu orebodies is frozen in the drillcore. Since footwall breccia plumes contain (and have transported upwards) fragments of sulphides and lower level SIC lithologies to upper levels in the stratigraphy. As the mafic units of the SIC were nearly crystallized, the brecciated and subsequently partially melted gneissic and granitic rocks in the footwall were likely still well above their solidus temperature.

During cooling of the SIC, the walls of the impact crater were still prone to structural deformation and experienced slumping events that simultaneously created faults, allowing for upward migration of the partial melted centres of the embayments. This hypothesis is well supported by (i) cross-cutting relationships between the sublayer, mafic norite, and felsic norite and the plume structures, indicating that the lower layers of the SIC cooled

significantly before the breccia plumes migrated upwards and, (ii) the observation that the lower units of the SIC display a relatively constant thickness

surrounding the plumes, with the exception of the sublayer at some depths whose thickness is controlled partly by the morphology of the basement contact where footwall breccia is absent. Petrographic observations suggest that the degree of partial melting involved in ridge formation varied slightly, with some plumes being emplaced as clast-rich, liquid-rich crystal-liquid mushes and others being emplaced in the plastic regime with little interstitial liquid present (plumes A and D, respectively). Presumably, the extent of partial melting would have partially controlled the height to which the plumes would be emplaced in the SIC, and the size and volume of the ridge structures themselves.

Figure 2.21 shows a basic model for the interaction of late style partial melt with the SIC, mineralization and fluids in a plume. Interaction of infiltrating fluids from the footwall with sulphide-rich zones at the base of the plumes, and interaction between SIC-derived magmatic fluids and footwall (plume-derived) groundwater/water released during partial melting influenced the relative halogen abundances and ratios in these environments. First, in zones where contact mineralization occurs at the base of the plume structure, sulphides that accumulated accumulated at the base of the plume near the footwall-Levack gneiss contact acted as a source for I that could be leached by infiltrating hydrothermal fluids. As sulphides crystallized, I was released and would have been enriched locally in the vicinity of sulphides (presumably as salts on sulphide grain surfaces). Brecciation of sulphides during plume emplacement would have promoted the

release of I-rich fluids/salts. As hydrothermal fluids passed through the system, sourced from the footwall or from minerals that were dehydrating and melting at the contact region, they leached I and carried it to shallower level throughout the plume.

As these footwall/partial melting-derived fluids reached upper levels in the plumes, they would have mixed with SIC-derived magmatic fluids at the plume-SIC contact. Fluid mixing also occurred in the barren environmens, but without the associated I enrichment observed in mineralized embayments. The overall halogen budget of the footwall breccias and adjacent SIC rocks near plumes would have depended on the relative abundances of footwall vs. SIC-derived fluids trapped in inclusions (or having interacted with growing or re-equilibrating halogen bearing mineral phases). A more dominant footwall halogen signature (i.e., lower Cl^-/Br^-) ratios is a characteristic of footwall breccia plumes with mineralization at their base. This may be related to the relative volumes of footwall material and SIC rocks that interacted with one another. In areas where plumes were larger (mineralized environments), greater overall volumes of footwall-derived fluids would be introduced. In areas where plumes were small (barren environments), SIC fluids would constitute a more significant proportion of the overall fluid volumes circulating through the partially crystallized footwall breccias in the plumes.

It is apparent that the total abundance of footwall breccia at the contact region in barren environments is less than in mineralized embayments, arguing that it is the volume of footwall breccia partial melt that controls the development of plumes reated to development of the plumes. The abundance of footwall partial melt at the SIC base associated with mineralized embayments may have been controlled in turn by the extend

of hydrothermal activity in those embayments, since it should be expected that increased amounts of water and other volatiles would lower the solidus temperature for footwall gneisses and promote the formation of larger volumes of melt. If this is the case, then the contrasting soluble halogen ratios are largely coincidental and related to plume size. The reasons for the differences in halogen abundance are not entirely clear at present and will require a more extensive study of the morphology of footwall breccia plumes in mineralized and barren environments.

2.7.6 Implications for mineral exploration in the Sudbury basin

The distinct footwall breccia geochemical fingerprint of barren and mineralized environments can be used in conjunction with standard petrological and structural analysis for exploration purposes. As discussed early, prerequisites for locating sulphide-bearing embayments should include the presence of embayments (troughs) along the footwall contact as well as petrological evidence for extreme thermal recrystallization of the rocks beneath the embayment in the footwall. Once a potentially fertile embayment structure has been identified, focus should be placed on the identification of plume structures (if present) and, generally, sampling of any footwall breccias intersected in drill core in the embayment. If sulphides are recognized, this is not necessarily an indication that a large scale contact-style deposit will be present, as barren embayments may contact some disseminated sulphides formed by processes unrelated to the presence of large-scale deposits at the base of plumes. Footwall breccias in embayments containing potentially

economic deposits of massive contact-style sulphide can be identified by the following four most conclusive criteria (for exploration purposes):

1. *Cl^-/Br^- ratios* – This study has shown that the ratio is particularily useful in the Sudbury environment because it allows discrimination of footwall-dominated halogen endowments in rocks (mineralized embayments) and SIC-dominated signatures (barren embayments) in the system, as well as the extent of fluid interaction. Low Cl^-/Br^- values in footwall breccia indicate mineralization potential. High Cl^-/Br^- values indicate poorly mineralized or barren environments. A low Cl^-/Br^- value represents a possibly mineralized zone because this fluid is sourced from the footwall and is related to the development of large scale plume structures.

2. *Iodine* – Iodine abundance is a key indicator because it is sourced from mineralized zones where sulphides occur and its enrichment can extend far away from the actual sulphide source to shallow depths in the embayment. If I abundances alone are considered, a large population of samples are required for analysis, since it was recognized that truly anomalous I abundances only occur in a small % of samples.

3. *Relevance of whole rock data* – With the exception of the soluble halogens, major and trace data are not useful in discriminating mineralized from barren footwall breccias. From a geochemical standpoint, the two environments are more or less the same and no clear differences were recognized. Even when bulk rock halogens (not soluble halogens)

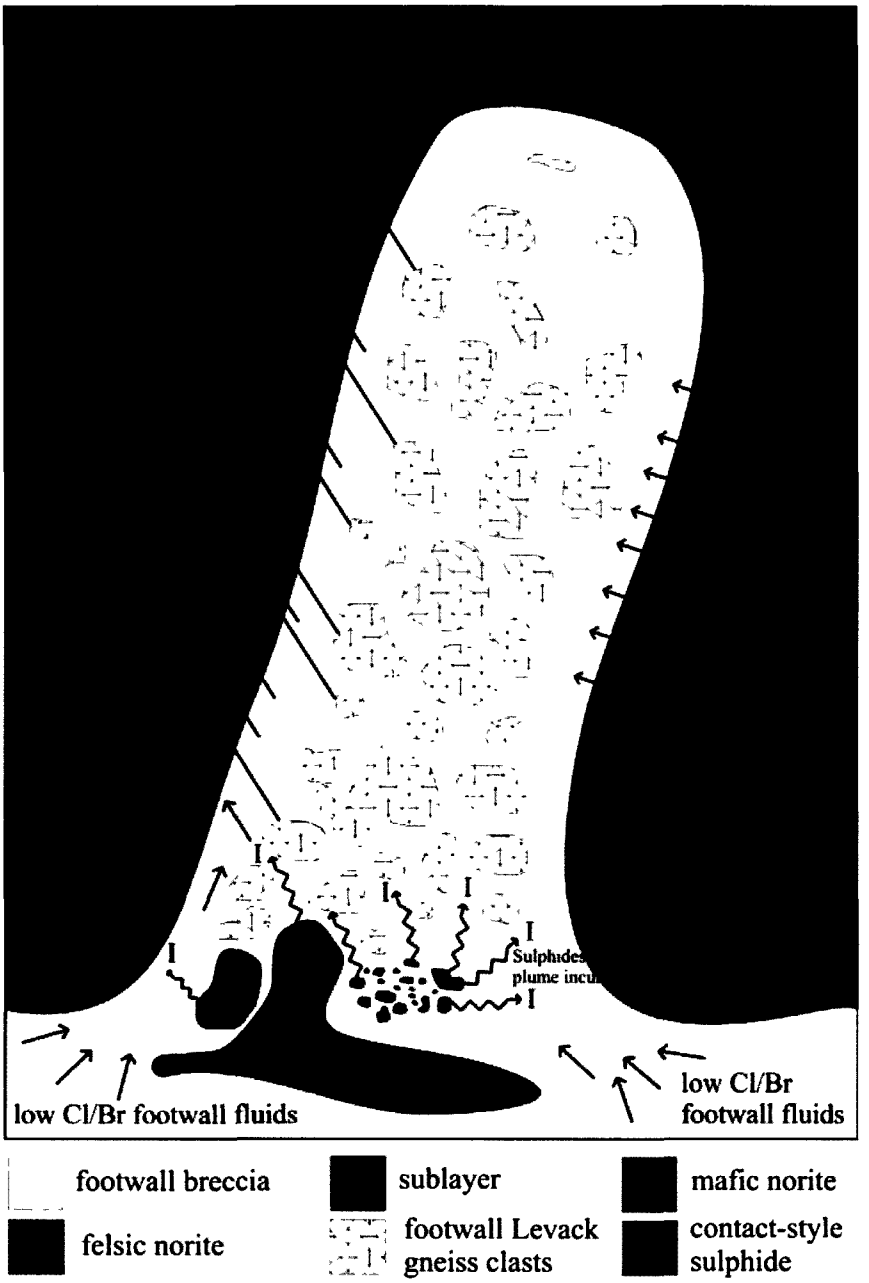

Figure 2.21. Schematic cross section of a primary plume structure showing interaction and sources of fluids and sulphide accumulation. Crimped arrows indicate the release of I from crystallizing sulphides and its migration through the plume to shallower depths. Straight arrows extending into the plume indicate the interaction of SIC fluids with the plume. Straight arrows extending from footwall breccia clasts indicate fluids released from silicate clasts by partial melting or groundwater migrating out of the plume. The plume itself contains several variably melted clasts of Levack gneiss interdispersed within proper footwall breccia, and brecciated sulphides at its base.

were examined, differences between mineralized and barren embayments were difficult if not impossible to recognize because multiple sites of halogen deposition (minerals and trapped fluids) related to several different events that were common in both areas are present in the rocks. Traditionally assayed elements (Cu, Ni) show non-systematic variations from lithology to lithology and are not always enriched in samples from mineralized embayments. This questions their use as pathfinders for embayment scale exploration.

4. *Use of discrimination diagrams* – Discrimination diagrams for differentiating barren and mineralized environments were investigated and the use of specific diagrams developed here should be encouraged during routine exploration. As discussed, I enrichment can be used as an indicator for mineralization. Use of the Cl-Br-I ternary is recommended as it differentiates environments by showing this I enrichment trend in breccias from mineralized embayments coupled with the higher soluble Cl^- abundance contributing to bulk rock Cl in barren rocks. A Br vs. I diagram will also allow differentiation of mineralized from barren embayment rocks. Soluble halogens are also important in distinguishing the two environments. Barren samples of footwall breccia have higher Cl^-/Br^- ratio while samples from mineralized embayments have a lower ratio. This discrimination factor is not apparent when bulk Cl/Br ratios are evaluated because the insoluble fraction masks the diagnostic soluble criterion. The range in Cl^-/Br^- ratio indicates that at least two distinct fluid types are trapped in the breccias altered the

system. The F^--Cl^--Br^- ternary diagram is recommended as it shows that barren samples are slightly enriched in Cl^- relative to mineralized samples.

2.8 Conclusions

"Plume" structures were formed at the SIC-footwall by partially melted footwall breccia rising buoyantly into the still partially crystallized SIC. The criteria put forward here may allow a more robust evaluation of the likelihood that massive sulphides occur at the bottom of footwall breccia ridges. The results of the study can also be extended to any footwall breccia units intersected along the SIC-footwall contact and those intersected at high levels within the SIC.

It is remarkable how the major and trace element geochemistry of barren and mineralized SIC lithologies are so similar. The only significant chemical differences between the two systems when all lithologies are compared are with respect to some bulk and soluble halogen parameters, and Na_2O (related to albitization and Br). Present day halogen anomalies fingerprint former fluids migrating through the SIC stratigraphy. While most F is hosted in insoluble mineral phases, a significant amount of Cl and Br occur in both soluble and insoluble phases. Correlations between I, Cl and Br suggest that all three of these elements are controlled by common sites of deposition (common mineral species grown at specific times, or common fluid generations). There were two dominant fluid types: a higher Cl-/Br- fluid indicating SIC involvement, and a lower Cl-/Br- fluid indicating fluid interaction within the footwall. The volume of footwall breccia in mineralized embayments and the vertical extent of their interaction with the SIC

resulted in a dominantly footwall halogen signature preserved in the rocks, whereas footwall breccias in barren embayments appear to have been dominated chemically by halogen-bearing fluids originating from the SIC. There is also a diagnostic I-enrichment within mineralized rocks caused by the release of I during sulphide leaching at footwall-Levack gneiss contact. Iodine was released during crystallization and has since migrated to shallower depths within and around footwall breccia plumes in mineralized embayments. Analyses of I and water-soluble halogen elements used in conjunction with the discrimination diagrams developed in this paper allows for differentiation between the two environments and potentially provide a useful indicator for mineralized embayments in the SS.

Chapter 3 – Mineral chemistry of halogen-bearing phases

3.1 Abstract

The mineral chemistry of some halogen-bearing phases in heterolithic footwall breccias and associated lithologies of the Sudbury Igneous Complex (Ontario, Canada) were studied. Halogen-bearing silicate phases (amphibole, biotite) have mineral chemical compositions that are consistent with typical halogen-poor, high Mg# magmatic silicates as opposed to late stage, Fe- and Cl-rich hydrothermal silicates. Apatite-biotite and calcic amphibole thermobarometry for barren and mineralized samples of footwall breccia yielded minimum crystallization/re-equilibration temperatures of ~320-680°C and ~400-575 °C, respectively, and low pressures (<5 kbar). These conditions represent the lowest temperature at which halogen exchange occurred and indicate that remobilization of halogens by fluids and resetting of primary magmatic halogen chemistry in the minerals proceeded to temperatures well below the solidus conditions for the footwall breccia. Biotites show significant enrichment in Ni and Cr in mineralized embayments and provide another valuable exploration indicator. This enrichment is important as it is possible to analyze Ni by EMP, allowing for an inexpensive and easily accessible method for locating mineralized zones for exploration using mineral chemistry. Aside from elevated Ni in biotite, and a possible enrichment (on average) of Cl and F in amphiboles from the mineralized embayment compared to the barren one, no other chemical characteristics of halogen-bearing minerals allow for discrimination between barren and mineralized embayments.

3.2 Introduction

The halogen elements (F, Cl, Br, I) are found in various concentrations in the crust surface, hosted both in minerals and fluids. In the mantle, halogens are hosted in mica, amphibole, and apatite (Smith, 1981). Fluorine is hosted primarily in apatite, chlorine is hosted in both amphiboles as well as in fluids, while bromine and iodine are hosted in fluids inclusions and in salts as their ionic radii is too large to allow them to partition into melts and mineral structures (Aiuppa et al., 2009). In the crystalline rocks within and surrounding the Sudbury Igneous Complex (SIC), Ontario, Canada, the characteristics of halogens in minerals found in both the footwall and SIC have been detailed by several authors (Farrow, 1994; McCormick and McDonald, 1998; Warner et al., 1998; McCormick and McDonald, 1999; Magyarosi et al., 2002; Hanley and Mungall, 2003; and authors therein). The most common halogen-bearing minerals (amphibole, biotite) can contain up to 4.0 wt. % Cl, while some F-enriched magnesiohornblende also occurs and can contain up to 1.1 wt. % F.

Halogen abundance in these minerals varies systematically with distance to ore in the Archean-age footwall gneisses of the SIC (Hanley and Mungall, 2003). Halogen mineralogy in the footwall sulphide ore deposits is complex; Farrow (1994) identified several generations/varieties, including actinolite, ferro-actinolite, magnesiohornblende, and actinolitic hornblende, at the Fraser mine. It was also reported that these minerals show a characteristic Fe- and Cl-enrichment with increasing alteration intensity in the footwall.

While the halogen mineralogy of the footwall deposits has been studied extensively, few studies have been carried out to identify mineral chemical differences between halogen-bearing phases in the SIC itself or at its contact with the footwall gneisses. At the contact between the SIC and the footwall, in the footwall breccia unit formed by partial melting of the basement gneisses underneath the SIC, McCormick and McDonald (1999) reported that all amphiboles examined were all calcic amphiboles, regardless of their halogen content. These amphiboles may contain low concentrations of halogens (Cl or F < 0.5 wt. %), although rare and extremely high fluorine abundances were also reported (up to 1.1 wt.%). McCormick and McDonald (1999) also noted that it amphiboles containing elevated Cl and F were rarely observed. Though there is no direct relationship between F and Cl in these minerals, amphiboles containing elevated halogen values are confined to only mineralized samples containing sulphides.

This mineralogical study of halogen-bearing phases in Sudbury involves a comparison of the contact-ore hosting lithology footwall breccia with the surrounding SIC and basement gneiss rock types. Samples of a variety of lithologies taken from drill core were obtained from two environments: a "barren" environment located in the Windy Lake area, absent of economic-grade Ni-Cu-PGE mineralization, and a "mineralized" environment located near Levack, both along the north range of the Sudbury Structure. Mineral chemistry analyzed by LA-ICP-MS and EMP was used to compare compare the chemistry of halogen-bearing mineral phases from both environments with the goal of identifying any differences in mineral chemistry that might be used to discriminate between barren and mineralized segments of the SIC and contact region along the north

range. Simple thermobarometric techniques were applied to ascertain the temperature and pressure of crystallization to determine if magmatic and/or hydrothermal processes were primarily responsible for their formation.

3.3 Geological Setting

The Sudbury Igneous Complex ('SIC') is located at the centre of the Sudbury Structure ('SS'; Fgure 3.1.1.) and is probably the result of a ~1.85 Ga bolide impact (e.g. - Dietz and Butler, 1964; Grieve et al., 1991; Naldrett, 1999). This impact left a depression (the Sudbury basin) on the Earth's surface that was infilled with the Whitewater Group, consisting of the Onaping, Onwatin, and Chelmsford formations. Footwall breccia is the primary lithology observed in this study and is the partially melted basal contact f the SIC. The SIC consists of three primary lithological layered units: norite (subdivided into felsic and mafic), granophyre, and quartz gabbro (Dressler et al., 1992). There is also a transition zone called the contact sublayer, occurring at the bottom of the SIC and above the footwall breccia (Pattison, 1979; Morrison, 1984). Most of the sublayer is heterogeneous and contains abundant Ni-Cu mineralization and xenoliths derived from local country rock or mafic-ultramafic rocks of an unknown source; however they can be genetically linked to the Sudbury complex (Therriault et al., 2002).

The footwall breccia is a discontinuous, 100-150m wide, irregular lithological unit between the basement gneiss and the sublayer (Coats and Snajdr, 1984). Generally speaking, the footwall breccia occurs as either mineralized (gray colour) or barren (pink and white colour). The footwall breccia is a matrix-supported, polymictic unit that

contains subrounded fragments that vary in size on a scale of millimetres to tens of meters in length (McCormick et al., 2002). The mineralogy of the footwall breccia matrix includes andesitic to albitic plagioclase feldspar, quartz, potassium feldspar, chlorite, epidote, pyroxene, biotite, amphibole, as well as accessory phases including apatite, titanite, ilmenite, magnetite, sulphides, etc. The unit serves as the most important host for contact-style deposits (high Ni, pentlandite-rich, massive-disseminated sulphides) along the north range of the SIC. The bulk composition of the footwall breccia matrix varies depending on proximity to the upper and lower footwall contact (dioritic to granitic, becoming increasingly more granitic with increasing proximity to the footwall contact; McCormick et al., 2002). The texture of the footwall breccia matrix also changes with proximity to the footwall contact, occurring granular at the footwall-basement gneiss contact and becoming increasingly igneous with increasing proximity to the sublayer-SIC contact (Lakomy, 1990). The footwall breccia contains clasts of local footwall rocks (i.e. – gneiss, mafic norite, felsic norite, etc.) and pyyhotite-pentlandite-chalcopyrite massive orebodies.

The sublayer norite (also known as the contact sublayer) is a gradational contact between the SIC and the footwall breccia. The contact between the sublayer and norite of the SIC occurs over tens of meters while the contact between the sublayer and the basal contact with the footwall breccia occurs over only a few meters (Therriault et al., 2002). The sublayer is medium to coarse grained and heterogeneous. It is composed mainly of sericitized labradorite-andesine grains, as well as altered enstatite and diopside. There are also minor phases of amphibole, biotite, chlorite, apatite, olivine, and disseminated

sulphides. Sulphides are primarily pentlandite, pyrrhotite, and chalcopyrite, as well as minor pyrite. There are minor inclusions that vary in size from millimetre to meter scale (Therriault et al., 2002). There are also monomineralic inclusions of plagioclase and quartz xenocrysts. Though the felsic norite occurs throughout the SIC, the mafic norite is only present in the North Range. All of these units are a product of in situ fractional crystallization. With some exceptions involving local structural controls, the felsic norite overlies the mafic norite in the North Range. The felsic norite is coarse-grained and contains cumulus

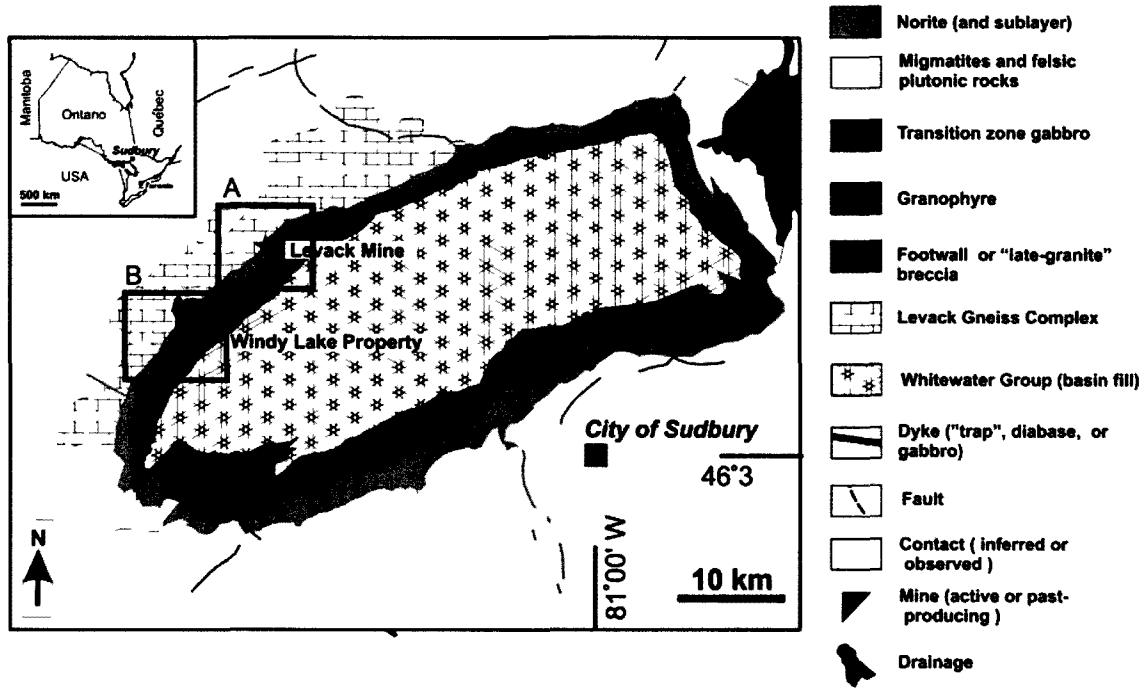

Figure 3.1. Regional map figure of Sudbury Structure. Area A (boxed in) contains the mineralized embayment, and the locations of the studied diamond drill holes FNX6103 and FNX6061 at the Levack Mine. Area B contains the barren environment, and diamond drill WWL-022 at the Windy Lake Property.

plagioclase, orthopyroxene, and intercumulus augite, as well as quartz, biotite, and quartz-feldspar micrographic intergrowth. In the upper portion of the felsic norite the orthopyroxene is no present and the augite displays a cumulus texture. The mafic norite underlies the felsic norite. The mafic norite has ~40-60% orthopyroxene compared to ~20% in the felsic norite. Also, the majority of the mafic norite is an orthopyroxene cumulate where the grains are totally enclosed by plagioclase as a poikolitic texture. Plagioclase in the mafic norite increases upward with increasing proximity to felsic norite (Naldrett and Hewins, 1984).

The SIC and footwall breccia are underlain by the Archean Levack gneiss complex (basement gneiss). The complex is approximately 2711+/-7 Ma years old (Dietz, 1960). The complex contains banded and migmatitic tonalitic, granodioritic, and dioritic gneisses as well as metapyroxenite. The Levack gneiss contains plagioclase, quartz, clinopyroxene, biotite, hornblende, as well as orthopyroxene, garnet, apatite, and magnetite. The complex also contains a gneissic foliation that is defined by felsic bands (plagioclase +- quartz) alternating with mafic bands (clinopyroxene, hornblende, biotite, +- orthopyroxene) (Lafrance et al., 2008). Compositional layering is present throughout the complex with individual units ranging in thickness from a millimetre scale to tens of meters. Most gneisses are grey and fine grained. In certain areas (i.e. – the Levack area) the unit exhibits granulite and amphibolite facies mineralogy. Contact metamorphic overprinting and retrograde metamorphism are present (Dressler, 1984).

3.4 Analytical methods

3.4.1 Electron microprobe

Mineral compositions were determined using a JEOL Superprobe 8200 located at Dalhousie University in Halifax, Nova Scotia, Canada. It is equipped with five wavelength-dispersive spectrometers and an Oxford Link eXL energy-dispersive system. The wavelength-dispersive system was used in the present case. The beam current was 15 nA; the accelerating voltage was 15 kV. Count time varied between 30 and 60s. A beam diameter of 1-2 μm was used in the majority of minerals analyzed which includes biotite, apatite, amphibole, and titanite. Two analytical routines were created: one for silicates and the other for apatites. Silicate standards included KK (K, Ca, Ti, Al, Si, Na, Mg, Fe), fluoroapatite (P, F), tugtupite (Cl), Cr metal (Cr), CuS (S), rhodonite (Mn), and Ni metal (Ni). Apatite standards included fluoroapatite (P, Ca, F), pyrolusite (Mn), garnet (Fe), tugtupite (Cl), CuS (S), KK (Mg), and various rare earth standards for La, Ce, Pr, and Nd. Data were reduced using Link's ZAF matrix correction program. Detection limits for the major elements reported here are in the order of 0.1%.

3.4.2 LA-ICP-MS

Biotite was analyzed in standard polished thin sections (30 μm thick) using laser ablation inductively coupled plasma mass spectrometer (ICP-MS) that was operated in dual detector mode at the Geological Survey of Canada's geochemical facility in Ottawa, Ontario. Simon Jackson assisted with this methodology and implementation. Major element compositions were determined by electron probe microanalysis. The system

comprises a Photon Machines Analyte.193 laser ablation sampler coupled to an Agilent 7700x ICP-MS.

The Analyte 193 employs a short pulse width (FWHM *ca.* 4 ns), energy-stabilized ArF excimer laser beam (λ = 193 nm), which is aperture-imaged onto the sample. Ablation was performed in a flow of He carrier gas, which was combined with Ar make-up gas prior to entering the ICP. In this study, the system's operating parameters were optimized daily for maximum sensitivity at low oxide production rate (*i.e.*, $ThO^+/Th^+ < 0.5\%$) by line scan ablation (nominal spot diameter = 52 μm, energy density = *ca.* 7 J/cm^2, laser repetition rate = 10 Hz, sample translation rate = 5 μm/s) of NIST SRM 612 glass (nominally 50 ppm). This typically resulted in signals for mono-isotopic mid- to high-mass elements (La, Lu) in excess of 500,000 c.p.s. and background measured at a.m.u. 220 of 1-2 c.p.s.

Data were acquired on 34 isotopes using the instrument's time-resolved analysis data acquisition software and a fast peak hopping protocol (dwell time per isotope 10 ms) to ensure representative measurement of rapidly transient signals typical of laser ablation sampling. The time-resolved analysis software reports signal intensity data (c.p.s.) for each mass sweep, allowing subsequent inspection of signals as a function of time (ablation depth or sample travel), and thus assessment of chemical heterogeneity within the ablation volume (*e.g.,* inclusions, penetration into slide glass). The signals can then be selectively integrated during data processing.

Nominal spot diameters used ranged from 34 to 86 μm, depending upon grain size. Typical analyses yielded 15-25 s of data before the laser penetrated through the mineral

into the underlying slide-glass substrate, as indicated by a sudden rapid increase in signals for, in particular, Na, Sr and Zr. Line scans (4 μm/s) were employed where possible to extend ablation times. Total analysis time was 120 s - instrumental background (*ca.* 50 s) followed by ablation (up to *ca.* 50 s for line scans)

Analyses were performed in runs of up to 20 analyses, which comprised 2 analyses of a calibration standard, NIST SRM 610, at the beginning and end of each run, bracketing up to 15 biotite analyses and one analysis of USGS BCR-2G basaltic glass microbeam standard for QC purposes.

Raw signal intensities (c.p.s.) *vs.* time data were exported from the ICP-MS for data processing using LAMTRACE (Jackson, 2008). LAMTRACE allows selective integration of signals for representativeness, and then performs calculation of concentrations by referencing background-corrected ablation signal intensities of the sample against a calibration standard (NIST SRM 610) and correction for ablation yields via Si internal standardization. Concentration values used for NIST SRM 610 glass were the preferred average values of Pearce et al. (1997). Electron microprobe SiO_2 measurements were used for internal standardization. Data were filtered for detection limits that were calculated for each analysis using the algorithm derived by Longerich et al. (1996). Detection limits for mid- to high-mass elements in this study were generally < 10 ppb. Precision and accuracy data, as determined by 7 analyses of BCR-2G, are presented in the Appendices.

3.4.3 Thermobarometry

3.4.3.1 Biotite-apatite thermometry

A biotite-apatite halogen geothermometer was developed by Zhu and Sverjensky (1992) to constrain the lowest (i.e. latest) temperature of mineral equilibrium. This is possible by calculating the exchange of F between biotite and apatite grains; however the two grains must be in contact with one another and show textural evidence for equilibrium. When analyzing the minerals by EMP, selected probe points must be on the rim of the grain closest to the paired mineral. These data are then recalculated to determine partition coefficient (K_D) for the distribution of fluorine between the biotite and apatite grains in equilibrium. The F exchange is described in the following equation (Zhu and Sverjensky, 1992):

$$KMg_3AlSi_3O_{10}(F)_2 + 2Ca_5(PO_4)_3(OH) = KMg_3AlSi_3O_{10}(OH)_2 + 2Ca_5(PO_4)_3(F)$$

(fluorbiotite) (hydroxyapatite) (hydroxybiotite) (fluorapatite)

The halogen exchange coefficient for this reaction is defined as:

$$\ln K_D = \ln [(X_F/X_{OH})_{Apatite}]/[(X_F/X_{OH})_{Biotite}]$$

Oxide to cation recalculations per formula were calculated using geochemical software developed by MinPet geological software. Mole fractions for fluorine (X_F) and hydroxyl

(X_{OH}) were ascertained and then partition coefficients were determined to calculate K_D. Temperature was determined using the following calculation (Zhu and Sverjensky, 1992):

$$T = [((8852 - (0.024 * P) + (5000 * X_{Fe})]/(1.987 * \ln K_D) + 3.3666) - 273.1$$

Where P represents pressure in bars and X_{Fe} is the mole fraction of Fe, determined from mineral recalculations (site assignments, determined using MinPet). Note that while P comprises a parameter in the expression above, the calculated T is relatively insensitive to P and most sensitive to variations in the halogen exchange constant.

3.4.3.2 Semi-quantitative calcic amphibole thermobarometry

Ernst and Liu (1998) described a method of estimating pressure and temperature using the Al and Ti abundances in calcic amphiboles from mafic igneous rocks. They determined that in these systems, with increasing P and T, an increases in Mg# and Na, Ti, K, and Al occur. There are also decreases in total Fe + Mg + Mn + Ca and Si (Femenais et al., 2006, and Ernst and Liu, 1998). Calcic amphibole transforms to anhydrous phases + free H_2O over a small P-T range at subsolidus temperatures, however these changes diminish slowly over a larger range of temperatures (Ernst and Liu, 1998). High pressure experiments have shown that a negative P-T slope exists from the amphibole-out reaction. This process is caused by the higher entropy assemblage (garnet + clinopyroxene + minor aqueous fluid) possesses a smaller volume than the equivalent amount of calcic amphibole (Ernst and Liu, 1998). Below solidus temperatures, the

preserved Al and Ti content of amphibole are the best overall indicators of pressure and temperature and are the least sensitive cation parameters to changes in other site occupancies. Ernst and Liu (1998) recalibrated the dependance of Al and Ti (quantifiable by electron microprobe) on P and T and provide a robust graphical technique.

3.5 Results

3.5.1 Petrography of footwall breccia and associated units

The footwall breccia is a felsic granitic rock that shows a wide range of textures, varying from true heterolithic breccia containing a fine-grained igneous matrix and clasts of variably digested footwall gneiss (and restitic clasts) to more equigranular, clast-free, plastically deformed equivalents of the footwall gneiss. In some cases, rocks logged as footwall breccia in drill cores, appear identical to the Levack Gneiss in hand sample. This suggests that large blocks of Levack Gneiss become mobilized during partial melting and footwall breccia formation and rise up to stratigraphic levels in the plumes but do not melt completely or only experience some thermal metamorphism. Therefore, footwall materials cannot be heated too far above their solidus temperature during interaction with the SIC. Figure 3.2 shows typical variations in textures and colour of the footwall breccia. Figure 3.2a shows the true heterolithic breccia variety. Felsic clasts composed of quartz, albitic plagioclase, and alkali feldspar are visible and mafic clasts with amphibolitic compositions are also present in a fine-grained, granular, grey matrix. These clasts are residual rounded fragments from the partially and dynamically melted Levack Gneiss. Figures 3.2b-d show more equigranular footwall breccia varieties (leucocratic and

melanocratic). The colour of the rocks are related to the proportions of felsic and mafic minerals from the original (parental) gneisses. Secondary alteration veins and patches of granophyric intergrowth related to cooling of the footwall breccia and post-crystallization hydrothermal alteration are visible in Figure 3.2b and c. The granophyric matrix material is also common to the adjacent SIC lithologies and may be a late stage residue from the footwall breccia as it recrystallizes in the plumes. Figure 3.2e shows a mafic clast rich footwall breccia sample with a fine grained, grey igneous matrix infilling the spaces between the clasts. For comparison, Figure 3.2f shows the Levack Gneiss several hundred metres below the SIC contact. Its textural similarities to the footwall breccia suggest that many samples logged as breccia are actually large pods of weakly altered and thermally metamorphosed gneiss that were emplaced with partial melt during plume formation, as described above. Evidence for fluids released from the footwall breccia into adjacent SIC rock types is shown in Figure 3.2g-h in which normal felsic norite and a coarse-textured pegmatitic equivalent are compared.

In thin section (Figure 3.3), footwall breccias show three main textural changes that may be related to the extent of partial melting of the original gneiss from which they were sourced. In relatively fresh Levack Gneiss or weakly developed footwall breccia, many of the original characteristics of the gneiss are visible including large, subhedral to euhedral polycrystalline quartz aggregates containing triple junctions and well defined matrix domains containing large oikocrysts of plagioclase containing tabular albite crystals (Figure 3.3a). As melting proceeded, domains of quartz aggregates and feldspar rich matrix became poorly defined, quartz and albite grains became anhedral as they melted

and recrystallized to form large complexely intergrown masses, and grain boundaries developed sawtooth like morphologies (Figure 3.3b) similar to stylolites in chemical sedimentary rocks. Grain boundary migration continued as melting advances and quartz and albite grains develop highly irregular grain boundaries. Sieve texture indicates resorption of feldspars (Figure 3.3c-d). Partial melt that collected in the matrix of the footwall breccia recrystallized to a graphic-textured intergrowth (granophyre; Figure 3.3e), accompanied by the growth and recrystallization of halogen-bearing silicates (fibrous actinolite, Figure 3.3f; and lathy biotite, Figure 3.3g). In the surrounding SIC rock types (norite, gabbro, sublayer) fresh igneous textures are generally preserved but are coarsened locally and show evidence of replacement of primary pyroxene by biotite (Figure 3.3i) and infiltration of granophyric liquid (Figure 3.3j).

Typical textural relationships between biotite and apatite were observed by scanning electron microscope (SEM). Evaluation of the timing of biotite and apatite growth was important because textural equilibrium between the two was required to use apatite-biotite thermometry. Figure 3.4 shows that amphibole is also spatially associated with biotite and apatite. Grain boundary contacts are smooth between these mineral phases and no evidence for replacement of one mineral by another or zonation were apparent in the footwall breccia. This is in contrast to the felsic norite where apatite and biotite often show evidence of resorption (e.g., see apatite grains in Figure 3.4e).

Some relevant petrographic characteristics are summarized in Tables 3.1.1-3.1.2. Included in this table are the modal abundances of all halogen bearing minerals. No differences in halogen mineral abundances in common lithologies were identified

between the barren and mineralized environments. Also summarized are colour indicators for footwall breccia and other lithologies. For the footwall breccias this indicates the gneissic parentage of the breccia (i.e., melanocratic vs. leucocratic, where melanocratic breccia contains > 50% dark minerals). Indicators of footwall breccia maturity (extent to which the breccia represents a fully developed partial melt) are also summarized Indicators for this include a lack of euhedral quartz and albitic plagioclase in the matrix of the breccias, and the presence of granophyric intergrowth.

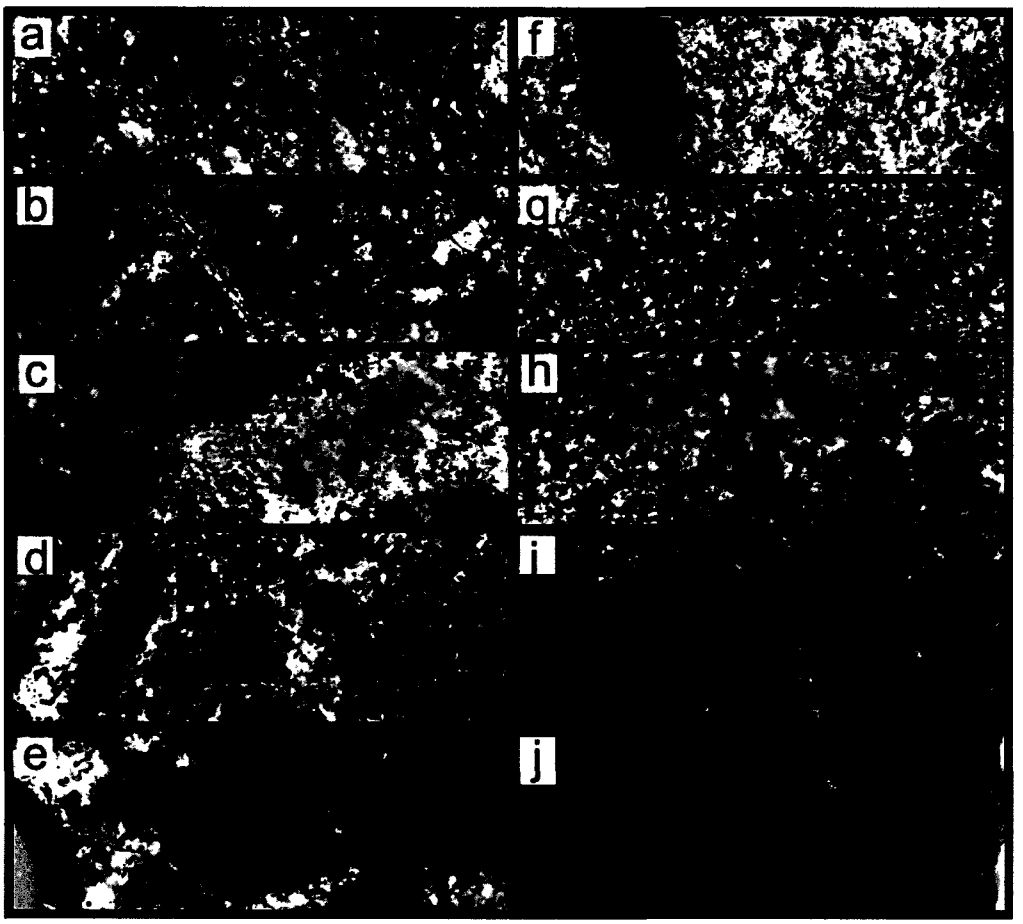

Figure 3.2. Petrographic characteristics of studied lithologies in hand sample. (a-d) Footwall breccias showing a range of textures resulting from a combination of varying clast compositions (from melted protoliths) and degree of melting. In fully developed footwall breccia (a), a variety of restitic and relict clasts from melted gneissic rocks occur in a grey, fine-grained, granular to granophyric granitic matrix. Lesser developed breccias (b-d) show microtextural evidence of partial melting but macroscopically preserve characteristics of the primary footwall gneiss with variable mafic content resulting from variations in the in original proportions of mafic and felsic bands in the protolith gneisses. Image (a-c) show more leucocratic varieties of footwall breccia whereas image (d) shows a melanocratic variety. Image (c) shows a large patch of quartz-alkali feldspar granophyric intergrowth within the breccia matrix. Note in image (d) the lack of any discernable "brecciated" textures. (e) Leucocratic footwall breccia matrix hosting several large mafic restitic clasts. (f) Typical Levack Gneiss from the region near the contact with the SIC showing pink hematitic-K-feldspar alteration, mafic clasts (from the original gneiss, not from partial melting). (g) Felsic norite (fine-grained). (h) Felsic norite (coarse-grained pegmatitic variety from immediately adjacent to footwall breccia.(i) Mafic norite. (j) Sublayer containing abundant pyroxenitic inclusions in a noritic matrix.

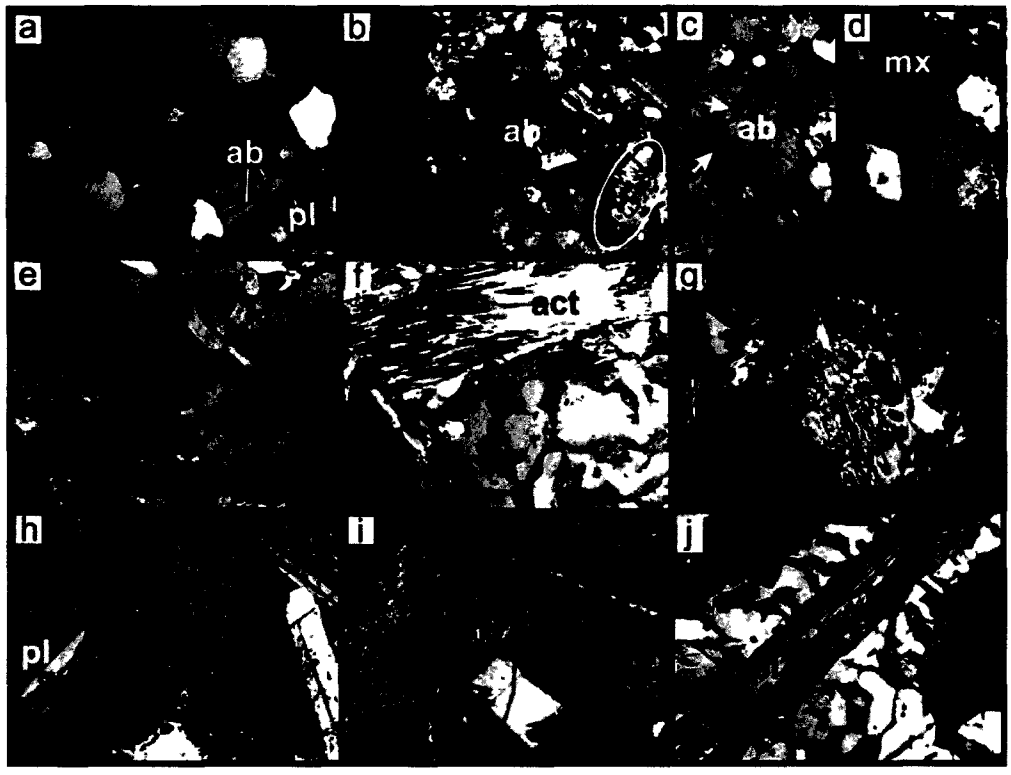

Figure 3.3. Petrographic characteristics of studied lithologies in thin section. All images have a height of field of 500 mm. (a) thermally metamorphosed but unmelted Levack Gneiss from adjacent to the SIC contact along an embayment. Note the occurrence of polycrystalline quartz (qtz) forming a patch or "eye" with relatively smooth grain boundaries and abundant trip junctions, and a matrix containing euhedral (tabular) albitic alkali feldspar (ab) included in plagioclase (pl). Matrix and quartz patches form discrete domains within the gneiss. (b) Footwall breccia showing partially melted footwall gneiss. As melting progressed, quartz (qtz) grain boundary migration occurred resulting in anhedral "sawtooth" or stylolite-like grain surfaces (area outlined in white oval), and the euhedral character of matrix feldspars (ab) became greatly diminished. (c-d) Fully developed footwall breccia showing extensively melted footwall rock. In (c) sieve texture in remnant feldspars is well developed (arrows), resulting from resorption, and in (d) domains of remnant quartz and matrix are still visible, the matrix (mx) has a granular appearance and relict quartz grains have a highly irregular grain shape. (e) granophyric matrix within footwall breccia, occurring as a mm-size vuggy infilling within the matrix. (f) Lathy, acicular amphibole (var. actinolite; mx) surrounding in granophyric matrix from a footwall breccia sample. (g) Platy biotite (bt) within the matrix of a footwall breccia sample; circular dark areas are LA-ICPMS pits. (h-i) Typical noritic and sublayer rock types showing the occurrence of ophitic plagioclase (pl) - orthopyroxene (opx) intergrowth with secondary (or late magmatic) replacement of orthopyroxene by biotite (bt). Image (j) shows a resorbed plagioclase lath surrounding in granophyric matrix potentially introduced as a partial melt from the adjacent footwall breccia plume.

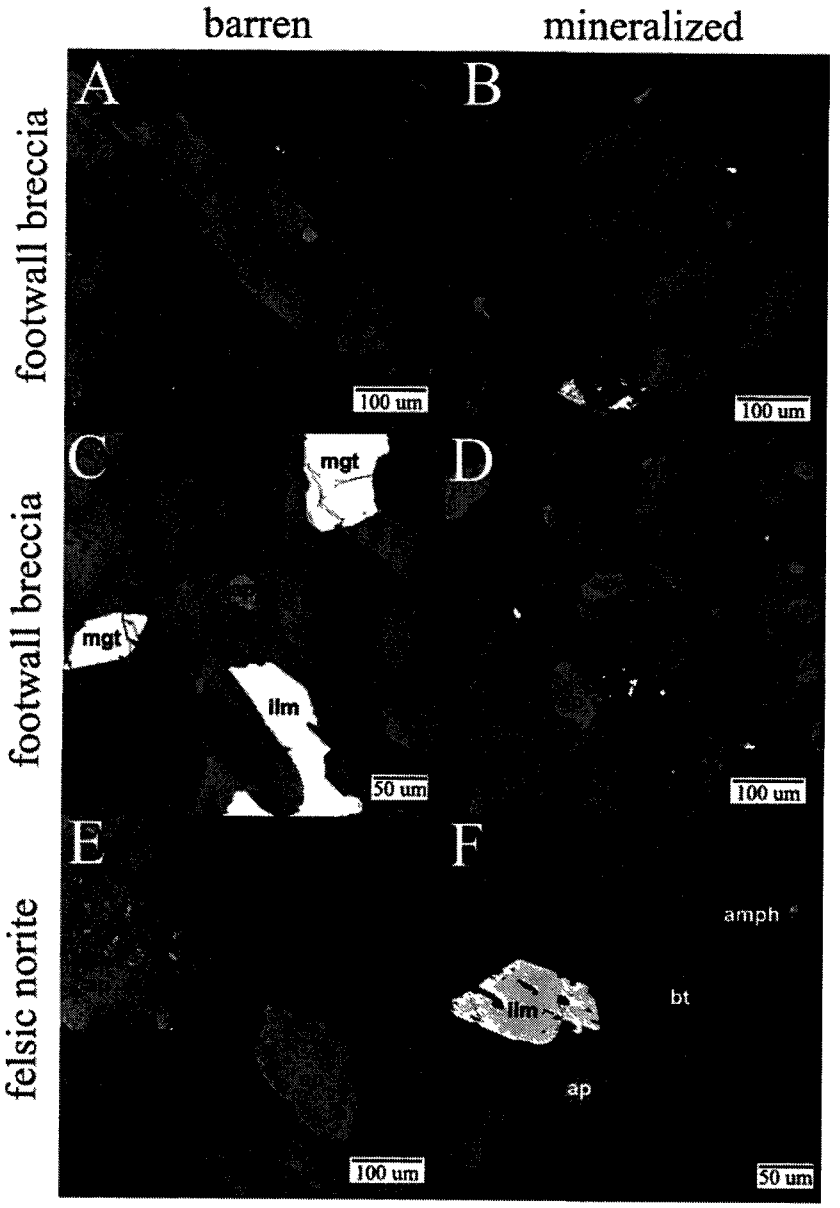

Figure 3.4. SEM backscatter images of representative sample textures. These images show examples of equilibrium and disequilibrium textures between biotite and apatite grains in the footwall breccia and felsic norite. Other accessory minerals present include chlorite, amphibole, magnetite, and ilmenite. Samples: A. CS62a; B. CS107; C. CS85a; D. CS124; E. CS37a; F. CS101. Abbreviations: amph = amphibole; ap = apatite; bt = biotite; chl = chlorite; ilm = ilmenite; mgt = magnetite.

3.5.2 Mineral chemistry

Minerals grains from a representative sample set of each lithology were analyzed by electron microprobe (EMP) to determine in particular, their halogen content. Minerals analyzed included amphibole, biotite, apatite, chlorite and titanite. The majority of samples analyzed were from the footwall breccia; however representative samples from the other lithologies were also examined. The EMP strategy was to examine compositional variations between lithologies and between the barren and mineralized environments. All EMP data are tabulated in the Appendices.

In total, 353 amphibole analyses were collected: 261 from the barren environment and 92 from the mineralized. Amphibole from the mineralized footwall breccia contain 2-3 wt. % less SiO_2 than the barren footwall breccia. The FeO content is greater in the mineralized environment (~14-17 wt. %) than the barren (~1-10 wt. %). Amphibole from felsic norite contain slightly more Al_2O_3 in the barren than in the mineralized environments (~2.25 and 1.4 wt. %, respectively). Several EMP analyses were recalculated into cation abundances to determine their mineral classification. Figure 3.5 classifies amphiboles based on their Si p.f.u. and Mg# (Leake et al., 1997), and all appropriate criteria were met to implement this diagram. Average analyses are shown along with the number of analyses from each lithology. The majority of amphiboles are actinolitic, with a few analyses plotting as tremolite and magnesiohornblende.

A total of 513 apatite grains were analyzed. Almost half of the apatites analyzed were from footwall breccia. There are no significant differences in apatite composition (in terms of major elements) between the two environments in the footwall breccia.

A total of 181 biotite grains were analyzed from the barren and mineralized environments. Biotites exhibit greater fluctuation in FeO in the mineralized footwall breccia environment, ranging from 8.6 to 21.4 wt. %, while biotites from the barren environment ranges from ~12-18 wt. %. Sublayer biotites contain 17.3 wt. % FeO in the barren environment compared to 7-12 wt. % in the mineralized environment. There is a greater range and variability in MgO in the mineralized environment compared to the barren (10-17.5 and 14-16.8 wt. %, respectively).

Table 3.1.1. Major mineralogical and textural characteristics of studied lithologies

		Modal Abundance (%)				Petrographic summary					
Sample	Unit	amp	ap	bt	ttn	L/M	apx % sulph	graphic?	qtz gb	euhedral fsp	amp/bt?
barren											
CS2	apl	0.5	0.575	3	0	l	0	y	n	n	y
CS3	qtgb	1	3.6	2	0	m	0	y	n	n	y
CS4	fnor	8	0.275	4	0	m	0	n	n	n	y
CS5	fnor	0.5	0.3	2	0	m	0	n	n	n	y
CS9	fnor	5	0.175	1	tr	m	0	n	n	n	y
CS10b	fwb	4	0.775	1	tr	l	0	n	n	n	y
CS12	fwb	2	0.925	0	0	l	0	n	n	n	y
CS13a	fwb	3	0.475	0	tr	l	0	y	n	n	n
CS17a	fwb	13	0.45	0	0	l	0	y	n	n	y
CS18a	fwb	2	0.625	0.5	0	l	0	n	n	n	y
CS19a	fwb	1	0.55	0.5	tr	l	0	n	n	n	y
CS20	fwb	2	0.725	0	0	l	0	y	n	n	n
CS22	fwb	1	0.525	0	0	l	1	n	n	n	n
CS24	fwb	18	1.775	0	0	m	1	n	n	n	y
CS25a	fwb	2	0	0	0	l	2	n	n	n	n
CS27b	fwb	3	0.775	0	0	l	1	y	n	y	y
CS31a	fwb	1	0.5	0	tr	l	1	n	y	n	n
CS34b	fwb	2	1.15	0	tr	l	2	y	n	n	y
CS35	fwb	40	0.75	1	tr	l	0.5	n	n	y	y
CS37a	fnor	4	0.425	0.5	tr	l	1	n	n	n	y
CS38	fnor	3	0.4	1	0	l	2	y	n	y	n
CS41b	fwb	4	0	0.5	tr	m	0	y	n	n	y
CS42b	fwb	5	0.15	0	tr	m	0	n	n	n	n
CS43	mnor	0	0.725	0.5	0	m	0	n	y	n	n
CS44a	mnor	22	0.125	1	0	m	9	y	n	n	y
CS44b	mnor	15	0.125	1	0	m	7	y	n	n	y
CS47b	fwb	2	0.675	1	0	l	0.5	n	n	n	y
CS49a	fwb	7	0.675	0	0	m	0	y	n	n	n
CS51a	fwb	0.5	0.525	0	tr	l	0	n	y	n	n
CS56a	fwb	4	0.4	0	0	l	4	n	n	n	y
CS57a	fwb	15	0.325	1	0	m	2	n	n	y	n
CS58a	fwb	10	0.15	1	0	m	4	n	n	n	y
CS60	fwb	28	0.225	0	tr	m	2	y	n	n	y
CS62a	fwb	30	0.2	1	0	m	0	y	n	n	y
CS66	fwb	4	0.225	4	0	m	1	y	n	n	n

Notes:

L/M = leucocratic or melanocratic

apx. % sulph = approximate percentage of sulphide minerals in thin section

Lithologies: apl = aplite dike; fnor = felsic norite; fwb = footwall breccia; gn = Levack gneiss; grano = granophyre; mnor = mafic norite; qtgb = quartz gabbro; sl = sublayer norite

Petrographic abbreviations: L/M = leucocratic or melanocratic; graphic? = graphic textured matrix (alb felds-qtz intergrowth; amp/bt = amphibole or biotite present as replacement mineral; qtz gb = euhedral quartz grain boundaries; euhedral fsp = euhedral feldspars in matrix

Ttn: tr = few grains per sample (ttn =>1 % modal abundance)

Apatite modal abundance calculated based on bulk P_2O_5 from chapter 2

Table 3.1.2. Major mineralogical and textural characteristics of studied lithologies

		Modal Abundance (%)				Petrographic summary					
Sample	Unit	amp	ap	bt	ttn	L/M	apx % sulph	graphic?	qtz gb	euhedral fsp	amp/bt?
CS68	fwb	3	0.15	2	0	m	3	n	n	n	n
CS69b	fwb	4	0.225	1	0	m	5	n	n	n	y
CS70a	fwb	2	0.675	0.5	0	l	0	n	y	n	y
CS71a	fwb	2	0.575	0.5	0	l	1	n	n	n	n
CS73b	fwb	1	0.5	1	tr	l	1	n	y	n	y
CS76a	fwb	1	0.575	0	0	l	1	y	y	n	n
CS78b	sl	0	0.3	1	0	m	0.5	n	ab	n	n
CS79	sl	10	0.45	0.5	0	m	15	n	ab	y	y
CS80b	sl	3	0.575	1	0	m	11	y	n	y	n
CS84a	fwb	0	0.375	1	0	m	2	n	n	n	n
CS85a	fwb	0	0.625	1	0	m	2	n	n	y	n
CS89	fwb	1	0.475	0	0	l	2	n	y	n	n
CS90a	fwb	2	0.35	0	0	l	2	n	n	n	n
CS93a	gn	1	0.375	0.5	0	l	1	n	y	n	n
CS95a	gn	8	0.375	0	0	l	2	n	n	n	n
CS96	grano	4	1.225	2	0	l	2	y	n	n	n
mineralized											
CS101	fnor	1	0.275	4	0	l	0	n	n	y	n
CS104	grano	4	0.175	1	0	l	0	n	n	n	n
CS107	fwb	1	0.55	2	0	m	3	n	n	y	n
CS110	mnor	1	0.325	2	tr	m	1	n	n	n	y
CS112	sl	0	0.15	1	0	m	0.5	n	n	n	n
CS115	fwb	1	0.55	1	0	l	1	n	n	n	n
CS116	gn	2	1.1	1	0	l	0	n	n	n	n
CS119	gwb	2	0.35	0.5	0	l	2	n	y	n	n
CS120	gn	3	0.35	1	0	l	1	n	y	n	n
CS122	gwb	8	0.3	0	0	m	3	y	y	n	n
CS123	gn	2	0.25	1	0	l	0.5	n	y	n	n
CS124	fwb	1	0.225	1	0	l	0	n	n	n	n
CS127	fwb	0	0.5	3	0	m	4	n	n	n	n
CS133	sl	0	0.125	1	0	m	0	n	n	n	n
CS137	fwb	0	0.125	0	0	l	0	n	n	n	n
CS139	sl	0.5	0.425	0	0	l	0	n	n	n	n
CS140	sl	0.5	0.425	5	0	m	1	n	n	n	y
CS142	gn	2	0.625	1	0	m	0.5	y	n	n	y
CS143	gn	1	0.275	0	0	l	1	n	y	n	n

Notes:

L/M = leucocratic or melanocratic

apx. % sulph = approximate percentage of sulphide minerals in thin section

Lithologies: apl = aplite dike; fnor = felsic norite; fwb = footwall breccia; gn = Levack gneiss; grano = granophyre; mnor = mafic norite; qtgb = quartz gabbro; sl = sublayer norite

Petrographic abbreviations: L/M = leucocratic or melanocratic; graphic? = graphic textured matrix (alb felds-qtz intergrowth; amp/bt = amphibole or biotite present as replacement mineral; qtz gb = euhedral quartz grain boundaries; euhedral fsp = euhedral feldspars in matrix

Ttn: tr = few grains per sample (ttn =>1 % modal abundance)

Apatite modal abundance calculated based on bulk P_2O_5 from chapter 2

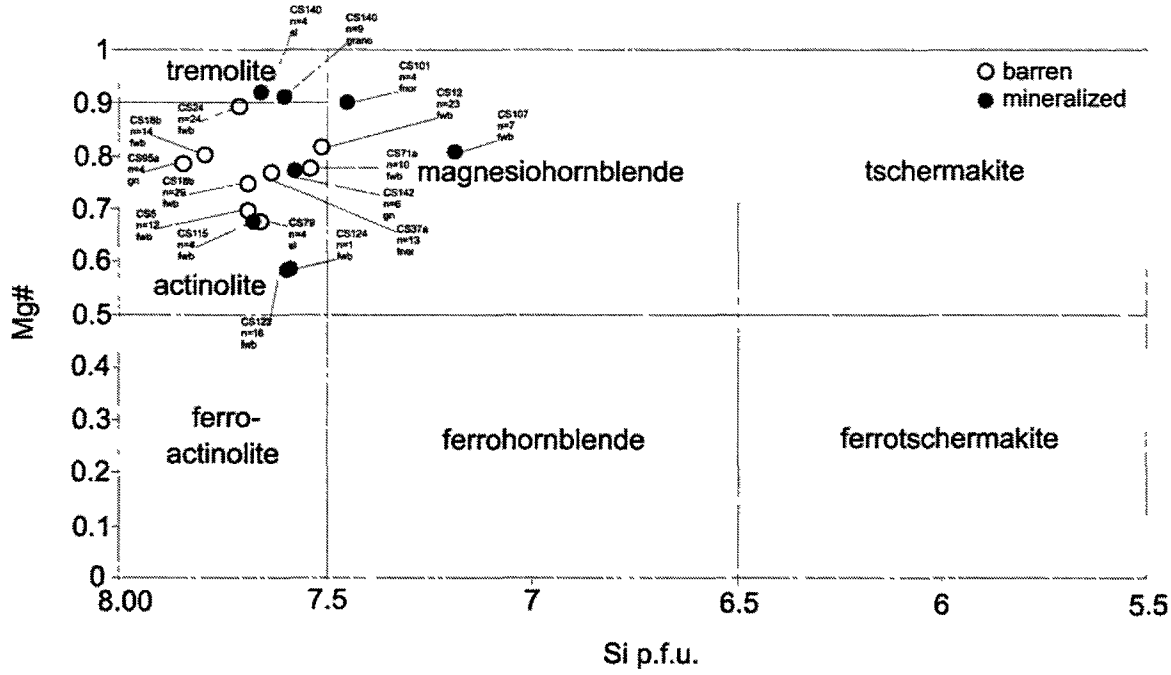

Figure 3.5. Si vs. Mg# diagram for amphibole data (based on classification criteria of Leake et al., 1997). The term 'n' is the number of analysis per sample, averaged to plot the data point. Lithologies: wb = footwall breccia; fnor = felsic norite; sl = sublayer norite; grano = granophyre; gn = Levack gneiss. p.f.u. = per formula unit.

Abundance of Na_2O from biotites in the sublayer samples are both slightly greater in the mineralized environment (0.08 and 0.71 wt. %, respectively). Biotites in basement gneiss contained elevated K_2O and TiO_2 in mineralized samples. Biotites from the barren environment are enriched Na_2O. On a diagram classifying biotite according to their Al^{IV} and Fe# (Bailey, 1984) the majority of micas are classified as phlogopite-annite, plotting along the phlogopite-annite joint but closer to the phlogopite end-member (Figure 3.6). There is no obvious difference between the two lithologies, however two samples of barren footwall breccia and one of barren felsic norite plot below the extent of the diagram (their Al^{IV} falls below the diagram plot area). One mineralized felsic norite sample also plots slightly outside the diagram (Al^{IV} = 1.93). Barren samples also plot more consistently with a smaller variation in both Si and Mg#.

Chlorite grains from footwall breccia contain more FeO (24-28 wt. %) than barren grains (~15-21 wt. %), with one barren sample containing an anomalous value. There is also enrichment in Na_2O and K_2O in mineralized grains, though only slight. There is slightly less Mg in chlorite grains from the mineralized environment. Titanites show no differences in chemistry between the environments.

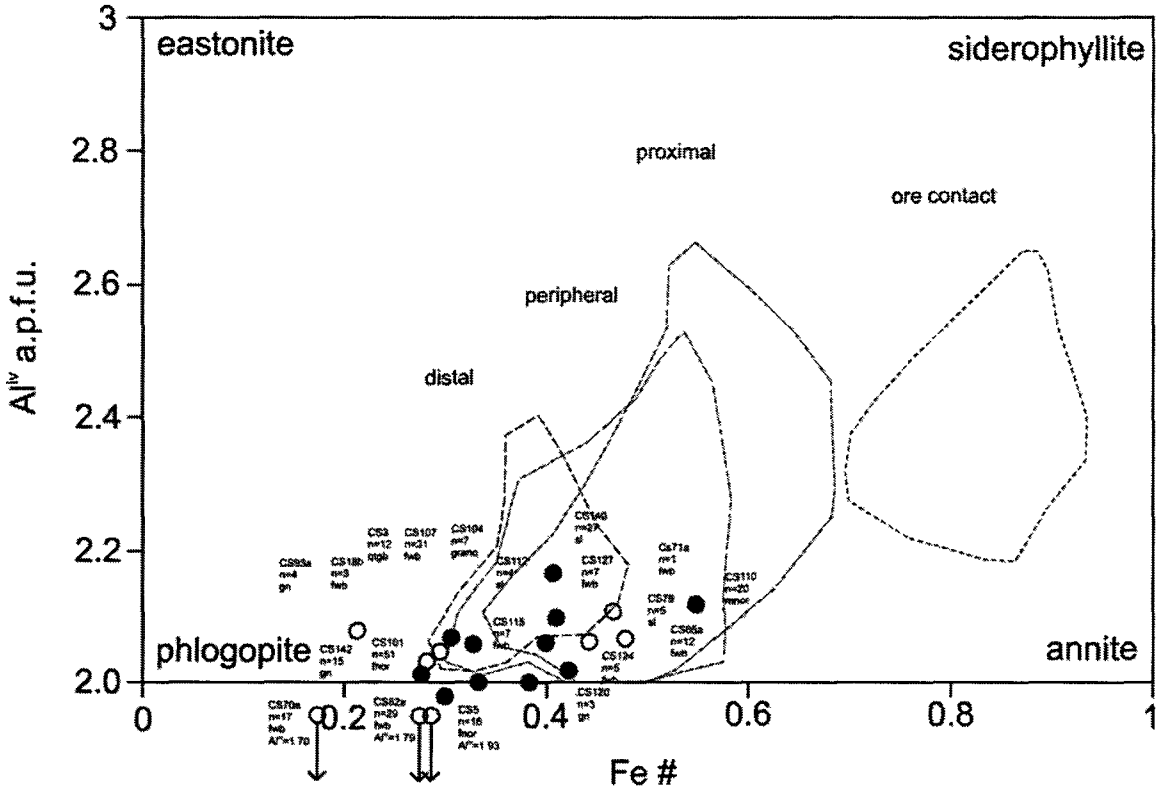

Figure 3.6. Fe# vs. Al^{IV} diagram for micas (after Bailey, 1984). Empty circles represent barren samples while filled circles represent mineralized samples. Lithologies: fwb = footwall breccia; fnor = felsic norite; mnor = mafic norite; sl = sublayer norite; grano = granophyre; gn = Levack gneiss. a.p.f.u. = atoms per formula unit. Four fields on diagram represent biotites from Sudbury breccia samples from ore distal, peripheral, and proximal samples in the footwall from Hanley and Mungall (2003), sampled at varying distances from footwall-style sulphides. n = number represents number of analysis per sample.

3.5.3 Halogen abundances in mafic hydroxysilicates and apatite

Figures 3.71-3.73 summarize average halogen abundances from individual samples by environment. Complete analyses (used to generate these diagrams) for all minerals are summarized in the Appendices. The majority of analyzed samples were from footwall breccia.

The average Cl and F contents of amphiboles (Figure 3.71) are greater in most samples from the mineralized embayment compared to the barren environment. This is particularly true for F which fell below routine detection limits for all amphibole grains except in one sample (CS60) which had unusually high F levels. The Cl contents of amphiboles are very low (< 0.12 wt, %), typical of amphiboles with high Mg# in the Sudbury environment. The F contents of amphibole in all lithologies are generally 2-3 times higher than Cl, averaging several thousand ppm in most samples (max ~ 0.5 wt. %).

On average, Cl values in apatite (Figure 3.7.2) are higher in the barren environment but highly variable (ranging from b.d.l. to up to ~ 1 wt. %), with little variation in corresponding F content. Interestingly, F values are lower in samples taken from shallower depths in the barren environment. Mineralized apatites can be similar in composition to fluorapatite, containing up to an average of ~3.5 wt. % F from individual samples. There are two populations of barren apatite; one averaging ~3.5 wt. % F (similar to mineralized samples), and a second group containing between ~2.0-2.5 wt. % F; this second group contains generally lower and less variable Cl than the first group. Samples from the mineralized environment contain about the same amount of F as the deeper samples from the barren environment, sampled from core at a similar stratigraphic level.

Biotites from the mineralized embayment contain similar amounts of Cl (and show a similar range in values) as in the barren rocks. The data are highly scattered and samples containing biotites with elevated F tend to be poor in Cl, whereas biotites rich in Cl tend to be poor in F. With the exception of one outlier sample, the mineralized samples contain more F on average, although individual analyses vary quite widely and this difference is only recognizable if average values are considered.

Titanite was found as an accessory mineral in a few samples but was absent in most of the samples from the mineralized environment. This made it difficult to obtain representative samples for all lithologies and to compare the sampled embayments. Halogen contents in titanite are variable but generally low suggesting that it cannot contribute much to bulk halogen abundances.

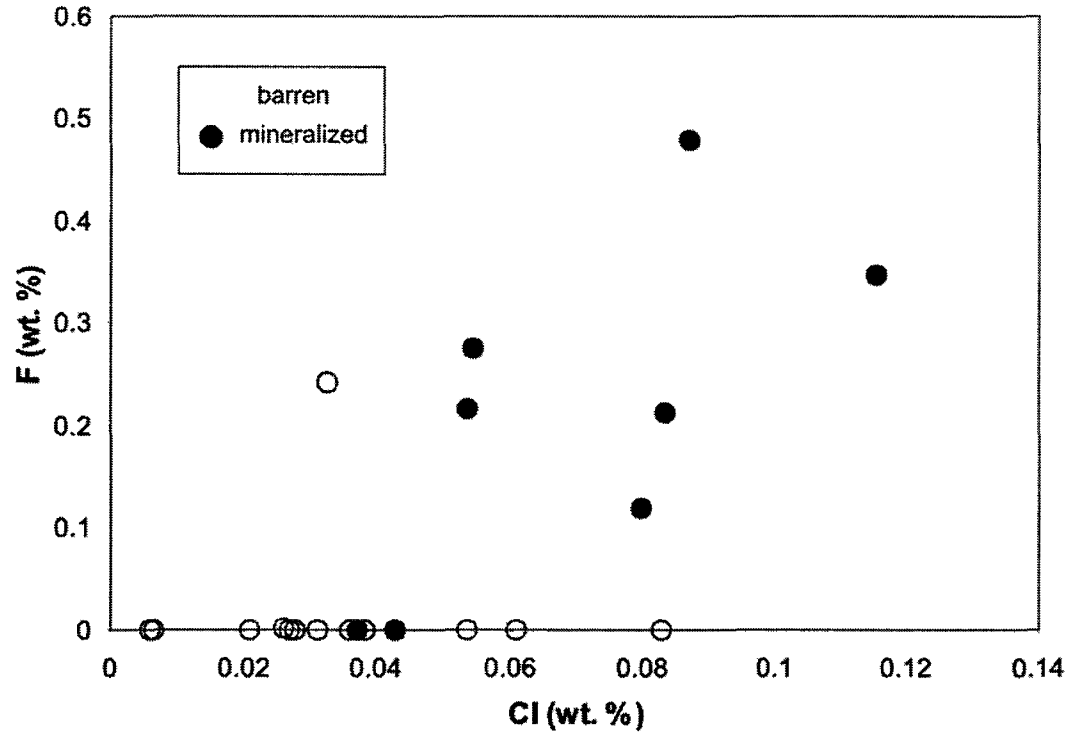

Figure 3.7.1. Cl vs. F in amphibole. Each point represents the average of several analyses from a single sample. The majority of grains from barren samples contain no F.

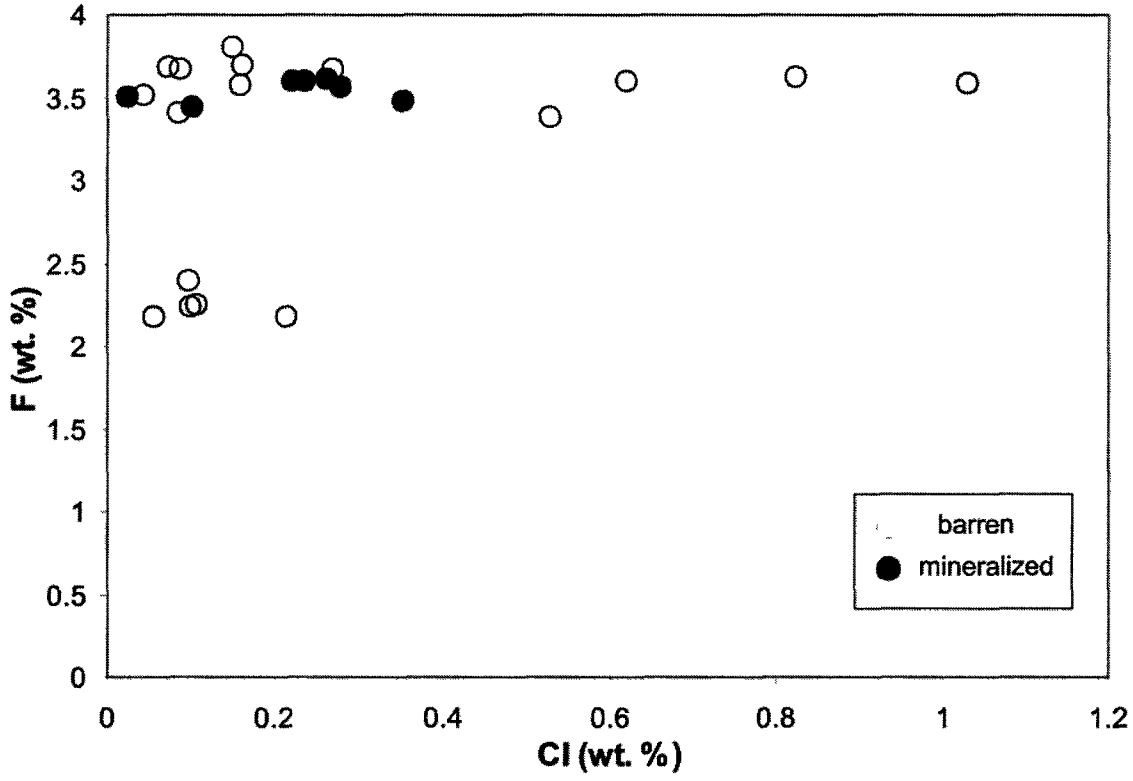

Figure 3.7.2. Cl vs. F in apatite. Each point represents the average of several analyses from a single sample. Fluorine remains relatively consistent for most samples from both environments, with the exception of five barren samples. Chlorine varies between samples but does not exceed 0.4 wt. % for mineralized samples.

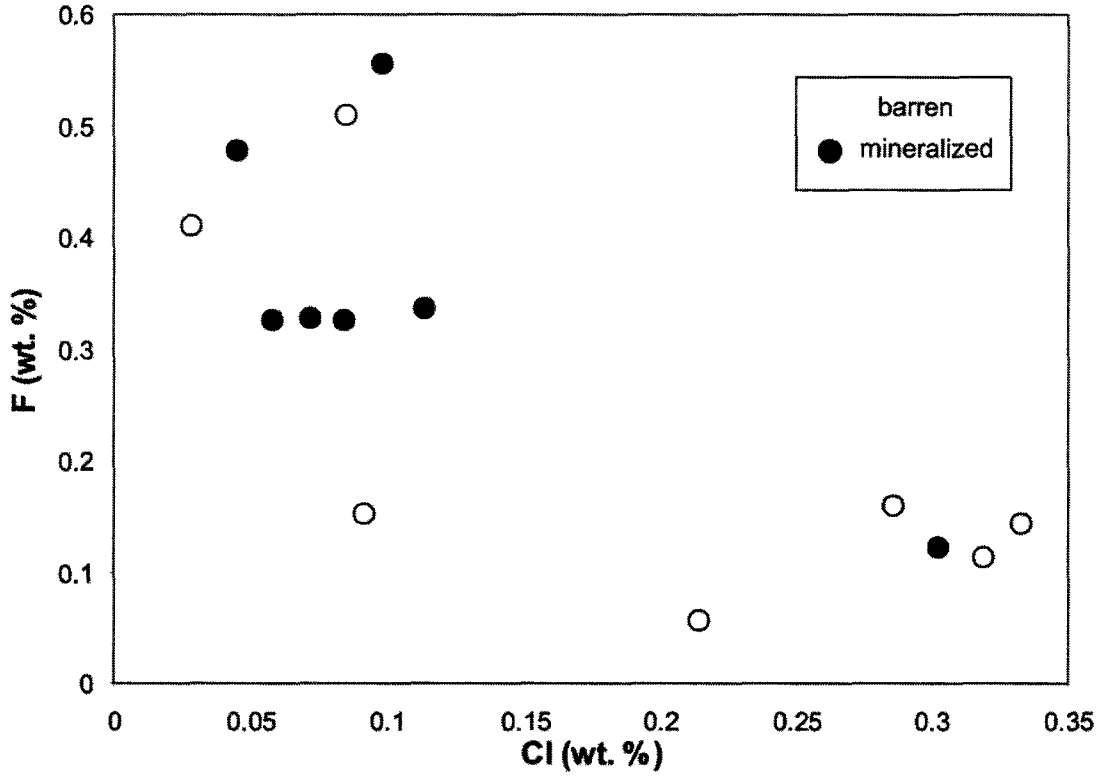

Figure 3.7.3. Cl vs. F in biotite. Each point represents the average of several analyses from a single sample. The majority of mineralized samples are enriched in F. On average, barren samples are enriched in Cl.

3.5.4 LA-ICP-MS analysis of cations in biotite

Biotite grains were analyzed by LA-ICP-MS to determine if there were any significant variations in their trace element chemistry from environment to another. A sample suite covering all lithologies from both environments was selected and fresh, unaltered grains were preferred (i.e., unaltered to chlorite).

With respect to variations in trace element chemistry between lithologies, some sublayer biotite samples showed marked depletion in Ce and Y compared to other lithologies. Generally, all biotites analyzed became increasingly enriched in Ba with increasing depth. Biotites in the footwall breccia have the highest abundance of Ba. However, this enrichment in Ba drops in the basement gneiss below the footwall breccia; biotites in the basement gneiss contained the lowest amount of Ba.

The most significant differences in biotites between environments was their Ni and Cr contents. Generally, the lowest amounts of Ni were found in biotites from the gneiss and norite samples. The sublayer and footwall breccia biotites contain the highest amounts of Ni. When comparing barren and mineralized biotites, the mineralized samples contained substantially higher amounts of Ni. There were four footwall breccia samples analyzed. Three of the four samples were from the mineralized environment. Two of the three samples (CS107, CS124) from the mineralized embayment were from one drill hole while the other (CS127) was from the second drill hole. All of these samples, with the exception of two analyses from mafic norite, showed Ni contents exceeding ~500 ppm whereas biotites from the barren environment showed Ni contents consistently below this value. Some Ni contents reach more than ~0.1 wt% in the mineralized embayment.

Similarily, Cr concentrations are higher in most samples in the mineralized embayment, although a greater number of barren biotite grains show overlap with grains from the mineralized embayment. Figure 3.8 summarizes analyses of Ni and Cr in biotites, exemplifying the marked enrichment in both elements in grains analyzed from the mineralized system. Barren samples are also depleted in Y compared to the mineralized samples.

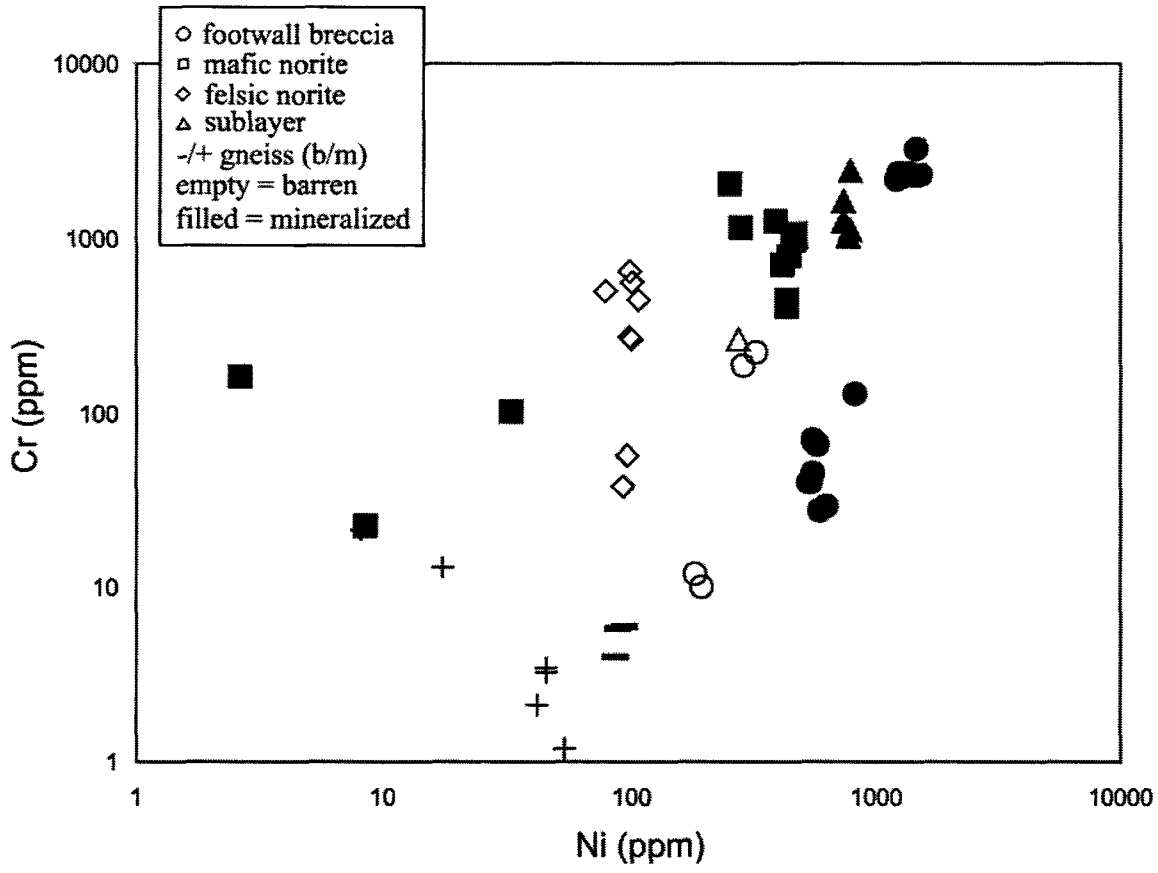

Figure 3.8. Biotite data showing Ni vs Cr concentrations and a pronounced enrichment in both elements in biotite grains from the mineralized embayment. Samples analyzed using a LA-ICP-MS.

3.6. Discussion

3.6.1 Comparison to other studies

McCormick and McDonald (1999) identified two distinct types of Cl-bearing amphibole in the footwall breccia, comprised of distinctly halogen poor and halogen rich phases. These two types have distinguishable optical properties. The halogen-poor phase is pale yellow to olive green in plane-polarized light, while the Cl-rich phase displays deep blue-green to green colour characteristic of amphiboles that are also enriched in alkalis (Na_2O and K_2O). These halogen-rich grains were also observed rimmed by ferrohastingsite and/or tschermakite. These two amphiboles are commonly associated with one another. The Cl-rich phase in the footwall breccia is also associated with and found in zones containing Cu-Ni mineralization and sulphides while the halogen-poor phase is commonly associated and found in barren zones. These two phases of amphibole are also associated with biotite and chlorite and commonly occur as rims on halogen-poor amphibole and as intergrowths with Cl-rich amphibole. Amphiboles are also associated, to a lesser degree, with orthopyroxene, clinopyroxene, epidote, and F-bearing apatite. These mineral associations were also present in rocks observed in this study, though to a varying degree depending on lithology. The majority of amphiboles in this study were classified as calcic (regardless of their halogen content), as were the samples examined by McCormick and McDonald (1999). The majority of amphibole grains observed and analyzed by McCormick and McDonald (1999) contain magnesiohornblende or actinolite cores and have lower concentrations of halogen elements (Cl + F = <0.5 wt. %). Amphiboles from this study were classified as actinolite, with two mineralized samples

classified as tremolite and another two as magnesiohornblende. Some rare amphibole grains contained up to 1.1 wt. % F. These distinct amphibole types were also observed in samples from this study, both geochemically and optically suggesting that the range in halogen contents may reflect analysis of different generations of amphibole in the samples.

Apatite is a unique mineral as it is one of the only volatile-bearing rock forming minerals found in stratiform mafic igneous complexes, such as the SIC. By sampling with respect to depth, microprobe analyses of apatite grains can lead to a greater understanding of the geochemistry in the evolving melt as detailed by relative proportions of F, Cl, and OH with respect to lithological contacts. Apatite occurrence and composition vary in different units of the SS, however it is found as an accessory phase in all units. Warner et al. (1998) described the distribution of apatite in the SS, including the SIC, Sudbury basin, and footwall. They were able to use bulk rock abundances of P2O5 to determine modal abundance of apatite at depth, a method that was also utilized in this study. The authors found that apatite at the bottom of the SIC (the lower norite units) is present as an intergranular accessory mineral, with less that 1% overall volume, while in the upper units it can be present in concentrations as high as 7% (in the quartz gabbro). A similar anomaly was observed in samples from this study; with vol. % apatite significantly greater in the quartz gabbro, granophyre and upper units, and its occurance lessen towards the footwall-Levack gneiss contact. The quartz gabbro shows an abrupt increase in bulk P (up to 2.9 wt.% P2O5). Warner et al. (1998) described changes in apatite chemistry and distribution in three areas of the Sudbury region. One of the three areas is located close to

the barren and mineralized zones discussed in this paper and the best locality for comparison. They determined that out of the three locations observed in the study, the apatites from the NW location yielded the best quantitative analyses. They concluded that apatites from this area are F-rich and Cl and OH abundances in apatite increase with depth in the SIC. The authors reported an increase in F with increasing depth. They also showed that the composition of apatite grains evolves up-section where the lowest units of the SIC exhibits Cl-rich, post-cumulus apatite grains that are enriched in LREE and the upper units exhibit F-rich cumulus and intergranular apatite. A significant increase in F with depth was not noticed in this study, but again can be attributed to the complexity of the Sudbury structure and its alteration history. The distribution of F varied, however F is hosted primarily in minerals and therefore is dependent on modal abundance and not as much on alteration like other halogens. Apatites from the "NW" section of their study were enriched in Cl, Na, Si, and LREE when compared to the "SW" and "NE" sections.

Halogen elements are also present as a solid phase in biotite. Biotites in this study contained 0.06 – 0.61 wt. % F and 0.2 – 0.35 wt. % Cl. A mineralogical study was conducted by Magyarosi et al. (2002). Several biotite grains from the Copper Cliff South mine were examined. Although this area is located in the South range of the Sudbury Structure, these data can still be used for comparison. They reported biotite as both a primary magmatic phase as well as secondary alteration. It is present as inclusions in massive sulphides, but also as a replacement mineral for amphibole in the quartz diorite. It is also present as an intergrowth with chlorite. All biotite grains in the Copper Cliff South area are classified as annite. Biotites from this study were primarily phlogopite,

however textural characteristics and occurance described by Magyarosi (2002) are much the same. Magyarosi et al. (2002) compared biotite grains from the south range. They found that biotites from the area were present both as primary magmatic phase and as an alteration mineral, similar to this study. The group discussed biotites present in massive sulphides and along/within sulphide veins are richer in Fe and Mn and poorer in M and Si. Though we did not find any massive suphides in the holes, these observations were compared to samples from the mineralized footwall breccia. We found Si to be lower in the barren environment but Mg fluctuates and is inconsistent in both lithology and increasing depth. Fe and Mn are variable and do not correlate well, although there is more Mn in the mineralized environment. Magyarosi et al. (2002) also noted that Cl content in biotites are generally greater in samples that contain PGM, but never exceeds 0.2 wt. %. We found that there is no Cl pattern within biotites, but Cl values do exceed 0.2 wt. % in several samples from all lithologies. Individual samples from the south range show a positive correlation between Fe and Cl, especially in samples containing PGM. This phenomenon was not present in our study. Biotite grains from massive sulphides and within sulphide veins are enriched in Fe and Mn and depleted in Mg and Si. The Cl content of biotites is generally greater in samples containing platinum-group minerals, but no sample exceeded 0.2 wt. % Cl. This pattern was also observed in apatites from this study as maximum Cl in barren apatite was 0.49 wt.% and mineralized was 0.39 wt.%. Positive correlations between Fe and Cl were present in many samples, especially samples containing platinum-group minerals. Ratios of Cl/(Cl+F) in biotites were plotted against Mg# (Figure 3.9). Mineralized amphiboles from footwall breccia contained more

F than Cl. All other mineralized samples as well most barren samples (except two barren footwall breccia samples) did not contain any detectable F. Biotite data were also plotted along with data from Sudbury breccia (Hanley and Mungall, 2003). No definitive correlation was present for any lithologies or either environment. However, most biotite analyzed lie within the magmatic compositional range for Ni-Cu-PGE-bearing mafic-ultramafic intrusions, characterized by high Mg/(Mg+Fe) ratios and typically low Cl/(Cl+F) contents. Similar to amphiboles, most biotite samples contain much more F than Cl. Also there is a slight depletion in Mg# for barren samples compared to the mineralized environment.

3.6.2 Preliminary estimates of minimum equilibration conditions

Biotite and apatite grains that showed equilibrium textures were analyzed by EMP for thermobarometric calculations. Details on the thermobarometric calculation are outlined in section 3.3.1. All EMP data and cation recalculations relevant to the calculations are summarized in Table 3.2. In total, six samples were analyzed for apatite-biotite thermobarometry. Two samples were from the barren environment, one of footwall breccia and the other of quartz gabbro. The other four samples were taken from the mineralized environment. One of the footwall breccia samples was taken from the upper hole, while the other two were taken from the lower hole. Thermobarometric calculations yielded minimum crystallization temperatures of ~320–680° C. Biotite-apatite pairs in samples from the barren environment yielded minimum crystallization temperatures ranging from of ~320° C in the quartz gabbro to ~370° C in the footwall breccia. Felsic

norite in the mineralized embayment yielded minimum crystallization temperatures of ~450-515° C, whereas The footwall breccia samples from the upper mineralized hole yielded crystallization temperatures of ~330-515° C and the lower hole was ~640-680° C. For comparison, the Al and Ti content of calcic amphibole grains were used in a graphical determination of final equilibration T and P (method of Ernst and Liu, 1998). The data for amphibole and apatite-biotite pairs are plotted together on a simplified P-T diagram showing isopleths of Al_2O_3 and TiO_2 (for amphibole) and solid lines for the T data from the apatite-biotite pairs (Figure 3.10). Amphiboles yielded similarily low temperatures (~400-450 °C for the barren embayment, and ~400-575 °C for mineralized environment)

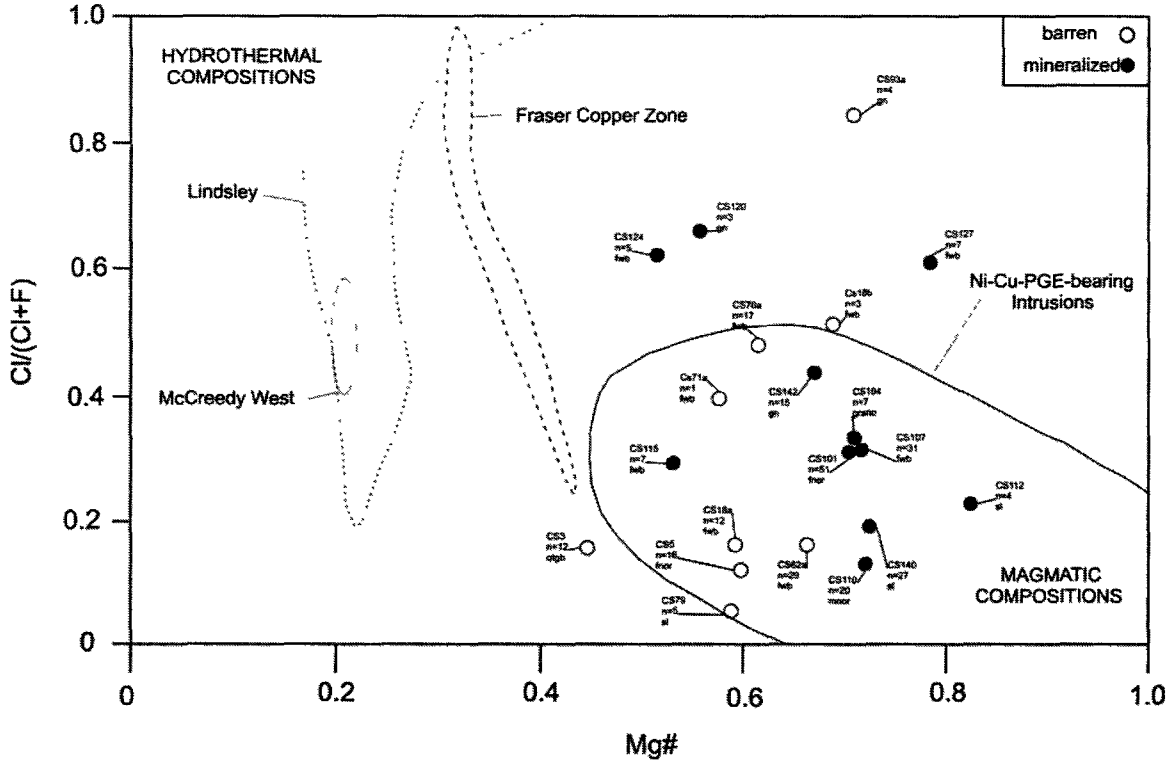

Figure 3.9. Mg# vs. Cl/(Cl+F) diagram for biotites. Lithologies: fwb = footwall breccia; fnor = felsic norite; sl = sublayer norite; grano= granophyre; gn = Levack gneiss. Fields from Farrow and Watkinson (1999). n = number represents number of analysis per sample.

and low pressures (0.1-0.6 GPa for barren, 0.1-0.5 GPa for mineralized) of final equilibration.

It must be noted that these calculations and diagrams describe the lowest pressure and temperature for exchange of the halogens, not just minimum temperature of crystallization, so the low temperature and pressures are not representative of the cooling of the SIC and associated units. These temperatures are well below hydrous granitic solidus temperatures indicating that significant halogen exchange occurred long after the emplacement of the footwall breccia. For comparison, Holz et al (1992) reported a crystallization temperature of ~780 °C for a granitic melt with a high water activity. Significant down-temperature requilibration occurred and that primary halogen abundances in the minerals cannot possibly be preserved. However, it is interesting to note that final halogen exchange occurred at lower temperatures at shallower depths in the mineralized hole. The reasons for this are unknown at present.

Table 3.2. Electron microprobe analyses (EMP) of apatite and biotite pairs from various lithologies of the Sudbury Structure

Apatite data	**Barren**				**Mineralized**												
Sample	CS3	CS3	CS62a	CS62a	CS101	CS101	CS101	CS101	CS107	CS107	CS107	CS115	CS115	CS124	CS124	CS124	CS124
Lithology	qtgb	qtgb	fwb	fwb	fnor	fnor	fnor	fnor	fwb	fwb	fwb	fwb	fwb	fwb	fwb	fwb	fwb
CaO (wt%)	57.34	57.29	56.85	56.25	55.96	55.62	56.40	56.21	54.75	54.40	54.66	56.23	56.44	52.79	52.80	52.52	51.93
P_2O_5	42.75	41.97	41.32	42.13	41.31	40.70	41.30	41.23	41.07	41.19	41.19	41.11	41.82	38.62	38.73	38.58	37.84
La_2O_3	0.48	0.45	0.48	0.50	0.48	0.53	0.52	0.52	0.26	0.27	0.25	0.23	0.20	1.16	1.33	1.33	1.44
Ce_2O_3	0.11	0.10	0.08	0.08	0.14	0.12	0.13	0.10	0.12	0.08	0.08	0.10	0.11	0.13	0.15	0.12	0.16
SO_3	0.08	0.08	0.07	0.09	0.07	0.07	0.08	0.07	0.09	0.11	0.10	0.08	0.07	0.64	0.77	0.76	0.84
F	3.83	3.80	4.00	3.93	3.66	3.63	3.77	3.78	3.67	3.64	3.74	3.92	3.82	3.43	3.54	3.41	3.52
Cl	0.64	0.63	0.27	0.44	0.44	0.47	0.43	0.28	0.89	0.67	0.71	0.27	0.27	0.06	0.07	0.06	0.06
Total	105.23	104.32	103.07	103.41	102.05	101.14	102.63	102.18	100.84	100.36	100.74	101.95	102.73	96.83	97.40	96.78	95.79
[1] *Thermobarometric parameters from apatite recalculation*																	
X_F	0.87	0.88	0.94	0.91	0.86	0.86	0.88	0.89	0.87	0.87	0.89	0.92	0.89	0.85	0.87	0.85	0.89
X_{Cl}	0.08	0.08	0.03	0.06	0.06	0.06	0.05	0.04	0.11	0.09	0.09	0.03	0.03	0.01	0.01	0.01	0.01
X_{OH}	0.05	0.05	0.03	0.03	0.09	0.08	0.06	0.08	0.01	0.05	0.02	0.04	0.08	0.14	0.12	0.15	0.11
X_F/X_{OH}	18.41	19.27	29.68	26.39	10.05	10.97	13.90	11.61	62.36	18.26	48.14	22.55	11.63	5.96	7.54	5.77	8.27
[2] *Thermobarometric parameters from coexisting biotite recalculation*																	
X_F	0.01	0.01	0.04	0.04	0.07	0.07	0.06	0.06	0.06	0.08	0.07	0.03	0.04	0.08	0.08	0.06	0.16
X_{Cl}	0.01	0.02	0.00	0.01	0.01	0.01	0.00	0.01	0.01	0.01	0.01	0.01	0.01	0.01	0.01	0.01	0.01
X_{OH}	0.99	0.98	0.96	0.95	0.92	0.92	0.94	0.94	0.93	0.91	0.92	0.95	0.95	0.91	0.91	0.93	0.83
X_{Fe}	0.54	0.57	0.32	0.30	0.27	0.28	0.27	0.27	0.30	0.24	0.24	0.51	0.48	0.45	0.45	0.47	0.31
X_F/X_{OH}	0.01	0.01	0.04	0.04	0.08	0.08	0.06	0.06	0.06	0.09	0.07	0.04	0.04	0.09	0.09	0.06	0.19
Thermobarometric calculations																	
[3] $K_{D,F}$	7.91	8.18	6.61	6.43	4.82	4.93	5.39	5.24	6.97	5.32	6.49	6.45	5.63	4.21	4.43	4.50	3.77
[4] **T (°C)**	**331**	**321**	**358**	**368**	**515**	**504**	**450**	**467**	**327**	**445**	**344**	**431**	**498**	**670**	**636**	**636**	**680**

[1]Determined from apatite compositions recalculated assuming 2 OH and 12 (OH, O, F, Cl)

[2]Determined from biotite compositions recalculated assuming 2 OH and 24 (OH, O, F, Cl)

[3]Calculated F-OH exchange coefficient for coexisting apatite-biotite using formulation of Zhu and Sverjensky (1992)

[4]Calculated temperature of final equilibration using the F-OH exchange thermometer expression of Zhu and Sverjensky (1992)

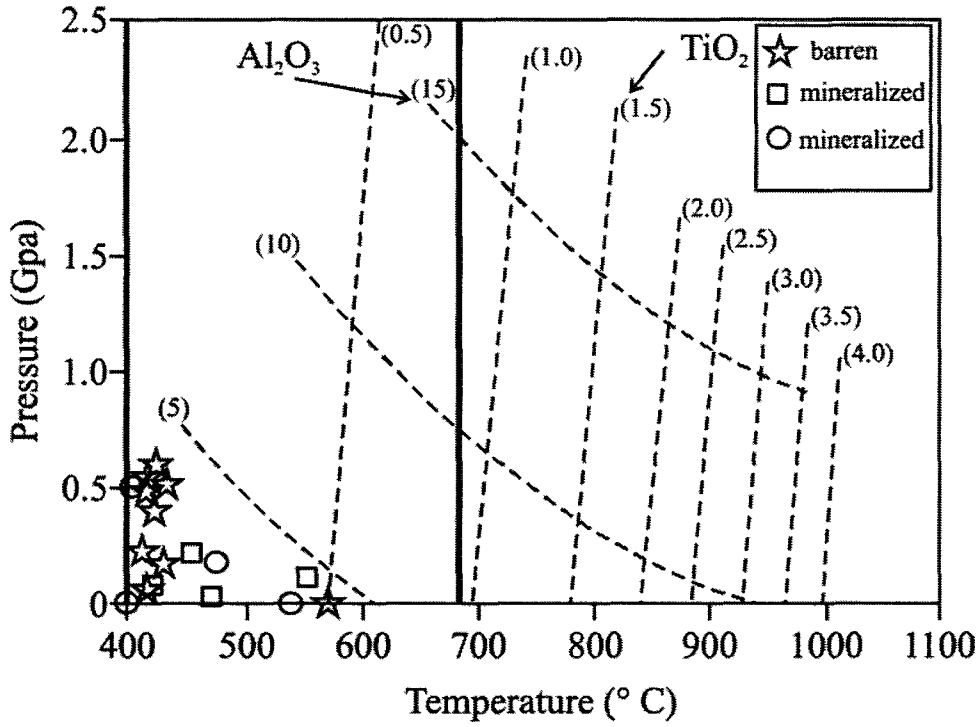

Figure 3.10. Ernst and Liu (1998) calcic amphibole thermobarometric diagram. Vertical lines (temperature sensitive) represent TiO_2 (wt%) abundances for amphibole grains while semi-horizontal lines (pressure sensitive) represent Al_2O_3 (wt%) abundances. Each point represents the average analyses for amphiboles from various samples. The vertical solid line represents the maximum crystallization temperatures for the mineralized environment calculated from biotite-apatite thermometry. The minimum temperature from biotite-apatite thermometry for the mineralized environment and the range in temperatures by this method for the barren environment calculated by this method (320 – 370 °C) are outside of the T range for this diagram.

3.6.3 Variations in mineral chemistry by rock type and environment

Relevant mineral data were evaluated in graphic logs showing the distribution and changes in data with respect to lithology and depth. Such graphical techniques readily allow for observations of patterns and correlations within the data set. In the mineralized hole, it is evident that halogens and some major elements within analyzed minerals correlate with one another. For example, in one of the two holes from the mineralized embayment, Cl and Al_2O_3 in amphibole increase with increasing depth. This correlation is apparent in both mineralized holes but are absent in the barren hole. In the shallow hole, they increase together with increasing depth in the felsic norite. There is a similar pattern in the deep hole where Al_2O_3 and Cl decrease with depth when moving from the footwall breccia to the basement gneiss.

A pattern was also observed in the apatite chemistry. Chlorine and F abundance in apatite are inversely correlated in the shallow mineralized hole but correlate in the deep mineralized hole and the barren hole.

3.6.4 Exploration implications and significance to the Sudbury ore-forming model

Though the focus of this study was on understanding the behaviour of halogens relation to ndiscordant footwall breccia plumes in the footwall deposits, the objective was to accumulate a criterion for locating zones of mineralization using bulk geochemical and mineralogical techniques associated with the halogens. Mineralogically, the two environments studied were more similar than anticipated. EMP mineral data did not indicate many significant differences between the two environments.

Three significant findings came from the study: (i) Ni and Cr enrichments occur in biotites from mineralized embayments; (ii) the final equilibration temperatures from halogen-bearing minerals in the mineralized embayment are higher and show a wider range than in the barren embayment but are still well below expected solidus conditions for the studied lithologies, and (iii) amphiboles in the mineralized embayment tend to be more enriched in Cl and F. Observation (ii) is particularly important because it demonstrates that all of the studied lithologies in the contact zone have re-equilibrated with hydrothermal solutions to low temperatures (321-368 °C in mineralized environment, 327-680 °C in barren environment) . The parameters described above require only EMP data to determine and evaluate.

3.7 Conclusions

Halogen mineral chemistry can be used to differentiate between zones of footwall breccia and associated lithologies that are mineralized and barren. The mineral chemistry of some halogen-bearing phases in the footwall breccias in the plumes are consistent with typical halogen-poor, high Mg# magmatic silicates as opposed to late stage, Fe- and Cl-rich hydrothermal silicates. Apatite-biotite and calcic amphibole thermobarometry for barren and mineralized samples of footwall breccia yielded minimum crystallization/re-equilibration temperatures of ~320-680°C and ~400-575 °C, respectively, and low pressures (<5 kbar). These conditions represent the lowest temperature at which halogen exchange occurred and indicate that remobilization of halogens by fluids and resetting of primary magmatic halogen chemistry in the minerals proceeded to temperatures well

below the solidus conditions for the footwall breccia. Biotites show significant enrichment in Ni and Cr in mineralized embayments and provide another valuable exploration indicator. This enrichment is important as it is possible to analyze Ni by EMP, allowing for a cheap and easily accessible method for locating mineralized zones for exploration using mineral chemistry. Aside from elevated Ni in biotites, and a possible enrichment (on average) of Cl and F in amphiboles from the mineralized embayment compared to the barren one, no other chemical characteristics of halogen-bearing minerals allow for discrimination between barren and mineralized embayments.

Chapter 4 - Conclusions

4.1 Significant findings

In this study, it has been shown that the absolute and relative abundances, and distribution of, the halogens in SIC main mass and contact lithologies are likely the result of complex magmatic-hydrothermal activity related to the incursion of partially melted footwall rocks and associated fluids into the still hot and partially crystallized SIC main mass. Various techniques were used to obtain a large variety of geochemical and mineralogical data that provides a preliminary understanding of the halogen budget of the magmatic rocks of the Sudbury environment. Overall, several key conclusions were drawn from the study, some with considerable significance to exploration for contact style deposits, and mineralized embayments in general:

1. With the exception of the halogens, the bulk rock geochemistry of all units studied (footwall country rock predating the SIC, contact lithologies, and SIC main mass units) are very similar and do not show any variation from mineralized to barren embayments. Slight variations (within an order of magnitude) in absolute trace element abundances vary within single embayments, and subtle enrichments and depletions in certain trace elements are recognized. These reflect primary magmatic processes (differentiation and fractionation) and not the accumulation of sulphides. Bulk rock analyses do not provide a good means for discrimination during exploration.

2. There are some significant differences in the halogen chemistry of the two environments. Whereas F is slightly higher in unmineralized (barren) footwall breccia, it shows significant (and inconclusive) variability in other lithologies. In mineralized embayments, sublayer is significantly more enriched in Br (up to 400%) compared to barren sublayer, and some footwall breccia and sublayer samples show highly anomalous I contents. While bulk rock halogen ratios were deemed not useful for discrimination (owing to the contribution of both soluble halogens from fluid inclusions, and insoluble halogens from minerals), the soluble halogen ratio Cl^-/Br^- (determined by analyses of leachates) is distinctly higher in barren lithologies, and must be related to variations in the relative abundance of high Cl^-/Br^- fluids trapped in inclusions.

3. Correlations between Cl, Br and I indicate that common sides of residence are controlling their abundance, most likely fluid inclusions. A weak correlation between Na_2O and Br suggests that albitization of feldspars in footwall breccias was linked to bulk rock enrichment in Br which in turn results in low Cl^-/Br^- ratios. Therefore, albitization of footwall breccia may be a mineralogical proxy for groundwater incursion during plume formation.

4. There were likely three dominant sources for halogens in the contact environment where footwall breccias developed. The first primary fluid source in the system was a low Cl^-/Br^- fluid originating from the footwall, the second was a high Cl^-/Br^- fluid originating

from the SIC, and the third was a high I phase that may have originated from the sulphides themselves during their crystallization.

5. While halogen-bearing minerals (apatite, amphibole, biotite) may contribute significantly to bulk rock F contents, and to a lesser extent Cl, there are no significant differences in major and minor element halogen-bearing mineral chemistry between the two environments. The major and minor element mineral compositions are also consistent, as are their abundances and general textural characteristics in relation to their host rocks. The bulk halogen and major element contents of amphibole and biotite are consistent with "magmatic" compositions recognized in other deposit types and lithologies at Sudbury, being relatively poor in F and Cl and having high Mg#, in contrast to the Cl-rich and Fe-rich varieties observed in "hydrothermal" deposits in the footwall deposits. Micas were primarily phlogopite with accessory biotite, and amphibole were primarily actinolite with some tremolite and magnesiohornblende.

6. Biotites from the mineralized environments are significantly enriched in Ni and Cr. Chromium abundances varied (for multiple analyses per sample) while Ni remained consistent. In particular, the enrichment in Ni may be detectable by electron microprobe. Whereas Ni is possibly remobilized from contact-style sulphides, Cr is unlikely to be significantly soluble in hydrothermal fluids and, therefore, may be locally derived.

7. Semiquantitative minimum crystallization temperatures for various phases in the footwall breccia (apatite-biotite, amphibole) indicate conditions well below the typical granite solidus, even at water-saturated conditions and the results of two independent thermombers are consistent with one another. Circulation of halogen-bearing fluids occurred long after both the SIC units and footwall breccia had solidified and shows that the halogen endowment of these minerals, despite being generally consistent with magmatic parentage, have been probably significantly modified by post-cumulus events.

8. Plumes in the mineralized environment are well defined. Extensive interaction between thick zones (concordant) and vertically extensive (discordant plumes) partially melted footwall materials with the SIC main mass units are manifested by a characteristic "footwall signature" for the halogens within mineralized embayments (for example, low Cl^-/Br^- ratios in leachates). This is in contrast to barren environments where minimal interaction between footwall partial melts and the SIC occurred, in which halogen ratios indicate a predominance of a primary "magmatic signature" (e.g., high Cl^-/Br^-).

9. Key exploration indicators to discriminate between footwall breccia occurring within a mineralized vs. barren embayment are anomalously high bulk I, low bulk Br/I ratios, low Cl^-/Br^- ratios in leachates, and Ni- and Cr-enrichment in biotites that reequilibrated with hydrothermal fluids at subsolidus temperatures. Bulk rock enrichments in Ni and Cu are not diagnostic of lithologies occurring within mineralized embayments.

4.2 Future work

There are few aspects of the study that could require more investigation. Halogens ratios and halogen discrimination diagrams provided insight into source of halogen-rich fluids migrating through the SIC and footwall breccia. However, it was shown clearly that bulk and soluble halogen analyses of such complex lithologies are somewhat ambiguous. Future work should focus on a comprehensive study of mineral Cl and O isotope analyses in order to better constraint source of the halogen-bearing fluids. A fluid inclusion study would also give further insight into the source and composition of fluids in the system. Fluid inclusion analysis would potentially yield composition of the original, primary fulids (from groundwater and magmatic sources) and their geochemical signature as trapped fluids within the rocks. The possible interaction of these two fluids has been previously indicated from fluid inclusion studies in the footwall (e.g., Marshall et al., 1999; Molnar et al., 2001; Hanley et al., 2004; Hanley et al., 2011), but a fluid inclusion study of the SIC and footwall breccia (which has never been undertaken) would produce additional data to support/refute the preliminary findings of this project. Due to the scope of this project and a focus on delineating exploration methods, a fluid inclusion study was not realistic.

A larger and more stratigraphically continuous sample set would improve uncertainties with some interpretations, particularly in the mineralized environment. Samples were collected from three boreholes: one from the barren environment and two from the mineralized environment but 99 samples were collected from the barren hole and only 46 from the mineralized holes.

Though at least half of the collected samples were from the footwall breccia, additional samples within this unit would have allowed confirming the validity of some of the discrimination diagrams proposed. Additional samples from other lithologies would provide a more statistically representative data set for the Sudbury Ni-Cu-PGE mining district.

References

Aiuppa, A., Baker, D. R., and Webster, J. D., 2009, Halogens in volcanic systems: Chemical Geology, v. 263, p. 1-18.

Ames, D.E., and Farrow, C.E.G., 2007, Metallogeny of the Sudbury mining camp, Ontario, *in* Goodfellow, W.D., ed., Mineral Deposits of Canada: A Synthesis of Major Deposit-Types, District Metallogeny, the Evolution of Geological Provinces, and Exploration Methods: Geological Association of Canada, Mineral Deposits Division, Special Publication No. 5, p. 329-350.

Ames, D. E., Watkinson, D. H., and Parrish, R. R., 1998, Dating of a regional hydrothermal system induced by the 1850 Ma Sudbury impact event: Geology, v. 26, no. 5, p. 447-450.

Aranovich, L. Y., and Newton, R. C., 1996, H2O activity in concentrated NaCl solutions at high pressures and temperatures measured by the brucite-periclase equilibrium: Contributions to Mineral Petrology, v. 125, p. 200-212.

Bai, T. B., and Koster van Groos, A. F., 1999, The distribution of Na, K, Rb, Sr, Al, Ge, Cu, W, Mo, La, and Ce between granitic melts and coexisting aqueous fluids: Geochimica et Cosmochimica Acta, v. 63, p. 1117-1132.

Berndt, M. E., and Seyfried Jr., W. E., 1990, Boron, bromine and other trace elements as clues to the date of chlorine in mid-ocean ridge vent fluids: Geochimica et Cosmochimica Acta, v. 54, p. 2235-2245.

Botcharnikov, R. E., Behrens, H., Holtz, F., Koepke, J., and Sato, H., 2004, Sulphur and chlorine solubility in Mt. Unzen rhyodacitic melt at 850 °C and 200 MPa: Chemical Geology, v. 213, p. 207-225.

Boudreau, A.E., Mathez, E.A., and McCallum, I.S., 1986a, Halogen geochemistry of the Stillwater and Bushveld Complexes: Evidence for transport of the platinum-group elements by Cl-rich fluids: Journal of Petrology, v. 27, p. 967-986.

Card, K.D., 1976, Geology of the Espanola-Whitefish Falls area. District of Sudbury: Ontario Division of Mines. Geosci. Rep. 131, p. 70.

Card, K.D., Gupta, V.K., McGrath, P.H., and Grant, F.S., 1984, The Sudbury Structure: Its Regional Geological and Geophysical Setting: The Geology and Ore Deposits of the Sudbury Structure, O.G.S. Special Volume 1, p. 25-44.

Carroll, M. R., and Holloway, J. R. (Eds.), 1994, Volatiles in magmas: Reviews of Mineralogy, p. 30.

Cathelineau, M., 1988, Cation site occupancy in chlorites and illites as a function of temperature: Clay Mineralogy, v. 23, p. 471-485.

Chandler, F.W., 1973, Clastic dykes at Whitefish Falls, Ontario and the base of the Huronian Gowganda Formation. In: Young, G.M. (Ed.), Huronian Stratigraphy and Sedimentation. Geological Association of Canada, Toronto, p. 199–209.

Churakov, S. V., Tkachenko, S. I., Korzhinskii, M. A., Bocharnikov, R. E., and Shmulovich, K. I., 2000, Evolution of composition of high-temoerature fumarolic gases from Kudryavy volcano, Ituruo, Kiril Islands: the thermodynamic modeling: Geochemical International, v. 38, p. 436-451.

Coats, C.J.A., Snajdr, P., 1984, Ore deposits of the North Range, Onaping-Levack area, Sudbury, *in* The Geology and Mineral Deposits of the Sudbury Structure, eds. E.G. Pye, A.J. Naldrett, P. Giblin, Ontario Geological Survey, Spec. Pub. No.1, p. 328-346.

Correns, C. W., 1956, The geochemistry of the halogens: Physics and Chemistry of the Earth, v. 1, p. 181-233.

De Caritat, P., Hutcheon, I., and Walshe, J. L., 1993, Chlorite Geothermometry: A review: Clays and Clay Minerals, v. 41, no. 2, p. 219, 239.

Dietz, R., 1960. Meteorite impact suggested by shatter cones in rock. Science, v. 73, p. 1781-1784.

Dietz, R.S., and Butler, L. W., 1964, Shatter-cones orientation at Sudbury, Canada: Nature, v. 204, p. 280-281.

Dixon, J. E., 1997, Degassing of alkalic basalts: American Mineralogist, v. 82, p. 368-378.

Dolejs, D., and Baker, D. R., 2004, Thermodynamic analysis of the system Na2O-K2O-CaO-Al2O3-SiO2-H2O-F2O-1: stability of fluorine-bearing minerals in felsic igneous suites: Contributions to Mineral Petrology, v. 146, p. 762-778.

Dolejs, D., and Baker, D. R., 2007, Liquidus equilibria in the system K_2O-Na_2O-Al_2O_3-SiO_2-$F2O_{-1}$-H2O to 100 MPa: I. Silicate-fluoride liquid immiscibility in anhydrous systems: Journal of Petrology, v. 48, p. 785-806.

Dressler, B.O., 1984, General Geology of the Sudbury Area, *in* The Geology and Mineral Deposits of the Sudbury Structure, eds. E.G. Pye, A.J. Naldrett, P. Giblin, Ontario Geological Survey, Spec. Pub. No.1, p. 57-82.

Dressler, B. O., Peredery, W. V., and Muir, T. L., 1992, Geology and mineral deposits of the Sudbury structure: Ontario Geological Survey Guidebook, v. 8, p. 38.

Duc-Tin, Q., Audetat, A., and Keppler, H., 2007, Solubility of tin in (Cl,F)-bearing aqueous fluids at 700 °C, 140 MPa: a LA-ICP-MS study on synthetic fluids inclusions: Geochimica et Cosmochimica Acta, v. 71, p. 3323-3335.

Ernst, W. G., and Liu, J., 1998, Experimental phase-equilibrium study of Al- and Ti-contents of calcic amphibole in MORB – A semiquantitative thermobarometer: American Mineralogist, v. 83, p. 952-969.

Farrow, C.E.G., 1994, Geology, alteration, and the role of fluids in Cu-Ni-PGE mineralization of the footwall rocks in the Sudbury Igneous Complex, Levack and Morgan Townships, Sudbury District, Ontario, Ph.D. thesis, Carleton University.

Farrow, C. E. G., Watkinson, D. H., and Jones, P. C., 1994, Fluid inclusions in sulphides from North and South Range Cu-Ni-PGE deposits, Sudbury Structure, Ontario: Economic Geology, v. 89, p. 647-655.

Femenias, O., Mercier, J.-C. C., Nkono, C., Diot, H., Berza, T., Tatu, M., and Demaiffe, D., 2006, Calcic amphibole growth and compositions in calc-alkaline magmas: Evidence from the Motru Dike Swarm (Southern Carpathians, Romania): American Mineralogist, v. 91, no. 1, p. 73-81.

Flynn, R. T., and Burnham, C. W., 1978, An experimental determination of rare earth partition coefficients between chloride containing capor phase and silicate melts: Geochimica et Cosmochimica Acta, v. 42, p. 658-701.

Foriel, J., Philippot, P., Rey, P., Somogyi, A., Banks, D., and Menez, B., 2004, Biological control of Cl/Br and low sulphate concentration in a 3.5-Gyr-oild seawater from North Pole, Western Australia: Earth and Planetary Science Letters, v. 228, p. 451-463.

Frape, S.K., and Fritz, P., 1987, Geochemical trends for groundwaters from the Canadian Shield; *in* Saline water and gases in crystalline rocks, Editors: Fritz, P., and Frape, S.K.: Geological Association of Canada Special Paper 33, p. 19-38.

Gao, S., Liu, Xiaomin, Yuan, Honglin, Hattendorf, Bodo, Gunther, Detlef, Chen, Liang, and Hu, Shenhong, 2002, Determination of forty two major and trace elements in USGS and NIST SRM glasses by laser ablation-inductively coupled plasma-mass spectrometry: The Journal of Geostandards and Geoanalysis, v. 26, n. 2, p. 181-196.

Giordano, D., Romano, C., Dingwell, D. B., Poe, B., and Behrens, H, 2004, The combined effects of water and fluorine on the viscosity of silicic magmas : Geochimica et Cosmochimica Acta, v. 68, p. 5159-5168.

Giordano, D., Russell, J. K., and Dingwell, D. B., 2008, Viscosity of magmatic liquids: A Model: Earth and Planetary Science Letters doi: 10.1016/j.epsl.2008.03.038.

Grieve, R. A. F., Stoffler, Dieter, and Deutsch, A., 1991, The Sudbury Structure: Controversial or Misunderstood?: Journal of Geophysical Research, v. 96(E5), p. 753-764.

Golightly, J.P., 1994, The Sudbury Igneous Complex as an Impact Melt: Evolution and Ore Genesis, *in* Proceedings of the Sudbury – Noril'sk Symposium, O.G.S. Special Volume 5, p. 105-117.

Hanley, J. J., and Mungall, J. E., 2003, Chlorine enrichment and hydrous alteration of the Sudbury breccia hosting footwall Ni-Cu-PGE mineralization at the Fraser mine, Sudbury, Ontario, Canada: The Canadian Mineralogist, v. 41, p. 857-881.

Hanley, J. J., Ames, D. E., Barnes, J., Sharp, Z., and Guillong, M., 2010, Interaction of magmatic fluids and silicate residues with saline groundwater in the footwall of the Sudbury Igneous Complex, Ontario, Canada: New evidence from bulk rock geochemistry, fluid inclusions and stable isotopes: Chemical Geology, in press.

Hanley, J. J., Mungall, J. E., Bray, C. J., and Gorton, M. P., 2004, The origin of bulk and water-soluble Cl and Br enrichments in ore-hosting Sudbury breccia in the Fraser Copper Zone, Strathcona Embayment, Sudbury, Ontario, Canada: The Canadian Mineralogist, v. 42, p. 1777-1798.

Hanley, J., Mungall, J., Pettke, T., Spooner, E., and Bray, C., 2005, Ore metal transport by hydrocarbon vapour in the footwall of the Sudbury igneous complex, Canada: Geochimica et Cosmochimica Acta, v. 69, p. A738.

Haynes, S.J., 1978, Joint determination of fluorine and chlorine in granitic rocks with ion-selective electrodes: Talanta, v. 25, p. 85-89.

Heinrich, C. A., 2007, Fluid-fluid interactions in magmatic-hydrothermal ore formation, In: Leibscher, A., and Heinrich, C. A. (Eds.), Fluid-fluid Interactions: Reviews in Mineralogy and Geochemistry, v. 65, p. 363-387.

Holloway, J. R., 1976, Fluids in the evolution of granitic magmas: consequences of finite CO_2 solubility: Geological Society of America Bulletin, v. 877, 1513-1518.

Holtz, F., Dingwall, D. B., and Behrens, H, 1993, Effects of F, B2O3, and P2O5 on the solubility of water in haplogranitic melts compared to silicate melts: Contributions to Mineral Petrology, v. 113, p. 491-501.

Ionov, D. A., Hofmann, A. W., Merlet, C., Gurenko, A. A., Hellebrand, E., Montagnac, G., Gillet, P., and Prikhodko, V. S., 2006, Discovery of whitlockite in mantle xenoliths: Inferences for water- and halogen-poor fluids and trace element residence in the terrestrial upper mantle: Earth and Planetary Science Letters, v. 244, is. 1-2, p. 201-217.

Jackson, S.E., 2008, LAMTRACE data reduction software for LA-ICP-MS, in, Laser Ablation-ICP-Mass Spectrometry in the Earth Sciences: Current Practices and Outstanding Issues (Sylvester, P., Ed.), Mineralogical Association of Canada (MAC) Short Course Series, v. 40, p. 305-307.

Jago, B.C., Morrison, G.G., Little, T.L., 1994, Metal Zonation Patterns and Microtextural and Mincromineralogical Evidence for Alkali- and Halogen-Rich Fluids in the Genesis of the Victor Deep and McCreedy East Footwall Copper Orebodies, Sudbury Igneous Complex: *in* Proceedings of the Sudbury – Noril'sk Symposium, O.G.S. Special Volume 5, p. 65-75.

Jambon, A., Deruelle, B., Dreibus, G., Pineau, F., 1995, Chlorine and bromine abundance in MORB: the contrasting behaviour of the Mid-Atlantic Ridge and East Pacific Rise and implications for chlorine geodynamic cycle: Chemical Geology, v. 126, p. 101-117.

Jochum, K. P., Willbold, M., Raczek, I., Stoll, B., and Herwig, K., 2005, Chemical characterization of the USGS reference glasses GSA-1G, GSC-1G, GSD-1G, GSE-1G, BCR-2G, BHVO-2G, and BIR-1G using EMPA, ID-TIMS, ID-ICPMS and LA-ICPMS: Geostandards and Geoanalytical Research, v. 29, p. 285-302.

Johns, W. D., and Huang, W. W. H., 1967, Distribution of chlorine in terrestrial rocks: Geochemica et Cosmochemica Acta, v. 31, p. 35-49.

Jowett, E. C., 1991, Fitting iron and magnesium into the hydrothermal chlorite geothermometer: GAC/MAC/SEG Joint Annual Meeting (Toronto, May 27-29, 1991), Program with Abstracts 16, A62.

Keppler, H., and Wyllie, P. J., 1991, Partitioning of Cu, Sn, Mo, W, U, and Th between melt and aqueous fluid in the systems haplogranite-H2O-HCl and haplogranite-H2O-HF: Contributions to Mineral Petrology, v. 109, P. 139-150.

Kiprianov, A. A., 2006, Regular trends in uptake of halogens by alkali silicate glasses containing two glass-forming components: Russian Journal of Applied Geochemistry, v. 79, p. 20-28.

Kiprianov, A.A., and Karpukhina, N. G., 2006, Oxyhalide silicate glasses: Glass Physics and Chemistry, v. 32, p. 1-27.

Kovalenko, N. I., 1977, Then reactions between granite and aqueous hydrofluoric acid in relations to the origin of fluorine-bearing granites: Geochimica, v. 4, p. 503-515.

Kullerud, K., 1995, Chlorine, titanium and barium-rich biotites: factors controlling biotite composition and implications for garnet-bearing geothermometry: Contributions to Mineral Petrology, v. 120, p. 42-59.

Lafrance, B., Legault, D., and Ames, D. E., 2008, The formation of the Sudbury breccia in the North Range of the Sudbury impact structure: Precambrian Research, v. 165, p. 107-119.

Lakomy, R., 1990, Implications for cratering mechanics from a study of the footwall breccia of the Sudbury impact structure, Canada: Meteoritics, v. 25, p. 195-207.

Larson, J. F., Knittle, E., and Williams, Q., 2003, Constraints on the speciation of hydrogen in earth's transition zone: Physics of the Earth and planetary interior, v. 136, p. 93-105.

Leake et al., 1997, Nomenclature of amphiboles: Report of the subcommittee on amphiboles of the international mineralogical association, commission on new minerals and mineral names: Canadian Mineralogist, v. 35, p. 219-246.

Liebermann, K. W., 1966, The determination of bromine in terrestrial and extraterrestrial materials by neutron activation analysis: Ph.D., University of Kentucky.

Lightfoot, P. C., Keays, R. R., Morrison, G. G., Bite, A., and Farrell, K. P., 1997, Geochemical relationships in the Sudbury igneous complex; origin of the main mass and offset dikes: Economic Geology, v. 92, no. 3, p. 289-307.

Lightfoot, P. C., and Farrow, C. E. G., 2002, Geology, geochemistry, and mineralogy of the Worthington Offset Dike: A genetic model for offset dike mineralization in the Sudbury Igneous Complex: Economic Geoology, v. 97, p. 1419-1446.

Long, D.G.F., Young, G.M., Rainbird, R.H., Fedo, C.M., 1999, Actualistic and non-actualistic Precambrian sedimentary styles: examples from the Proterozoic, north shore of Lake Huron. Field Trip B5 Guidebook. Geological Association of Canada–Mineralogical Association of Canada, Joint Annual Meeting, p. 50

Longerich, H.P., Jackson, S.E., and Günther, D., 1996, Laser Ablation-Inductively Coupled Plasma-Mass Spectrometric transient signal data acquisition and analyte concentration calculation: Journal of Analytical Atomic Spectrometry, v. 11, p. 899-904.

Luders, V., Banks, D. A., and Halbach, P., 2002, Extreme Cl/Br and ∂37Cl isotope fractionation in fluids of modern submarine hydrothermal systems: Mineralium Deposita, v. 37, p. 765-771.

Magyarosi, Z., Watkinson, D. H., and Jones, P. C., 2002, Mineralogy of Ni-Cu-Platinum-group element sulphide ore in the 800 and 810 orebodies, Copper Cliff South mine, and P-T-X conditions during the formation of platinum-group minerals: Economic Geology, v. 97, p. 1471-1486.

Manning, D. A. C., 1981, The effect of fluorine on liquidus phase relationships in the system Qz-Ab-Or with excess H2O at 1kb: Contributions to Mineral Petrology, v. 76, p. 206-215.

Markl, G, and Piazolo, S., 1998, Halogen-bearing minerals in syenites and high-grade marbles of Dronning Maud Land, Antarctica: monitors of fluid compositional changes during late-magmatic fluid-rock interaction processes: Contributions to Mineralogy and Petrology, v. 132, n. 3, p. 246-268.

Mathez, E. A., and Webster, J. D., 2005, Partitioning behaviour of chlorine and fluorine in the system apatite-silicate melt-fluid: Geochimica et Cosmochimica Acta, v. 69, n. 5, p. 1275-1286.

Matson, D. W., Muenow, D. W., and Garcia, M. O., 1984, Volatiles in amphiboles from xenoliths, Vulcan's Throne, Grand Canyon, Arizona, USA: Geochimica et Cosmochimica Acta, v. 48, p. 1629-1636.

McCormick, K. A., Fedorowich, J. S., McDonald, A. M., and James, R. S., 2002, A textural, mineralogical, and statistical study of the footwall breccia within the Strathcona Embayment of the Sudbury Structure: Economic Geology, v. 97, p. 125-143.

McCormick, K.A., Lesher, C.M., McDonald, A.M., Fedorowich, J.S., and James, R.S., 2002, Chlorine and Alkali Geochemical Halos in the Footwall Breccia and Sublayer Norite at the Margin of the Strathcona Embayment, Sudbury Structure, Ontario: Economic Geology, v. 97, p. 1509-1519.

McCormick, K. A., and McDonald, A. M., 1999, Chlorine-bearing amphiboles from the Fraser mine, Sudbury, Ontario, Canada: Description and crystal chemistry: The Canadian Mineralogist, v. 37, p. 1385-1403.

McDonough, W.F. (1998). Earth's core. In: Encyclopedia of geochemistry. Marshall, C.P. and Fairbridge, R.W. (Editors), Kluwer Academic Publishers, Dordrecht. 151-156.

McDonough, W.F. and Sun, S.-S. (1995). Composition of the Earth. Chemical Geology 120: 223-253.

Molnar, F., and Watkinson, D. H., 2001, Fluid-inclusion Data for Vein-type Cu-Ni-PGE Footwall Ores, Sudbury Igneous Complex and Their Use in Establishing an Exploration Model for Hydrothermal PGE-enrichment Around Mafic-Ultramafic Intrusions: Exploration and Mining Geology, v. 10, no. 1-2, p. 125-141.

Morrison, G. G., 1984, Morphological features of the Sudbury structure in relation to an impact origin: Ontario Geological Survey Special Volume 1, p. 513-520.

Morrison, G.G., Jago, B.C., and White, T.L., 1994, Footwall mineralization of the Sudbury Igneous Complex: Proceedings of the Sudbury-Noril'sk Symposium, O.G.S. Special Volume 5, p. 57-64.

Mungall, J. E., and Brenan, J. M., 2003, Experimental evidence for the chalcophile behaviour of the halogens: The Canadian Mineralogist, v. 41, p. 207-220.

Mungall, J. E., Ames, D. E., and Hanley, J. J., 2004, Crustal redistribution in large bolide impacts: geochemical evidence from the Sudbury Structure: Nature, v. 6990, p. 546-548.

Muramatsu, Y., and Wedepohl, K.H., 1998, The distribution of iodine in the earth's crust: Chemical Geology, v. 147, p. 201-216.

Nagaseki, H., and Hayashi, K., 2008, Experimental study of the behaviour of Cu and Zn in a boiling hydrothermal system: Geology, v. 36, p. 27-30.

Nahnybida, T., Gleeson, S. A., Rusk, B. G., and Wassenaar, L. I., 2009, Cl/Br ratios and stable chlorine isotope analysis of magmatic-hydrothermal fluid inclusions from Montana and Bungham Canyon, Utah: Mineralium Deposita, v. 44, p. 837-848.

Naldrett, A.J., 1999, Summary: Development of ideas on Sudbury geology, 1992-1998: Geological Society of America Special Paper 339, p. 431-442.

Naldrett, A. J., and Hewins, R. H., 1984, The Main Mass of the Sudbury Igneous Complex, *in* The Geology and Mineral Deposits of the Sudbury Structure, eds. E.G. Pye, A.J. Naldrett, P. Giblin, Ontario Geological Survey, Spec. Pub. No.1, p. 235-251.

Newsom, H. E., 1995, Composition of the solar system, planets, meteorites, and major terrestrial reservoirs: Global Earth Physics, A Handbook of Physical Constants, AGU Reference Shelf, v. 1, American Geophysical Union, Washington.

Newman, S., and Lowenstern, J. B., 2002, VOLATILECALC: a silicate melt H2O-CO2 solution model written in Visual Basic for excel: Computers and Geosciences, v. 28, 597-604.

Pattison, E. F., 1979, The Sudbury sublayer: The Canadian Mineralogist, v. 17, is. 2, p. 257-274.

Pearce, N.J.G., Perkins, W.T., Westgate, J.A., Gorton, M.P., Jackson, S.E., Neal, C.R., and Chenery, S.P., 1997, A compilation of new and published major and trace element data for NIST SRM 610 and NIST SRM 612 glass standard reference materials: Geostandards Newsletter, v. 21, p. 115-144.

Peiffert, C., Nguyen-Trung, C., and Cuney, M., 1996, Uranium in granitic magmas: part 2: Experimental determination of uranium solubilita and fluid-melt partition coefficient in the uranium oxide-haplogranite-H2O-NaX (X= Cl, F) system at 770 °C, 2 kbar: Geochimica et Cosmochimica Acta, v. 60, p. 1515-1529.

Pentak, A., Molnar, F., Watkinson, D. H., Jones, P. C., 2008, Footwall-type Cu-Ni-PGE Mineralization in the Broken Hammer Area, Wisner Township, North Range, Sudbury Structure: Economic Geology, v. 103, n. 5, p. 1005-1028.

Peredery, W. V., and Morrison, G. G., 1984, Discussion of the Origin of the Sudbury Structure *in* The Geology and Ore Deposits of the Sudbury Structure, edited by E. G. Pye, A. J. Naldrett, and P. E. Giblin, Ontario Geological Survey, Special Volume 1, p. 491.

Rocholl, A., 1998, Major and trace element composition and homogeneity of microbeam reference material: Basalt glass BCR-2G: Geostandard Newsletter, v. 22, p. 33-45.

Seufert, H. M., and Jochum, K. P., 1997, Trace element analysis of geological glasses by laser plasma ionization mass spectrometry (LIMS): A comparison with other multielement and microanalytical methods: Fresenius Journal of Analytical Chemistry, v. 359, p. 454-457.

Shinonaga, T., Ebihara, M., Nakahara, H., Tomura, K., and Heumann, K. G., 1994, Cl, Br, and I in igneous standard rocks: Chemical Geology, v. 115, p. 213-225.

Simon, A. C., Frank, M. R., Pettke, T., Candela, P A., Piccoli, P. M., and Heinrich, C. A., 2005, Gold partitioning in melt-vapour-brine systems: Geochimica et Cosmochimica Acta, v. 69, p. 3321-3335.

Smith, J. V., 1981, Halogen and phosphorus storage in the Earth: Nature, v. 289, p. 762-765.

Smith, J. V., Delaney, J. S., Hervig, R. L., and Dawson, J. B., 1981, Storage of F and Cl in the upper mantle: geochemical implications: Lithos, v. 14, p. 133-147.

Symonds, R. B., Rose, W. I., Gerlach, T. M., Briggs, P. H., and Harmon, R. S., 1990, Evaluation of gases, condensates, and SO2 emissions from Augustine volcano, Alaska: the degassing of a Cl-rich volcanic system: Bulletin of Volcanology, v. 52, p. 355-374.

Symonds, R. B., Reed, M. H., and Rose, W. I., 1992, Origin, speciation, and fluxes of trace-element gases at Augustine volcano, Alaska: Insights into magma degassing and fumarolic processes: Geocimica et Cosmochimica Acta, v. 56, p. 633-657.

Symonds, R. B., Rose, W. I., Bluth, G. J. S., and Gerlach, T. M., 1994, Volcanic-gas studies: methods, results and applications, In: Carroll, M. R., Holloway, J. R., (Eds.), Volatiles in Magmas: Rev. Mineral., v. 30, p. 1-66.

Sugiura, T., 1968, Bromine to chlorine ratios in igneous rocks: Bulletin of the Chemical Society of Japan, v. 41, p. 1133

Sugiura, T., Mizutani, Y., Oana, S., 1963, Fluoine, chlorine, bromine and iodine in volcanic gases: Journal of Earth Sciences Nagoya University, v. 11, p. 272.

Therriault, A. M., Fowler, A. D., and Grieve, R. A. F., 2002, The Sudbury Igneous Complex: A Differentiated Impact Melt Sheet: Economic Geology, v. 97, p. 1521-1540.

Uitterdijk Appel, P. W., 1997, High bromine contents and low Cl/Br ratios in hydrothermally altered Archean komatiitic rocks, West Greenland: Precambrian Research, v. 82, p. 177-189.

Warner, S., Martin, R.F., Abdel-Rahman, A., and Doig, R., 1998, Apatite as a monitor of fractionation, degassing, and metamorphism in the Sudbury Igneous Complex, Ontario: Canadian Mineralogist, v. 36, p. 981-999.

Webster, J. D., 1990, Partitioning of F between H2O +- CO2 fluids and topaz rhyolite melt: implications for mineralizing magmatic-hydrothermal fluids in F-rich granitic systems: Contributions to Mineral Petrology, v. 104, p. 424-438.

Webster, J. D., 1992, Fluid-melt interactions involving Cl-rich granites: experimental study from 2 to 8 kbar: Geochimica et Cosmochimica Acta, v. 56, p. 679-687.

Webster, J. D., Hollowat, J. R., and Hervig, R. L., 1989, Partitioning of lithophile trace elements between topaz rhyolite melt and H2O and H2O + CO2 fluids: Economic Geology, v. 84, p. 116-134.

Webster, J. D., and DeVivo, B., 2002, Experimental and modeled solubilities of chlorine in aluminosilicate melts, consequences of magma evolution, and implications for exsolution of hydrous chloride melt at Mt. Somma-Vesuvius: American Mineralogist, v. 87, p. 1046-1061.

Wedepohl, K. H. (ed.), 1974, Handbook of Geochemistry, II/4, p. 35-E-1 to 35-E-5 and p. 53-E-3 to 53-E-5.

Webster, J. D., and Thomas, R., 2006, Silicate melt inclusions in felsic plutons: a synthesis and review: in: Webster, J. D. (Ed.), Melt Inclusions in Plutonic Rocks: Mineralogical Association of Canada, v. 36, p. 165-188.

Wedepohl, K.H. (1995). The composition of the continental crust. Geochimica et Cosmochimica Acta 59: 1,217-1,239.

White, W. M., 2005, Geochemistry: on line text book. http://www.geo.cornell.edu/geology/classes/geo455/chapters.html.

Williams, T. J., Candela, P. A., and Piccoli, P. M., 1995, The partitioning of Cu between silicate melt and 2-phase aqueous fluids – an experimental investigation at 1 kbar, 800 °C and 0.5 kbar, 850 °C: Contributions to Mineral Petrology, v. 121, p. 388-399.

Williams-Jones, A. E., and Heinrich, C. A., 2005, Vapour transport of metals and the formation of magmatic-hydrothermal ore deposits: Economic Geology, v. 100 (7), p. 1287-1312.

Wu, J., Milkereit, B., and Boerner, D., 1994, Timing constraints on deformation history of the Sudbury Impact Structure: Canadian Journal of earth Sciences, v. 31, p. 1654-1660.

Xiong, X., Zhao, A., Zhu, J., Bing, R., and Lai, M., 1998, Partitioning of F between aqueous fluids and albite granite melt and its petrogenetic and metallogenetic significance: Chinese Journal of Geochemistry, v. 17, p. 303-310.

Yardley, B. W. D., 2005, Metal concentrations in crustal fluids and their relationship to ore formation: Economic Geology, v. 100, p. 613-632.

Yoshida, M., Takahashi, K., Yonehara, N., Ozawa, T., and Iwasaki, I., 1971, The fluorine, chlorine, bromine, and iodine contents of volcanic rocks in Japan: Bulletin of the Chemical Society of Japan, v. 44, p. 1844.

Young, G.M., 1973, Origin of carbonate-rich early Proterozoic Espanola Formation, Ontario, Canada: Geological Society of America Bulletin 84, p. 135–160.

Young, G.M., 1983, Tectono-sedimentary history of Early Proterozoic rocks of the northern Great Lakes region. Geol. Soc. Am. Mem. 160, p. 15–32.

Young, G. M., Shaw, C. S. J., and Fedo, C. M., 2004, New evidence favouring an endogenic origin for supposed impact breccias in Huronian (Paleoproterozoic) sedimentary rocks: Precambrian Research, v. 133, is. 1-2, p. 63-74.

Zhu, C., and Sverjensky, D. A., 1992, F-Cl-OH partitioning between biotite and apatite: Geochimica et Cosmochimica, v. 56, p. 3435-3467.

Appendices

Element	SiO_2 (wt. %)	TiO_2	Al_2O_3	Fe_2O_3	MnO	MgO	CaO	Na_2O	K_2O	P_2O_5	LOI	Total
Detect Limit	0.01	0.01	0.01	0.01	0.01	0.01	0.01	0.01	0.01	0.01	0.05	
CS10	59.03	0.47	17.46	4.88	0.06	3.68	5.97	6.07	0.75	0.31	1.54	100.24
CS12	57.12	0.52	16.37	5.9	0.09	5.89	5.83	5.27	0.62	0.37	2.28	100.26
CS13	60.49	0.23	18.7	3.81	0.05	2.63	4.8	6.34	1.35	0.19	1.36	99.94
CS17	61.12	0.39	17.98	4.87	0.06	2.74	5.83	5.02	0.95	0.18	0.98	100.13
CS18	60.24	0.37	17.73	5.14	0.06	3.48	4.95	5.18	1.1	0.25	1.69	100.19
CS19	60.29	0.25	19.11	3.82	0.05	2.24	5.93	5.68	1.07	0.22	1.21	99.87
CS20	59.9	0.4	18.44	4.6	0.06	2.38	5.7	5.45	1.07	0.29	1.67	99.96
CS22	62.96	0.29	18.28	2.43	0.03	2.15	4.73	7.22	0.98	0.21	1.15	100.44
CS24	50.5	0.92	13.74	9.04	0.14	9.41	9.91	2.67	0.42	0.71	2.65	100.13
CS27	57.78	0.39	17.85	5.4	0.07	3.58	6.26	4.96	1.13	0.31	2.11	99.86
CS31	61.66	0.29	18.78	3.56	0.04	1.91	4.95	5.86	1.21	0.2	1.55	100.02
CS34	55.62	0.82	17.9	5.45	0.07	5.54	4.58	6.24	0.33	0.46	2.86	99.87
CS35	61.93	0.38	16.78	4.26	0.05	3.21	2.79	6.98	0.91	0.3	2.2	99.78
CS42	60.84	0.37	10.67	10.06	0.11	6.29	4.69	2.13	1.14	0.06	3.64	100
CS47	61.57	0.47	17.05	4.92	0.07	2.51	5.54	5.54	1.24	0.27	1.14	100.32
CS49	60.3	0.48	16	5.64	0.09	3.67	5.81	5.32	0.91	0.27	1.62	100.09
CS51	64.3	0.39	16.93	4.2	0.06	1.95	4.18	5.64	1.16	0.21	1.35	100.37
CS56	59.33	0.32	17.17	5.24	0.08	3.89	5.38	5.24	0.93	0.16	2.03	99.78
CS57	55.03	0.35	14.38	8.42	0.12	7.01	8.39	3.29	1.04	0.13	1.54	99.7
CS58	51.68	0.29	13.18	10.78	0.16	9.15	7.92	2.03	1.22	0.06	2.66	99.12
CS60	56.28	0.37	10.29	10.56	0.14	9.55	6.36	2.93	0.26	0.09	2.86	99.69
CS66	54.42	0.36	11.84	13.58	0.11	6.03	4.72	2.11	1.89	0.09	4.09	99.23
CS68	53.74	0.3	13.43	11.24	0.15	6.87	6.61	2.66	0.81	0.06	2.79	98.66
CS69	55.6	0.29	12.66	11.47	0.14	8.48	5.12	2.06	1.59	0.09	2.34	99.84
CS70	58.46	0.49	15.63	5.96	0.11	4.18	6.92	4.98	0.82	0.27	1.72	99.56
CS71	64.46	0.39	16.4	4.42	0.07	1.87	4.62	5.36	1.56	0.23	1.03	100.4
CS73	65.65	0.42	16.14	4.06	0.05	1.7	4.12	5.08	1.53	0.2	0.87	99.84
CS76	62.4	0.45	16.44	4.36	0.07	2.31	6.02	5.44	1.16	0.23	1.52	100.41
CS84	50.97	0.77	12.89	12.02	0.18	8.74	9.94	2.19	0.64	0.15	1.23	99.72
CS85	52.34	0.89	14.62	11.83	0.18	8.35	7.26	2.55	0.76	0.25	1.05	100.09
CS89	65.13	0.37	15.58	4.48	0.07	2.2	4.48	4.97	1.57	0.19	0.98	100.02
CS90	67.28	0.4	14.85	3.86	0.06	2.18	3.29	5.54	1.53	0.14	1.13	100.26
σ =	4.36	0.17	2.37	3.10	0.04	2.59	1.60	1.56	0.37	0.13	0.79	0.38
Minimum	50.5	0.23	10.29	2.43	0.03	1.7	2.79	2.03	0.26	0.06	0.87	98.66
Maximum	67.28	0.92	19.11	13.58	0.18	9.55	9.94	7.22	1.89	0.71	4.09	100.44
Average	59.01	0.43	15.79	6.57	0.09	4.56	5.74	4.63	1.05	0.22	1.84	99.93

A1: Bulk rock major element data for footwall breccia in barren environment. Sample depth increases with sample number.

Element	SiO_2 (wt. %)	TiO_2	Al_2O_3	Fe_2O_3	MnO	MgO	CaO	Na_2O	K_2O	P_2O_5	LOI	Total
Detect Limit	0.01	0.01	0.01	0.01	0.01	0.01	0.01	0.01	0.01	0.01	0.05	
CS107	58.31	0.44	15.68	7.27	0.13	6.4	6.55	3.72	0.67	0.22	0.5	99.89
CS115	61.71	0.66	16.1	5.27	0.07	2.62	5.77	5.34	0.9	0.22	0.93	99.6
CS119	66.77	0.49	15.39	4.82	0.07	1.47	4.47	4.7	1.21	0.14	0.75	100.29
CS122	55.68	0.84	14.5	10.13	0.16	4.88	7.52	3.42	1.18	0.12	1.34	99.75
CS124	67.67	0.29	15.71	4	0.05	1.3	3.46	4.91	2.09	0.09	0.91	100.47
CS127	55.17	0.68	15.01	9.5	0.17	5.73	7.29	3.89	0.61	0.2	1.38	99.65
CS137	65.27	0.13	19.48	1.98	0.03	0.85	5.51	5.85	1.01	0.05	0.39	100.54
σ =	4.84	0.23	1.51	2.75	0.05	2.13	1.37	0.83	0.46	0.06	0.35	0.37
Minimum	55.17	0.13	14.5	1.98	0.03	0.85	3.46	3.42	0.61	0.05	0.39	99.6
Maximum	67.67	0.84	19.48	10.13	0.17	6.4	7.52	5.85	2.09	0.22	1.38	100.54
Average	61.51	0.50	15.98	6.14	0.10	3.32	5.80	4.55	1.10	0.15	0.89	100.03

A2: Bulk rock major element data for footwall breccia in mineralized environment. These data are collected from two different boreholes, however they are both located in the same mineralized environment, spereated by ~100m.

Element	SiO_2 (wt. %)	TiO_2	Al_2O_3	Fe_2O_3	MnO	MgO	CaO	Na_2O	K_2O	P_2O_5	LOI	Total
Detect Limit	0.01	0.01	0.01	0.01	0.01	0.01	0.01	0.01	0.01	0.01	0.05	
Barren												
MNOR												
CS43	41.33	2.95	8.21	17.39	0.27	11.67	13.62	0.39	0.24	0.29	3.16	99.53
CS44	31.48	0.23	6.32	39.41	0.11	6.79	4.37	1.07	0.38	0.05	8.00	98.21
FNOR												
CS4	56.60	0.45	17.09	7.42	0.12	5.54	7.36	2.86	1.24	0.11	1.30	100.10
CS5	57.00	0.46	17.06	7.46	0.13	5.29	7.14	2.92	1.33	0.12	1.18	100.09
CS9	57.80	0.33	16.42	6.37	0.09	5.27	5.29	4.45	1.05	0.07	2.72	99.86
CS37	57.94	0.34	16.07	6.51	0.09	5.10	5.71	4.08	2.21	0.17	2.44	100.65
CS38	59.60	0.48	15.41	5.57	0.07	4.74	2.29	5.37	1.96	0.16	2.81	98.46
CS40	61.01	0.43	14.70	5.75	0.07	5.93	1.72	4.41	2.37	0.18	3.37	99.95
Minimum	31.48	0.23	6.32	5.57	0.07	4.74	1.72	0.39	0.24	0.05	1.18	98.21
Maximum	61.01	2.95	17.09	39.41	0.27	11.67	13.62	5.37	2.37	0.29	8.00	100.65
Average	52.85	0.71	13.91	11.99	0.12	6.29	5.94	3.19	1.35	0.14	3.12	99.61
Mineralized												
MNOR												
CS110	59.58	0.47	10.21	10.13	0.17	10.42	4.22	2.20	1.31	0.13	0.67	99.52
FNOR												
CS101	59.07	0.28	16.72	6.97	0.11	5.68	6.39	3.30	0.99	0.11	0.68	100.30
Minimum	59.07	0.28	10.21	6.97	0.11	5.68	4.22	2.20	0.99	0.11	0.67	99.52
Maximum	59.58	0.47	16.72	10.13	0.17	10.42	6.39	3.30	1.31	0.13	0.68	100.30
Average	59.33	0.38	13.47	8.55	0.14	8.05	5.31	2.75	1.15	0.12	0.68	99.91

A3: Bulk rock major element data for barren and mineralized norite.

Element	SiO_2 (wt. %)	TiO_2	Al_2O_3	Fe_2O_3	MnO	MgO	CaO	Na_2O	K_2O	P_2O_5	LOI	Total
Detect Limit	0.01	0.01	0.01	0.01	0.01	0.01	0.01	0.01	0.01	0.01	0.05	
Barren												
CS78	49.6	0.47	7.39	14.89	0.21	13.02	10.28	0.97	0.5	0.12	1.47	98.91
CS79	48.3	0.82	11.81	15.31	0.21	9.38	8.84	1.91	0.62	0.18	2.3	99.68
CS80	51.05	0.62	10.23	12.42	0.2	12.61	7.93	1.41	0.6	0.23	2.11	99.42
σ =	1.12	0.14	1.83	1.27	0.00	1.63	0.97	0.38	0.05	0.04	0.36	0.32
Minimum	48.3	0.47	7.39	12.42	0.2	9.38	7.93	0.97	0.5	0.12	1.47	98.91
Maximum	51.05	0.82	11.81	15.31	0.21	13.02	10.28	1.91	0.62	0.23	2.3	99.68
Average	49.65	0.64	9.81	14.21	0.21	11.67	9.02	1.43	0.57	0.18	1.96	99.34
Mineralized												
CS112	49.67	0.27	4.02	13.59	0.18	19.82	8.64	0.75	0.35	0.06	2.73	100.09
CS133	40.24	0.34	4.47	26.36	0.22	18.24	7.02	0.38	0.17	0.05	0.79	98.29
CS139	56	0.15	20.98	5.13	0.08	2.94	7.42	5.49	0.66	0.17	0.76	99.79
CS140	58.06	0.51	10.41	10.24	0.17	10.53	4.4	2.2	1.66	0.17	1.01	99.36
σ =	6.94	0.13	6.84	7.84	0.05	6.73	1.55	2.01	0.58	0.06	0.82	0.68
Minimum	40.24	0.15	4.02	5.13	0.08	2.94	4.4	0.38	0.17	0.05	0.76	98.29
Maximum	58.06	0.51	20.98	26.36	0.22	19.82	8.64	5.49	1.66	0.17	2.73	100.09
Average	50.99	0.32	9.97	13.83	0.16	12.88	6.87	2.21	0.71	0.11	1.32	99.38

A4: Bulk rock major element data for barren and mineralized sublayer norite.

Element	SiO_2 (wt. %)	TiO_2	Al_2O_3	Fe_2O_3	MnO	MgO	CaO	Na_2O	K_2O	P_2O_5	LOI	Total
Detect Limit	0.01	0.01	0.01	0.01	0.01	0.01	0.01	0.01	0.01	0.01	0.05	
Barren												
CS93	68.65	0.45	14.71	4.44	0.06	1.33	3.76	4.39	1.4	0.15	0.67	100
CS95	66.14	0.25	16.8	2.97	0.05	1.53	4.47	5.88	1.47	0.15	1.17	100.87
Mineralized												
CS116	57.21	0.69	13.04	7.45	0.12	8.48	7.46	3.08	1.03	0.44	0.73	99.74
CS120	68.1	0.47	15.11	4.5	0.07	1.16	3.92	4.67	1.44	0.14	0.74	100.33
CS123	64.63	0.44	15.3	5.02	0.08	1.99	5.24	4.81	1.1	0.1	1.13	99.84
CS142	58.43	0.57	15.99	6.7	0.1	4.66	6.41	4.21	1.53	0.25	0.84	99.68
CS143	66.58	0.36	17.03	3.38	0.04	1.23	4.31	5.33	1.21	0.11	0.85	100.44
σ =	4.26	0.13	1.26	1.52	0.03	2.54	1.28	0.82	0.18	0.11	0.18	0.40
Minimum	57.21	0.36	13.04	3.38	0.04	1.16	3.92	3.08	1.03	0.1	0.73	99.68
Maximum	68.1	0.69	17.03	7.45	0.12	8.48	7.46	5.33	1.53	0.44	1.13	100.44
Average	62.99	0.51	15.29	5.41	0.08	3.50	5.47	4.42	1.26	0.21	0.86	100.01

A5: Bulk rock major element data for barren and mineralized basement gneiss samples.

Element	Detect Limit	CS10	CS12	CS13	CS17	CS18	CS19	CS20	CS22	CS24	CS27	CS31	CS34
Ba (ppm)	0.8	339.3	265.1	525	548.5	539.7	648.2	613.8	474.5	733.7	613	795.9	105.1
Be	0.04	0.83	1.1	0.91	1.03	1.2	1.08	1.04	1.01	1.72	1.16	1.1	0.97
Cd	0.013	0.019	0.021	0.013	0.022	0.019	0.035	0.027	0.018	0.061	0.017	<0.013	0.026
Ce	0.12	87.04	56.17	24.84	26.51	39.01	25.56	31.89	26.2	126.86	53.71	27.61	92.45
Co	0.13	36.3	42.53	17.06	17.63	16.98	12.54	16.12	5.39	36.32	19.25	10.48	17.18
Cr	3	154	232	127	210	212	143	135	143	532	234	121	472
Cs	0.013	0.152	0.17	0.196	0.357	0.168	0.144	0.199	0.142	0.392	0.207	0.164	0.085
Cu	1.4	18.4	13.3	15.1	24.9	21.2	56.8	290.8	6.6	5	20	10.6	8.8
Dy	0.009	2.848	3.012	0.777	1.073	1.866	0.938	1.45	0.926	5.652	2.612	0.834	2.526
Er	0.007	1.206	1.466	0.36	0.502	0.883	0.436	0.682	0.426	2.573	1.26	0.376	1.032
Eu	0.0031	1.29	1.433	0.887	0.957	1.222	0.971	1.138	0.892	2.917	1.54	0.949	1.411
Ga	0.04	20.02	18.52	21.04	23.08	22.56	23.49	23.54	21.09	20.5	23.7	22.85	20.03
Gd	0.009	5.342	4.552	1.291	1.673	2.902	1.489	2.269	1.508	9.297	4.089	1.447	4.441
Hf	0.14	1.72	1.84	1.59	2.08	1.92	1.89	1.94	1.92	3.51	1.84	1.84	3.14
Ho	0.0025	0.476	0.539	0.134	0.195	0.337	0.166	0.261	0.165	0.979	0.47	0.146	0.417
In	0.0018	0.025	0.037	0.016	0.021	0.027	0.02	0.025	0.014	0.077	0.03	0.017	0.029
K	6	5507	4462	10175	7976	8696	8427	8489	7603	3053	8818	9809	2468
La	0.04	39.82	26.02	14.14	13.83	19.08	13.18	15.83	13.26	51.38	24.59	14.61	45.74
Li	0.4	6	10.3	5.8	8.3	12	8	7.8	3.7	20.8	11.4	7.2	13.2
Lu	0.002	0.13	0.19	0.044	0.062	0.105	0.045	0.076	0.048	0.309	0.145	0.04	0.117
Mn	6	493	702	411	443	499	376	452	240	1041	545	295	560
Mo	1	3	3	3	4	4	5	4	5	2	4	4	3
Na	25	42359	32390	42738	33654	33711	38278	37139	51941	17301	32232	36749	39303
Nb	0.028	2.494	2.454	1.694	2.497	2.542	2.113	2.551	1.998	6.611	2.837	1.833	4.469
Nd	0.06	43.64	31.22	11.45	13.01	20.87	12.57	16.58	12.67	72.15	31.23	12.59	44.12
Ni	1	56	72	37	44	45	30	36	27	128	53	25	87
P	5	1346	1499	819	806	1085	958	1307	934	2941	1352	891	1882
Pb	0.6	3.7	3.3	3.6	5.5	4.9	7	5.6	3.5	4.7	4.1	4.9	3.2
Pr	0.014	11.06	7.395	2.95	3.23	5.005	3.141	4.067	3.166	17.073	7.217	3.277	11.338
Rb	0.23	18.4	16.31	31.49	16.58	18.12	15.69	18.58	20.62	9.27	23.12	22.07	7.57
Sb	0.04	0.21	0.22	0.19	0.25	0.24	0.16	0.22	0.17	0.15	0.21	0.12	0.09
Sc	1.1	12.4	21.6	3.3	6.5	9.2	4	5.7	3.6	30.4	10.2	3.6	12.9
Sm	0.012	7.858	6.014	1.909	2.276	3.948	2.231	3.16	2.201	13.566	5.797	2.147	7.22
Sr	0.6	773	536.1	695.8	737.1	653.1	946.2	852.4	625.4	625.4	878.9	789.2	520.6
Ta	0.023	0.101	0.13	0.067	0.108	0.111	0.083	0.107	0.069	0.338	0.215	0.058	0.243
Tb	0.0023	0.604	0.575	0.151	0.206	0.358	0.182	0.277	0.18	1.124	0.492	0.168	0.525
Th	0.018	8.793	0.674	0.615	0.614	0.72	0.564	0.802	0.637	2.097	0.673	0.353	1.453
Ti	7	2779	2999	1423	2409	2335	1588	2323	1769	5584	2427	1752	4852
Tm	0.0019	0.156	0.204	0.047	0.068	0.121	0.056	0.091	0.057	0.344	0.169	0.049	0.14
U	0.011	0.158	0.152	0.134	0.107	0.151	0.144	0.178	0.245	0.547	0.134	0.074	0.11
V	0.8	83.6	98.8	33.4	69.9	80.8	42.6	69.2	49.2	202.1	72.9	44.5	85
Y	0.05	12.68	14.95	3.63	5.13	8.93	4.35	6.86	4.48	27.13	12.85	3.83	9.86
Yb	0.009	0.898	1.282	0.301	0.414	0.739	0.33	0.537	0.343	2.156	1.039	0.286	0.839
Zn	3	35	58	36	54	56	51	52	23	115	64	29	56
Zr	1	66	67	62	84	74	78	78	74	145	70	84	137

A6: Trace element data from barren footwall breccia (table 1 of 3).

Element	Detect Limit	CS35	CS42	CS47	CS49	CS51	CS56	CS57	CS58	CS60	CS62	CS66	CS68
Ba (ppm)	0.8	168.2	366.7	771	750.8	700.9	556.9	479	679.5	51.8	184.6	541.5	384.8
Be	0.04	0.83	0.74	1.27	1.16	1.35	1.03	0.83	0.57	0.62	0.52	0.68	0.76
Cd	0.013	nd	0.186	0.04	0.034	0.016	0.045	0.142	0.164	0.342	0.092	0.546	0.307
Ce	0.12	37.02	65.88	53.01	63.7	58.85	42.01	42.42	25.21	49.34	36.14	44.97	37.78
Co	0.13	54.32	116.82	17.59	20.68	12.78	17.83	49.49	85.62	108.58	59.25	187	114.71
Cr	3	178	358	202	216	136	215	371	470	287	805	386	236
Cs	0.013	0.088	0.514	0.484	0.208	0.164	0.143	1.341	1.958	0.209	0.776	1.238	0.874
Cu	1.4	13.3	690.4	67.9	20.7	30.2	48	208	438.9	449.4	102.1	2069.4	677.7
Dy	0.009	1.554	2.284	2.296	2.935	3.298	1.329	2.578	1.517	1.976	3.166	1.589	1.859
Er	0.007	0.739	1.189	1.177	1.507	1.877	0.701	1.378	0.834	1.009	1.751	0.86	1.04
Eu	0.0031	0.986	1.355	1.413	1.583	1.542	1.219	1.258	0.836	2.017	0.827	0.946	1.054
Ga	0.04	16.42	13.87	22.35	21.15	21.82	21.58	17.3	14.08	11.94	8.56	13.99	15.28
Gd	0.009	2.509	3.09	3.174	4.039	3.731	2.006	3.384	1.799	2.74	3.681	2.18	2.274
Hf	0.14	2.19	3.52	2.64	2.18	2.78	1.93	1.91	1.12	1.66	2.5	2.99	1.88
Ho	0.0025	0.276	0.434	0.426	0.542	0.656	0.249	0.488	0.295	0.369	0.614	0.301	0.363
In	0.0018	0.021	0.045	0.029	0.041	0.038	0.022	0.049	0.039	0.05	0.059	0.054	0.047
K	6	7554	9617	10855	7471	9707	7072	9114	10362	1937	4048	17548	7311
La	0.04	17.46	30.49	25.94	30.83	28.44	21.11	19.59	11.93	24.24	15.29	21.92	18.1
Li	0.4	8	18.1	7.9	7.8	6.7	10.6	12.4	18.5	12.8	10.5	11	12.7
Lu	0.002	0.09	0.17	0.142	0.182	0.224	0.104	0.186	0.119	0.131	0.251	0.119	0.148
Mn	6	384	740	483	648	405	653	865	1177	1028	1187	744	1063
Mo	1	5	4	5	4	5	3	3	2	3	2	4	3
Na	25	47219	13273	37457	37142	38225	33318	22186	13698	18346	8562	14272	17032
Nb	0.028	2.527	4.73	4.755	4.996	4.299	3.118	2.08	1.505	2.519	2.775	3.901	2.509
Nd	0.06	19.22	28.15	26.07	32.13	27.67	18.81	22.9	12.24	21.96	20.76	19.16	17.61
Ni	1	61	560	47	58	25	64	228	362	461	273	1430	611
P	5	1239	271	1130	1067	963	718	584	246	354	325	435	260
Pb	0.6	3	9.8	8.2	10.6	7.8	7	5.4	5	147.3	5.6	14.6	6.1
Pr	0.014	4.618	7.729	6.553	8.071	7.193	4.934	5.592	3.161	5.832	4.93	5.262	4.603
Rb	0.23	14.93	20.21	23.4	11.62	19.18	22.09	36.49	49.86	3.26	12.11	43.8	19.45
Sb	0.04	0.12	0.13	0.1	0.07	0.1	0.06	0.08	0.08	0.12	0.05	0.06	0.2
Sc	1.1	9.5	19.5	7.8	10.5	7.4	8.2	27.1	29	20.3	33.7	15.9	24.5
Sm	0.012	3.45	4.598	4.475	5.569	4.705	2.99	4.408	2.347	3.717	4.249	3.173	3.033
Sr	0.6	319.7	229.5	771.2	745.6	595.3	613.5	555.9	333.8	83.5	117.5	324	330.5
Ta	0.023	0.068	0.209	0.212	0.23	0.173	0.119	0.098	0.068	0.132	0.149	0.176	0.108
Tb	0.0023	0.308	0.417	0.407	0.53	0.541	0.253	0.453	0.253	0.36	0.535	0.286	0.319
Th	0.018	0.18	1.762	0.872	1.811	0.669	1.041	1.188	0.91	1.516	1.668	3.253	0.701
Ti	7	2319	2245	3088	3104	2463	2108	2165	1852	2152	2323	2301	1893
Tm	0.0019	0.1	0.175	0.161	0.205	0.257	0.101	0.197	0.12	0.14	0.257	0.123	0.152
U	0.011	0.07	0.268	0.197	0.178	0.111	0.136	0.186	0.121	0.311	0.25	0.373	0.129
V	0.8	43.7	81.7	80.7	82.9	59.4	60.2	121.3	127.2	133.2	113.2	90.7	104.5
Y	0.05	7.26	11.56	11.67	14.9	17.38	6.89	13.21	7.88	9.5	15.24	8.28	9.77
Yb	0.009	0.604	1.161	0.997	1.287	1.588	0.668	1.275	0.794	0.889	1.667	0.789	1.011
Zn	3	36	62	53	65	42	61	74	80	138	54	93	90
Zr	1	97	127	108	95	113	70	64	43	60	80	109	70

A7: Trace element data from barren footwall breccia (table 2of 3).

Element	Detect Limit	CS69	CS70	CS71	CS73	CS76	CS84	CS85	CS89	CS90	avg	σ=
Ba (ppm)	0.8	395.9	653.7	783	795.4	771.8	372.9	374.4	705	484.3	520.4	207.7
Be	0.04	0.78	1.45	1.2	1.32	1.12	0.75	0.83	1.24	1	1.01	0.26
Cd	0.013	0.268	0.088	0.055	0.062	0.036	0.241	0.162	0.047	0.014	0.102	0.122
Ce	0.12	33.18	53.28	53.78	54.82	40.86	44.91	45.18	42.36	37.14	47.87	21.15
Co	0.13	99.95	23.84	12.39	10.75	13.32	89.22	66.25	12.12	9.98	38.85	34.42
Cr	3	502	275	130	136	162	423	501	164	206	275	157
Cs	0.013	2.122	0.268	0.241	0.128	0.266	0.893	1.129	0.221	0.164	0.479	0.523
Cu	1.4	798.7	77.2	27.3	26.2	27.6	409.5	114.6	21.3	29.3	207.2	396.0
Dy	0.009	1.87	3.279	2.596	2.556	1.945	3.145	2.518	2.487	1.681	2.211	0.958
Er	0.007	1.099	1.705	1.342	1.429	0.965	1.669	1.425	1.368	0.874	1.125	0.483
Eu	0.0031	0.943	1.519	1.379	1.288	1.245	1.427	1.415	1.164	0.968	1.2725	0.3946
Ga	0.04	14.38	20.63	20.65	20.36	21.22	15.81	18.42	19.73	18.02	19.03	3.71
Gd	0.009	2.286	4.289	3.465	3.315	2.729	3.815	3.182	3.074	2.247	3.131	1.481
Hf	0.14	1.86	2.13	2.25	2.67	2.2	2.13	1.71	2.24	2.58	2.19	0.53
Ho	0.0025	0.381	0.62	0.491	0.486	0.357	0.598	0.498	0.47	0.317	0.4096	0.1743
In	0.0018	0.048	0.047	0.032	0.026	0.026	0.062	0.053	0.029	0.026	0.0358	0.0149
K	6	14534	6912	13542	13441	9794	6114	7453	14443	13310	8716	3540
La	0.04	16.1	25.02	25.77	24.58	19.61	21.33	22.7	20.18	19.2	22.767	8.902
Li	0.4	13.1	9.2	8.2	8.6	6	9.1	5.6	6	6.4	9.8	3.9
Lu	0.002	0.179	0.222	0.166	0.19	0.124	0.216	0.203	0.166	0.115	0.144	0.063
Mn	6	999	791	468	362	519	1224	1212	463	437	664	293
Mo	1	3	4	4	4	6	3	3	4	5	4	1
Na	25	12873	33819	37289	34391	38366	15268	16461	35049	39302	30344	11422
Nb	0.028	2.251	3.797	3.648	4.599	3.878	4.727	5.43	3.626	3.836	3.321	1.221
Nd	0.06	16.43	29.44	26.54	27.38	20.83	23.62	21.48	21.77	16.66	24.03	11.67
Ni	1	484	89	24	21	28	368	198	30	44	185	278
P	5	399	1184	1057	900	1037	706	1114	874	625	949	522
Pb	0.6	8.4	8.2	7.7	7.2	11.3	7.5	7.1	7.6	6.5	10.8	24.3
Pr	0.014	4.088	6.931	6.677	6.918	5.122	5.735	5.473	5.293	4.348	5.999	2.805
Rb	0.23	50.98	12.87	22.17	17.9	14.46	19.56	21.8	22.66	18.12	21.05	10.56
Sb	0.04	0.04	0.06	0.05	0.06	0.07	0.06	0.04	0.04	0.05	0.12	0.07
Sc	1.1	21.3	12.3	7.3	6.6	6.4	35.8	27.8	7.3	7	14.2	9.6
Sm	0.012	2.977	5.684	4.73	4.826	3.695	4.774	4.005	4.024	2.953	4.325	2.166
Sr	0.6	350.2	644.8	605.4	598.6	804.8	463.1	485.5	527.3	354.9	560.2	213.8
Ta	0.023	0.108	0.225	0.136	0.16	0.146	0.328	0.292	0.167	0.153	0.154	0.073
Tb	0.0023	0.32	0.578	0.464	0.449	0.351	0.542	0.44	0.423	0.297	0.4051	0.1823
Th	0.018	0.702	0.401	0.399	0.306	0.422	3.014	1.938	0.407	0.559	1.264	1.520
Ti	7	1753	3074	2471	2574	2717	4752	5457	2322	2586	2665	1022
Tm	0.0019	0.171	0.24	0.188	0.207	0.135	0.23	0.202	0.188	0.123	0.1568	0.0672
U	0.011	0.141	0.119	0.087	0.063	0.182	0.51	0.338	0.111	0.174	0.188	0.113
V	0.8	77.7	92.2	67.1	61.9	65.5	204.4	190.4	70.4	58.1	88.4	42.2
Y	0.05	10.09	16.77	13.45	14.1	10.09	15.57	13.11	12.9	8.72	11.00	4.76
Yb	0.009	1.117	1.51	1.169	1.347	0.848	1.46	1.337	1.175	0.78	0.989	0.432
Zn	3	93	80	56	45	47	87	98	57	51	63	25
Zr	1	66	76	95	112	86	69	63	86	108	85	23

A8: Trace element data from barren footwall breccia (table 3 of 3).

Element	Detect Limit	CS107	CS115	CS119	CS122	CS124	CS127	CS137	avg	σ =
Ba (ppm)	0.8	525.5	570.7	387.3	568.7	923.5	241.4	801.7	574.1	214.4
Be	0.04	0.7	1.06	0.83	1.02	0.71	0.42	0.59	0.76	0.21
Cd	0.013	0.102	0.099	0.073	0.327	0.084	0.889	0.04	0.231	0.283
Ce	0.12	47.02	74.01	30.37	42.51	18.88	34.87	14.04	37.39	18.53
Co	0.13	32.84	14.35	12.94	39.43	11.2	183.88	7.25	43.13	58.53
Cr	3	447	175	143	60	152	3420	117	645	1139
Cs	0.013	0.347	0.092	0.122	0.463	0.185	0.587	0.059	0.265	0.189
Cu	1.4	131.3	74.2	67.2	612.9	227.8	5902	72.5	1012.6	2004.2
Dy	0.009	1.964	2.906	1.446	2.919	0.729	3.166	0.386	1.931	1.036
Er	0.007	0.952	1.39	0.776	1.516	0.341	1.773	0.193	0.992	0.555
Eu	0.0031	1.263	1.911	0.809	1.226	0.827	0.724	0.968	1.1040	0.3814
Ga	0.04	18.9	20.22	18.86	18.44	19.81	6.95	20.2	17.63	4.41
Gd	0.009	3.031	4.278	1.808	3.467	1.077	3.232	0.55	2.492	1.266
Hf	0.14	2.16	2.87	3.4	2.87	1.83	2.48	1.52	2.45	0.61
Ho	0.0025	0.361	0.519	0.277	0.553	0.132	0.629	0.07	0.3630	0.1992
In	0.0018	0.036	0.035	0.031	0.062	0.022	0.139	0.01	0.0479	0.0400
K	6	6008	7217	10734	10114	18409	2247	8361	9013	4643
La	0.04	23.16	35.97	15.45	20.33	11.1	15.67	9.33	18.716	8.333
Li	0.4	4.8	7.1	7.1	9.9	7.8	5.1	2.9	6.4	2.1
Lu	0.002	0.121	0.166	0.103	0.185	0.043	0.229	0.026	0.125	0.069
Mn	6	882	494	489	1088	352	1499	206	716	426
Mo	1	3	4	5	3	5	3	4	4	1
Na	25	27222	36370	33917	22762	34041	2788	39684	28112	11598
Nb	0.028	2.881	4.722	4.082	5.175	1.624	3.197	0.842	3.218	1.471
Nd	0.06	22.47	35.09	12.85	19.79	7.62	17.56	4.92	17.19	9.38
Ni	1	189	37	13	208	128	7048	53	1097	2431
P	5	1036	1010	660	485	424	256	213	583	310
Pb	0.6	6.2	9.4	6.7	10.6	9.4	18.7	6.8	9.7	4.0
Pr	0.014	5.766	8.983	3.484	5.124	2.035	4.393	1.414	4.457	2.352
Rb	0.23	10.87	6.57	13.75	21.72	32.65	11.7	13.43	15.81	8.06
Sb	0.04	0.07	0.06	0.05	0.05	0.04	nd	nd	0.05	0.01
Sc	1.1	16.2	16.4	6.6	22.9	6.4	23.8	2.7	13.6	7.8
Sm	0.012	4.016	6.187	2.266	4.052	1.353	3.601	0.765	3.177	1.719
Sr	0.6	652.7	788.5	422	487.8	624.9	61.8	1059.1	585.3	288.4
Ta	0.023	0.177	0.236	0.189	0.304	0.06	0.172	0.037	0.168	0.087
Tb	0.0023	0.373	0.549	0.247	0.503	0.132	0.506	0.069	0.3399	0.1790
Th	0.018	1.742	1.717	0.399	3.275	0.259	4.49	0.236	1.731	1.520
Ti	7	2750	4334	3043	5136	1854	2131	853	2872	1361
Tm	0.0019	0.132	0.187	0.107	0.205	0.048	0.249	0.027	0.1364	0.0762
U	0.011	0.272	0.194	0.153	0.545	0.121	0.438	0.111	0.262	0.156
V	0.8	95.4	125.4	65.9	183.7	61.1	159	24.4	102.1	52.8
Y	0.05	9.26	13.59	7.34	14.61	3.53	16.48	1.9	9.53	5.21
Yb	0.009	0.833	1.162	0.694	1.3	0.304	1.531	0.172	0.857	0.470
Zn	3	83	54	57	87	49	158	20	73	41
Zr	1	85	134	159	111	78	88	59	102	32

A9: Trace element data from mineralized footwall breccia

Element	Detect Limit	CS43	CS44	avg	σ =	CS110
Ba (ppm)	0.8	127.2	140	133.6	6.4	435.1
Be	0.04	1.62	0.42	1.02	0.60	0.69
Cd	0.013	0.229	0.391	0.310	0.081	0.123
Ce	0.12	88.42	19.6	54.01	34.41	45.6
Co	0.13	147.38	187	147.38	0.00	55.67
Cr	3	271	586	429	158	1162
Cs	0.013	0.713	0.763	0.738	0.025	0.633
Cu	1.4	791.4	3749	2270.2	1478.8	210.5
Dy	0.009	4.803	1.372	3.088	1.716	2.271
Er	0.007	2.008	0.743	1.376	0.633	1.312
Eu	0.0031	2.688	0.65	1.6690	1.0190	0.847
Ga	0.04	15.45	8.23	11.84	3.61	12.74
Gd	0.009	6.98	1.739	4.360	2.621	2.857
Hf	0.14	6.87	1.05	3.96	2.91	2.87
Ho	0.0025	0.821	0.264	0.5425	0.2785	0.441
In	0.0018	0.104	0.158	0.1310	0.0270	0.047
K	6	2247	3209	2728	481	12769
La	0.04	38.83	8.44	23.635	15.195	22.3
Li	0.4	9.9	13.5	11.7	1.8	9.2
Lu	0.002	0.217	0.106	0.162	0.056	0.189
Mn	6	1836	754	1295	541	1121
Mo	1	3	3	3	0	3
Na	25	2315	6270	4293	1978	15476
Nb	0.028	36.317	1.334	18.826	17.492	3.529
Nd	0.06	46.78	10.78	28.78	18.00	20.81
Ni	1	760	7934	4347	3587	212
P	5	1218	200	709	509	589
Pb	0.6	6	6.4	6.2	0.2	9.3
Pr	0.014	11.582	2.599	7.091	4.492	5.457
Rb	0.23	14.73	16.61	15.67	0.94	27.77
Sb	0.04	0.07	0.05	0.06	0.01	0.08
Sc	1.1	24.2	19.3	21.8	2.5	23.1
Sm	0.012	8.916	2.197	5.557	3.360	3.693
Sr	0.6	414.2	108.1	261.2	153.1	277.8
Ta	0.023	3.317	0.065	1.691	1.626	0.197
Tb	0.0023	0.922	0.239	0.5805	0.3415	0.387
Th	0.018	3.385	0.61	1.998	1.388	2.772
Ti	7	19069	1467	10268	8801	2932
Tm	0.0019	0.258	0.105	0.1815	0.0765	0.186
U	0.011	0.401	0.112	0.257	0.145	0.516
V	0.8	347.4	86.6	217.0	130.4	141.3
Y	0.05	20.64	7.07	13.86	6.79	11.48
Yb	0.009	1.533	0.695	1.114	0.419	1.245
Zn	3	86	95	91	5	97
Zr	1	254	40	147	107	98

A10: Trace element data from mafic norite. Samples CS43 and CS44 are from the barren environment; sample CS110 is from the mineralized environment.

Element	Detect Limit	CS4	CS5	CS9	CS37	CS38	CS40	avg	σ =	CS101
Ba (ppm)	0.8	435.9	403.6	559.4	413.9	277.9	548.9	439.9	95.2	380.4
Be	0.04	1	1	1.2	0.74	0.78	0.72	0.91	0.17	0.54
Cd	0.013	0.08	0.089	0.442	<0.013	0.014	2.231	0.571	0.843	0.089
Ce	0.12	47.92	51.3	29.45	32.6	48.18	36.19	40.94	8.49	34.02
Co	0.13	32.05	31.85	29.33	36.45	103.62	19.05	42.06	28.04	31.25
Cr	3	277	260	201	195	223	219	229	30	491
Cs	0.013	1.815	1.906	0.685	0.142	0.14	0.219	0.818	0.761	0.408
Cu	1.4	27.9	28.3	54.7	3.6	8.4	63.3	31.0	21.9	85.1
Dy	0.009	2.644	2.656	1.43	1.371	1.943	1.667	1.952	0.527	1.316
Er	0.007	1.501	1.502	0.771	0.731	1.033	0.912	1.075	0.317	0.678
Eu	0.0031	1.251	1.245	1.18	1.153	0.947	1.034	1.1350	0.1106	1.037
Ga	0.04	18.68	18.71	18.4	18.48	12.62	12.7	16.60	2.79	17
Gd	0.009	3.07	3.148	1.807	1.986	2.722	2.197	2.488	0.521	1.805
Hf	0.14	2.49	2.52	1.86	1.38	2.66	2.38	2.22	0.45	2.2
Ho	0.0025	0.521	0.517	0.274	0.259	0.359	0.319	0.3748	0.1069	0.244
In	0.0018	0.038	0.036	0.029	0.03	0.019	0.03	0.0303	0.0061	0.031
K	6	10971	11836	7358	17198	16549	17502	13569	3783	9475
La	0.04	24.28	25.67	14.9	16.42	22.71	16.08	20.010	4.321	17.32
Li	0.4	13	13.3	42	12.1	13.5	30.3	20.7	11.4	8.1
Lu	0.002	0.213	0.214	0.114	0.098	0.155	0.12	0.152	0.046	0.091
Mn	6	834	922	706	702	536	571	712	135	789
Mo	1	5	4	3	3	4	4	4	1	4
Na	25	18331	19404	25923	24606	34591	22697	24259	5335	22654
Nb	0.028	5.038	5.364	2.592	1.767	3.449	3.616	3.638	1.263	2.434
Nd	0.06	20.46	21.99	13.34	15.04	21.98	17.73	18.42	3.35	14.87
Ni	1	30	28	26	48	27	28	31	8	114
P	5	542	591	254	737	662	710	583	161	520
Pb	0.6	8	6.5	19.7	3.3	4.1	7.4	8.2	5.4	6.1
Pr	0.014	5.514	5.943	3.446	3.917	5.846	4.478	4.857	0.967	3.988
Rb	0.23	48	54.35	27.1	33.43	29.52	30.12	37.09	10.30	17.14
Sb	0.04	0.45	0.49	0.4	0.09	0.12	0.1	0.28	0.17	0.06
Sc	1.1	17.4	17.8	14.2	14.5	16.9	10.6	15.2	2.5	12.4
Sm	0.012	3.775	3.929	2.373	2.64	3.874	3.067	3.276	0.619	2.45
Sr	0.6	470.6	440.8	359.6	711.6	242.8	101.8	387.9	190.7	660.3
Ta	0.023	0.331	0.349	0.116	0.072	0.176	0.155	0.200	0.104	0.112
Tb	0.0023	0.444	0.458	0.253	0.251	0.363	0.295	0.3440	0.0843	0.236
Th	0.018	4.934	5.406	0.87	0.955	4.82	1.034	3.003	2.059	1.187
Ti	7	2693	2856	2125	2032	2836	2649	2532	330	1716
Tm	0.0019	0.217	0.215	0.115	0.103	0.15	0.13	0.1550	0.0455	0.097
U	0.011	1.092	1.095	0.172	0.175	0.473	0.184	0.532	0.411	0.164
V	0.8	109.3	112.8	64.2	117.8	89.6	121.9	102.6	20.0	67.7
Y	0.05	14.02	13.93	7.42	7.29	9.61	8.45	10.12	2.83	6.2
Yb	0.009	1.416	1.427	0.753	0.665	0.992	0.827	1.013	0.305	0.619
Zn	3	71	103	219	46	50	680	195	225	77
Zr	1	86	90	68	53	95	87	80	15	82

A11: Trace element data from felsic norite. Samples CS4-CS40 are from the barren environment; sample CS101 is from the mineralized environment.

Element	Detect Limit	CS78	CS79	CS80	avg	σ =	CS133	CS139	CS140	CS112	avg	σ =
Ba (ppm)	0.8	149.4	297	240.7	229.0	60.8	471.6	533.8	541.5	130.1	419.3	169.1
Be	0.04	0.66	0.71	1.15	0.84	0.22	0.73	0.57	1.08	0.23	0.65	0.31
Cd	0.013	0.575	0.275	0.17	0.340	0.172	0.237	0.314	0.163	0.152	0.217	0.065
Ce	0.12	43.74	38.87	62.45	48.35	10.16	34.31	16.26	55.27	16.38	30.56	16.05
Co	0.13	71.82	160.35	81.06	104.41	39.74	39.16	32.48	55.57	170.84	74.51	56.25
Cr	3	1169	567	1136	957	276	351	109	974	1162	649	433
Cs	0.013	1.026	1.057	1.424	1.169	0.181	0.261	0.217	1.164	0.171	0.453	0.412
Cu	1.4	6431	640.4	153.5	2408.3	2851.4	404.2	919.5	197.2	335.3	464.1	273.3
Dy	0.009	4.6	2.924	2.891	3.472	0.798	3.675	0.683	3.438	1.575	2.343	1.257
Er	0.007	2.188	1.525	1.438	1.717	0.335	1.805	0.328	1.95	0.793	1.219	0.681
Eu	0.0031	1.275	1.291	1.414	1.3267	0.0621	1.224	1.093	1.033	0.62	0.9925	0.2259
Ga	0.04	12.5	14.34	13.3	13.38	0.75	21.05	24.77	13.15	5.71	16.17	7.35
Gd	0.009	5.833	3.559	4.225	4.539	0.955	4.847	1.049	4.024	2.027	2.987	1.518
Hf	0.14	1.67	1.58	2.27	1.84	0.31	1.67	0.8	3.5	1.23	1.80	1.03
Ho	0.0025	0.835	0.55	0.532	0.6390	0.1388	0.674	0.125	0.672	0.29	0.4403	0.2400
In	0.0018	0.098	0.07	0.059	0.0757	0.0164	0.064	0.028	0.05	0.034	0.0440	0.0141
K	6	4719	5597	5393	5236	375	5059	5460	15280	3177	7244	4719
La	0.04	16.71	17.91	29.08	21.233	5.570	14.78	9.08	27.08	7.17	14.528	7.769
Li	0.4	7.6	8.9	11.3	9.3	1.5	5.2	3.6	12.7	10.7	8.1	3.8
Lu	0.002	0.259	0.194	0.195	0.216	0.030	0.211	0.041	0.277	0.096	0.156	0.093
Mn	6	1476	1366	1366	1403	52	1152	589	1169	1311	1055	276
Mo	1	2	2	1	2	0	2	2	4	2	3	1
Na	25	6513	11420	8561	8831	2012	26769	35702	13896	5366	20433	11652
Nb	0.028	1.786	3.896	4.644	3.442	1.210	3.463	0.299	5.97	1.04	2.693	2.225
Nd	0.06	30.13	20.87	31.83	27.61	4.82	22.3	7.82	25.93	9.86	16.48	7.78
Ni	1	399	950	504	618	239	329	671	178	1866	761	663
P	5	574	817	1048	813	194	924	799	803	300	707	240
Pb	0.6	4.6	7.4	5.7	5.9	1.2	7.6	16.6	9.7	4.2	9.5	4.5
Pr	0.014	6.604	5.049	7.853	6.502	1.147	4.893	1.96	6.645	2.263	3.940	1.934
Rb	0.23	20.39	21.06	22.69	21.38	0.97	8.21	6.11	52.01	6.96	18.32	19.46
Sb	0.04	0.05	0.05	0.05	0.05	0.00	0.04	0.04	0.15	0.07	0.11	0.04
Sc	1.1	46.2	33.7	28.7	36.2	7.4	34.6	7.5	22.9	37.4	25.6	11.8
Sm	0.012	6.963	4.294	5.883	5.713	1.096	5.379	1.38	4.903	2.247	3.477	1.700
Sr	0.6	183.7	387.1	260.5	277.1	83.9	686	1164.8	260.9	127.1	559.7	405.7
Ta	0.023	0.099	0.248	0.299	0.215	0.085	0.212	nd	0.406	0.055	0.224	0.144
Tb	0.0023	0.806	0.498	0.538	0.6140	0.1367	0.66	0.129	0.576	0.279	0.4110	0.2157
Th	0.018	1.504	1.801	4.031	2.445	1.128	0.426	0.309	5.589	0.622	1.737	2.227
Ti	7	2875	4945	3740	3853	849	4198	942	3142	1540	2456	1288
Tm	0.0019	0.303	0.208	0.205	0.2387	0.0455	0.245	0.044	0.288	0.107	0.1710	0.0992
U	0.011	0.237	0.3	1.229	0.589	0.454	0.1	0.035	1.525	0.125	0.446	0.624
V	0.8	155.7	226.7	167.3	183.2	31.1	165.3	47.4	154.5	115.1	120.6	46.2
Y	0.05	22.34	14.52	14.27	17.04	3.75	17.75	3.26	18.26	7.17	11.61	6.55
Yb	0.009	1.87	1.323	1.301	1.498	0.263	1.474	0.282	1.832	0.657	1.061	0.619
Zn	3	140	91	90	107	23	87	60	86	87	80	12
Zr	1	54	54	89	66	16	60	34	123	41	65	35

A12: Trace element data from sublayer norite. Samples CS78-CS80 are from the barren environment' Samples CS112-CS140 are from the mineralized environment.

Element	Detect Limit	CS93	CS95	avg	σ =	CS116	CS120	CS123	CS142	CS143	avg	σ =
Ba (ppm)	0.8	369.4	640	504.7	135.3	1054.5	436.1	418.7	1036.3	540.9	697.3	287.3
Be	0.04	0.95	1.26	1.11	0.16	1.06	0.77	0.81	0.97	0.98	0.92	0.11
Cd	0.013	0.058	0.084	0.071	0.013	0.231	0.051	0.176	0.088	0.048	0.119	0.073
Ce	0.12	40.21	29.19	34.70	5.51	116.44	40.71	27.69	58.71	20.68	52.85	34.33
Co	0.13	9.79	7.67	8.73	1.06	36.77	9.55	16.37	26.35	9.54	19.72	10.52
Cr	3	156	128	142	14	559	125	121	213	129	229	168
Cs	0.013	0.217	0.16	0.189	0.029	0.795	0.169	0.112	0.54	0.082	0.340	0.281
Cu	1.4	65.7	12.2	39.0	26.8	284	40.9	85.4	50.5	9.4	94.0	98.0
Dy	0.009	1.349	1.715	1.532	0.183	3.679	1.688	1.427	2.32	0.587	1.940	1.032
Er	0.007	0.702	0.843	0.773	0.070	1.477	0.948	0.706	1.135	0.28	0.909	0.403
Eu	0.0031	0.761	1.029	0.8950	0.1340	2.313	0.927	0.911	1.69	0.856	1.3394	0.5759
Ga	0.04	19.59	20.25	19.92	0.33	17.68	18.46	19.19	19.7	20.43	19.09	0.96
Gd	0.009	1.87	2.298	2.084	0.214	6.984	2.082	1.822	3.564	0.975	3.085	2.121
Hf	0.14	4.11	1.38	2.75	1.37	5.22	3.54	2.21	2.38	2.87	3.24	1.09
Ho	0.0025	0.251	0.307	0.2790	0.0280	0.603	0.328	0.263	0.428	0.101	0.3446	0.1673
In	0.0018	0.022	0.03	0.0260	0.0040	0.05	0.029	0.037	0.037	0.017	0.0340	0.0108
K	6	13119	12712	12916	204	9715	12942	9353	14238	10279	11305	1933
La	0.04	21.71	14.64	18.175	3.535	52.84	21.26	14.89	28.6	11.99	25.916	14.624
Li	0.4	7.3	3.5	5.4	1.9	11.1	6.7	7.3	8.2	6.8	8.0	1.6
Lu	0.002	0.099	0.098	0.099	0.001	0.16	0.134	0.088	0.146	0.039	0.113	0.044
Mn	6	375	396	386	11	810	409	555	666	261	540	192
Mo	1	6	3	5	2	3	3	4	2	4	3	1
Na	25	33721	36388	35055	1334	23316	33169	35071	27853	36992	31280	5015
Nb	0.028	4.582	2.762	3.672	0.910	5.431	5.233	2.77	2.93	1.616	3.596	1.490
Nd	0.06	15.55	14.47	15.01	0.54	59.95	15.45	12.16	29.6	8.75	25.18	18.78
Ni	1	13	23	18	5	217	6	79	61	11	75	76
P	5	724	617	671	54	2101	697	450	1084	496	966	610
Pb	0.6	8.1	8.6	8.4	0.3	35.8	6.8	6.9	7.1	9.3	13.2	11.3
Pr	0.014	4.311	3.608	3.960	0.351	14.898	4.421	3.133	7.471	2.35	6.455	4.568
Rb	0.23	22.44	24.51	23.48	1.04	52.26	17.86	12.91	32.52	11.23	25.36	15.40
Sb	0.04	0.06	0.04	0.05	0.01	0.07	0.04	0.05	0.04	0.04	0.05	0.01
Sc	1.1	5.7	7.4	6.6	0.8	20.6	6.5	9.7	17	6.4	12.0	5.8
Sm	0.012	2.481	2.898	2.690	0.209	10.615	2.608	2.285	5.194	1.431	4.427	3.339
Sr	0.6	256.5	625.3	440.9	184.4	640.1	390.7	657.2	817.8	662.4	633.6	137.4
Ta	0.023	0.128	0.118	0.123	0.005	0.307	0.272	0.143	0.092	0.034	0.170	0.104
Tb	0.0023	0.244	0.311	0.2775	0.0335	0.788	0.287	0.25	0.425	0.112	0.3724	0.2305
Th	0.018	0.359	0.596	0.478	0.119	7.993	0.833	1.58	0.544	0.041	2.198	2.940
Ti	7	2812	1515	2164	649	4614	2870	2685	3533	2203	3181	834
Tm	0.0019	0.1	0.113	0.1065	0.0065	0.188	0.135	0.096	0.157	0.038	0.1228	0.0519
U	0.011	0.236	0.166	0.201	0.035	1.017	0.237	0.293	0.142	0.141	0.366	0.331
V	0.8	54.3	41.2	47.8	6.6	143.4	52.1	87.4	127.9	51.9	92.5	37.8
Y	0.05	6.84	8.48	7.66	0.82	15.62	9.02	6.93	11.28	2.86	9.14	4.26
Yb	0.009	0.622	0.704	0.663	0.041	1.12	0.878	0.591	0.994	0.244	0.765	0.314
Zn	3	56	43	50	7	131	57	44	72	41	69	33
Zr	1	157	55	106	51	177	187	95	111	112	136	38

A13: Trace element data from basement gneiss. Samples CS93-CS95 are from the barren environment; Samples CS116-CS143 are from the mineralized environment.

	Standard								Comparison				
	1a	1b	1c	1d	1e	2a	2b	avg	1	2	3	AVG	error (%)
SiO_2(wt %)	37.65	55.00	55.00	55.00	55.00	55.00	55.00	52.52	55			55.00	1.05
TiO_2	1.29	2.04	1.62	1.70	2.04	1.83	1.54	1.72	2.32			2.32	1.35
MnO	0.12	0.20	0.14	0.16	0.19	0.17	0.14	0.16	0.21			0.21	1.31
MgO	2.17	3.41	3.65	3.65	3.29	3.46	3.32	3.28	3.57			3.57	1.09
CaO	4.25	6.82	5.73	5.81	6.74	6.08	5.24	5.81	7.1			7.10	1.22
Na_2O	1.98	3.09	2.94	2.94	3.00	2.95	2.78	2.81	3.14			3.14	1.12
K_2O	1.30	2.07	1.59	1.78	2.04	1.77	1.58	1.73	1.77			1.77	1.02
Ag (ppm)	0.31	0.62	0.37	0.52	0.59	0.43	0.42	0.47					0.00
Ba	394	654	342	404	610	455	381	463	6.83	660	641	436	0.94
Ce	31.13	52.122	27.096	31.511	47.839	36.39	31.092	36.74	53.3	52	52	52.43	1.43
Cd	0.14	<0.267	0.18	0.14	0.19	0.22	0.18	0.17					0.00
Co	24.6	39.4	27.0	30.7	37.2	32.9	28.1	31.4		37.0	38.0	37.5	1.19
Cr	10.0	15.1	10.5	11.5	14.0	12.8	10.3	12.0	18.8	15.0	17.0	16.9	1.41
Cu	11.6	17.9	12.8	15.5	18.3	15.6	13.2	15.0	15.5	17.0	18.0	16.8	1.12
Mo	152	237	129	160	225	180	148	176		300		300	1.71
Nb	6.8	10.4	6.2	7.4	10.1	8.4	6.8	8.0	12.3	13.0		12.7	1.58
Ni	7.5	11.9	8.5	9.7	11.8	10.7	8.9	9.9	13.0	13.0	12.7	12.9	1.31
Pb	6.6	10.3	5.4	6.2	9.9	7.2	6.7	7.5	10.6			10.6	1.42
Pd	<0.101	<0.176	0.033	<0.045	0.06	0.035	0.028	0.039					0.00
Pt	0.12	0.39	0.14	0.19	0.27	0.19	0.16	0.21					0.00
Rb	31.8	52.4	29.5	35.1	50.1	39.1	31.1	38.4	47.0	46.0	51.0	48.0	1.25
Sb	0.24	0.31	0.13	0.17	0.28	0.33	0.14	0.23			0.51	0.51	2.24
Sn	1.2	1.9	1.1	1.2	2.0	1.4	1.2	1.4			2.4	2.4	1.70
Sr	201	320	202	224	310	247	195	243	342		321	332	1.37
V	264	425	310	332	411	355	300	342	414	420	425	420	1.23
Y	19.7	29.9	17.6	20.7	28.8	22.5	17.5	22.4	36.9	36.0	31.0	34.6	1.55
Zn	97	152	112	122	144	125	106	123		140	153	147	1.20
Zr	108	163	96	113	161	125	98	124	188	200	167	185	1.50

A14: BCR-2G data used as a standard for LA-ICP-MS. All major data are in wt. % and trace element data are in ppm. Sources: 1. Rocholl, 1998 (majors) and Jochum et al., 2005 (trace); 2. Gao et al., 2002; 3. Seufert and Jochum, 1997.

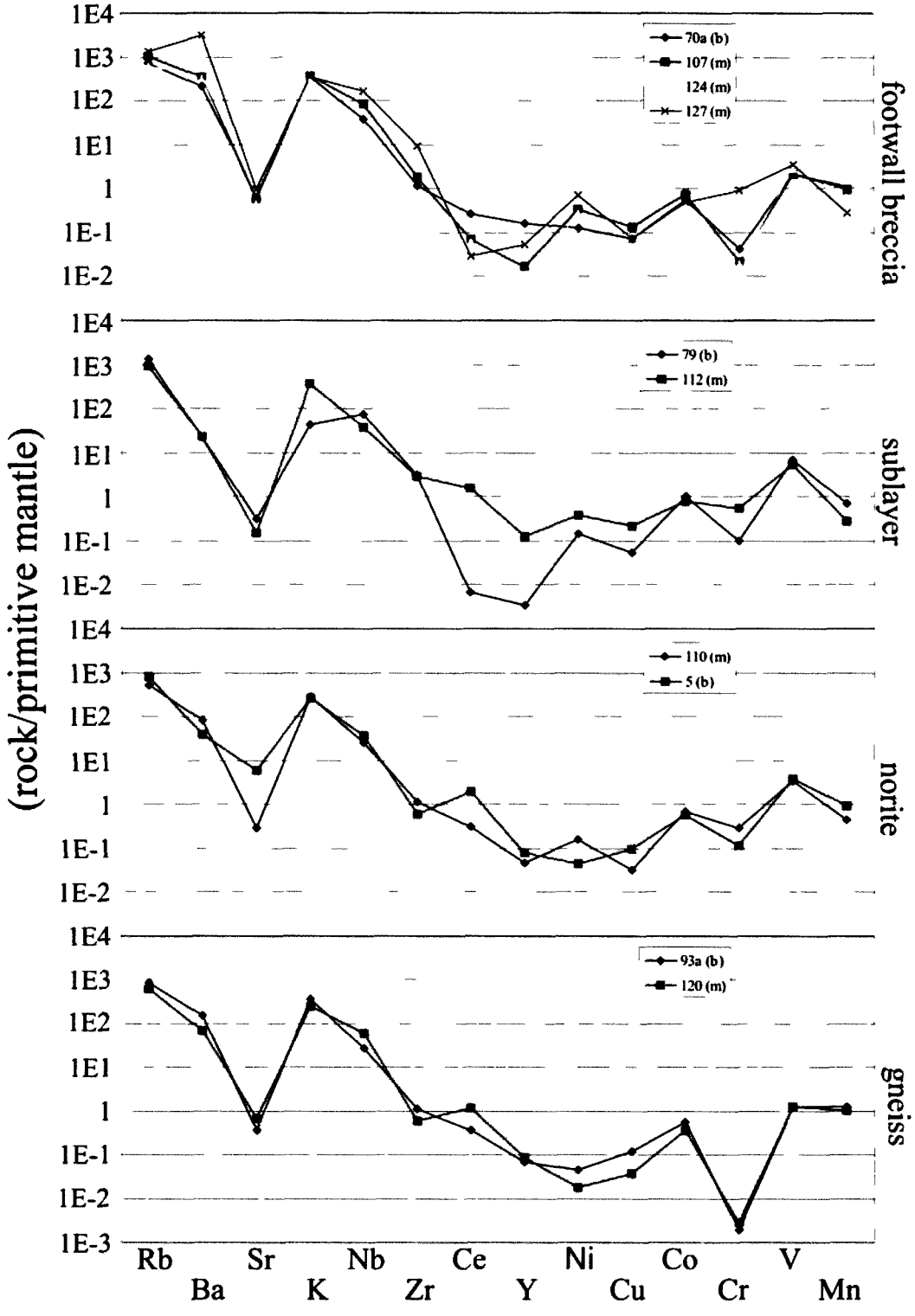

A15: Normative abundance diagram for biotites by LA-ICP-MS.

Sample	CS5	CS12	CS18b	CS20	CS24	CS37a	CS71a	CS79
n =	12	23	29	14	30	13	10	4
Lithology	fnor	fwb	fwb	fwb	fwb	fnor	fwb	sl
b/m	b	b	b	b	b	b	b	b
SiO_2	53.69	52.58	53.3	54.96	55.48	53.5	52.03	51.7
TiO2	0.06	0.06	0.13	0.06	0.26	0.11	0.54	0.15
$Al2O_3$	3.14	3.2	2.58	2.86	1.91	2.44	3.02	2.24
FeO	12.58	11.59	11.2	11.05	6.38	12.48	11.66	13.55
Cr_2O_3	0	0	0	0	0.07	0.01	0.01	0.06
MnO	0.37	0.41	0.34	0.41	0.09	0.36	0.4	0.39
MgO	15.21	16.87	16.31	16.57	20.4	16.41	16.22	14.45
CaO	12.7	11.93	12.38	11.22	12.87	12.02	11.78	12.75
Na_2O	0.1	0.23	0.28	0.13	0.23	0.24	0.28	0.28
K_2O	0.11	0.11	0.13	0.09	0.1	0.14	0.18	0.09
F	0	0	0.07	0	0	0	0.17	0
Cl	0.02	0.04	0.01	0.02	0.02	0.09	0.03	0.04
Subtotal	97.98	97.02	96.73	97.37	97.74	97.79	96.31	95.64
O = Cl, F	0	0.01	0.03	0	0	0.02	0.08	0.01
Total	97.98	97.01	96.7	97.37	97.74	97.77	96.23	95.63
Cations calculated on the basis of 23 (O, F, Cl) p.f.u. and the average ferric iron constraint (values obtained from the average 15eNK and 13eCNK)								
Si (p.f.u.)	7.69	7.51	7.69	7.79	7.71	7.63	7.54	7.66
Al	0.31	0.49	0.31	0.21	0.29	0.37	0.46	0.34
Fe^{3+}	0.00	0.00	0.00	0.00	0.00	0.00	0.00	0.00
Ti	0.00	0.00	0.00	0.00	0.00	0.00	0.00	0.00
T sites	8.00	8.00	8.00	8.00	8.00	8.00	8.00	8.00
Al	0.22	0.05	0.13	0.27	0.02	0.04	0.05	0.05
Cr	0.00	0.00	0.00	0.00	0.01	0.00	0.00	0.01
Fe^{3+}	0.09	0.53	0.15	0.34	0.21	0.38	0.36	0.13
Ti	0.01	0.01	0.01	0.01	0.03	0.01	0.06	0.02
Mg	3.25	3.59	3.51	3.50	4.23	3.49	3.50	3.19
Fe^{2+}	1.42	0.80	1.18	0.86	0.50	1.05	1.00	1.55
Mn	0.02	0.03	0.02	0.02	0.01	0.02	0.02	0.05
Ca	0.00	0.00	0.00	0.00	0.00	0.00	0.00	0.01
C sites	5.00	5.00	5.00	5.00	5.00	5.00	5.00	5.00
Mg	0.00	0.00	0.00	0.00	0.00	0.00	0.00	0.00
Fe^{2+}	0.00	0.06	0.02	0.11	0.03	0.05	0.06	0.00
Mn	0.02	0.03	0.02	0.03	0.01	0.02	0.03	0.00
Ca	1.95	1.83	1.91	1.71	1.92	1.84	1.83	2.00
Na	0.01	0.03	0.04	0.02	0.03	0.03	0.04	0.00
B sites	1.99	1.94	1.99	1.86	1.99	1.95	1.95	2.00
Ca	0.00	0.00	0.00	0.00	0.00	0.00	0.00	0.01
Na	0.01	0.03	0.04	0.02	0.03	0.03	0.04	0.08
K	0.02	0.02	0.02	0.02	0.02	0.03	0.03	0.02
A sites	0.03	0.05	0.06	0.03	0.05	0.06	0.07	0.11
cations	15.02	14.99	15.06	14.90	15.04	15.01	15.02	15.11
Cl	0.01	0.01	0.00	0.01	0.01	0.02	0.01	0.01
F	0.00	0.00	0.03	0.00	0.00	0.00	0.08	0.00
oxygen	23.00	23.00	23.00	23.08	23.00	23.00	23.00	23.00

A16: Average EMP data for amphibole grains from representative lithologies.

Sample	CS95a	CS101	CS104	CS107	CS115	CS122	CS124	CS140	CS142
n =	4	4	9	7	4	16	1	4	6
Lithology	gn	fnor	grano	fwb	fwb	fwb	fwb	sl	gn
b/m	b	m	m	m	m	m	m	m	m
SiO_2	55.11	53.08	54.52	49.76	52.17	51.54	50.64	54.9	53.52
TiO2	0.02	0.12	0.4	0.47	0.09	0.24	0.06	0.01	0.47
$Al2O_3$	1.17	1.46	2.42	4.41	2	2.22	3.01	1.06	2.07
FeO	9.21	15.17	12.83	14.35	13.99	17.16	16.72	11.55	12.76
Cr_2O_3	0	0.16	0.49	0.47	0.01	0.09	0.06	0.11	0.46
MnO	0.29	0.47	0.41	0.58	0.44	0.48	0.58	0.27	0.48
MgO	17.93	18 19	18.25	15.41	14.55	12.61	12.26	19.71	16.63
CaO	13.43	8.33	7.41	10.63	12.81	13.14	11.91	8.81	11.85
Na_2O	0.2	0.19	0.41	0.34	0.31	0.46	0.61	0.25	0.45
K_2O	0.06	0.08	0.52	1.08	0.09	0.16	0.21	0.06	0.21
F	0	0	0.33	0.35	0.22	0.12	0.37	0	0.4
Cl	0	0.04	0.08	0.12	0.03	0.11	0.16	0.04	0.07
Subtotal	97.42	97.13	97.58	97.5	96.7	98.24	96.53	96.66	98.91
O = Cl, F	0	0.01	0.16	0.17	0.1	0.08	0.19	0.01	0.18
Total	97.42	97.12	97.42	97.33	96.6	98.16	96.34	96.65	98.73
Cations calculated on the basis of 23 (O, F, Cl) p.f.u. and the average ferric iron constraint (values obtained from the average 15eNK and 13eCNK)									
Si (p.f.u.)	7.84	7.45	7.60	7.19	7.67	7.60	7.59	7.66	7.57
Al	0.16	0.24	0.27	0.73	0.33	0.38	0.41	0.16	0.35
Fe^{3+}	0.00	0.31	0.13	0.08	0.00	0.02	0.00	0.18	0.08
Ti	0.00	0.00	0.00	0.00	0.00	0.00	0.00	0.00	0.00
T sites	8.00	8.00	8.00	8.00	8.00	8.00	8.00	8.00	8.00
Al	0.04	0.00	0.13	0.02	0.02	0.00	0.12	0.01	0.00
Cr	0.00	0.02	0.05	0.05	0.00	0.01	0.01	0.01	0.05
Fe^{3+}	0.04	0.73	0.60	0.72	0.17	0.10	0.15	0.50	0.33
Ti	0.00	0.01	0.04	0.05	0.01	0.03	0.01	0.00	0.05
Mg	3.80	3.80	3.79	3.32	3.19	2.77	2.74	4.10	3.51
Fe^{2+}	1.06	0.41	0.37	0.81	1.55	2.00	1.94	0.36	1.03
Mn	0.04	0.03	0.02	0.04	0.06	0.06	0.04	0.02	0.03
Ca	0.02	0.00	0.00	0.00	0.01	0.04	0.00	0.00	0.00
C sites	5.00	5.00	5.00	5.00	5.00	5.00	5.00	5.00	5.00
Mg	0.00	0.00	0.00	0.00	0.00	0.00	0.00	0.00	0.00
Fe^{2+}	0.00	0.33	0.40	0.13	0.00	0.00	0.00	0.31	0.07
Mn	0.00	0.03	0.03	0.04	0.00	0.00	0.04	0.02	0.03
Ca	2.00	1.25	1.11	1.65	2.00	2.00	1.91	1.32	1.80
Na	0.00	0.03	0.05	0.05	0.00	0.00	0.05	0.03	0.06
B sites	2.00	1.63	1.59	1.86	2.00	2.00	2.00	1.68	1.95
Ca	0.03	0.00	0.00	0.00	0.01	0.04	0.00	0.00	0.00
Na	0.06	0.03	0.06	0.05	0.09	0.13	0.13	0.04	0.06
K	0.01	0.01	0.09	0.20	0.02	0.03	0.04	0.01	0.04
A sites	0.09	0.04	0.15	0.25	0.12	0.20	0.17	0.05	0.10
cations	15.09	14.68	14.74	15.11	15.12	15.20	15.17	14.72	15.05
Cl	0.00	0.01	0.02	0.03	0.01	0.03	0.04	0.01	0.02
F	0.00	0.00	0.15	0.16	0.10	0.06	0.18	0.00	0.18
oxygen	23.02	22.75	22.87	23.00	23.00	23.00	23.00	22.77	23.00

A17: Average EMP data for amphibole grains from representative lithologies.

Sample	CS2	CS3	CS12	CS18b	CS20	CS24	CS31a	CS37a	CS41b	CS51a	CS60	CS62a
n =	30	89	2	29	5	25	14	27	2	21	26	16
Lithology	apl	qtgb	fwb	fwb	fwb	fwb	fwb	fwb	fwb	fwb	fwb	fwb
b/m	b	b	b	b	b	b	b	b	b	b	b	b
SiO_2	0	0	0	0	0	0	0	0	0	0	0	0
FeO	0.15	0.38	0.11	0.18	0.1	0.23	0.36	0.29	0.12	0.19	0.11	0.14
MnO	0.05	0.1	0.03	0.03	0.03	0.03	0.24	0.16	0.08	0.04	0.06	0.04
MgO	0.02	0.1	0.05	0.09	0.05	0.12	0.2	0.18	0.04	0.04	0.05	0.04
SrO	0	0	0	0	0	0	0	0	0	0	0	0
CaO	55.06	54.79	55.44	55.01	54.98	54.66	55.13	55.3	54.06	54.03	55.73	54.2
Na_2O	0	0	0	0	0	0	0	0	0	0	0	0
K_2O	0	0	0	0	0	0	0	0	0	0	0	0
P_2O_5	38.7	38.34	39.66	39.89	39.5	38.86	39.71	39.54	38.54	37.48	41.79	37.67
SO_3	0	0.04	0.27	0.3	0.28	0.38	0.38	0.14	0.12	0.26	0.05	0.08
F	3.67	3.6	2.18	2.23	2.39	2.25	3.7	3.81	2.18	3.68	3.58	3.39
Cl	0.27	0.62	0.06	0.1	0.1	0.11	0.16	0.15	0.21	0.09	0.16	0.53
Subtotal	97.92	97.97	97.8	97.83	97.43	96.64	99.88	99.57	95.35	95.81	101.53	96.09
O=F, Cl	1.61	1.66	0.93	0.96	1.03	0.97	1.59	1.64	0.97	1.57	1.54	1.55
Total	96.31	96.31	96.87	96.87	96.4	95.67	98.29	97.93	94.38	94.24	99.99	94.54
Cations calculated on the basis of 2 OH and 212 (OH, O, F, Cl)												
Fe^{2+} p.f.u.	0.02	0.05	0.02	0.03	0.01	0.03	0.05	0.04	0.02	0.03	0.02	0.02
Mn	0.01	0.01	0.00	0.00	0.00	0.00	0.03	0.02	0.01	0.01	0.01	0.01
Mg	0.01	0.03	0.01	0.02	0.01	0.03	0.05	0.05	0.01	0.01	0.01	0.01
Sr	0.00	0.00	0.00	0.00	0.00	0.00	0.00	0.00	0.00	0.00	0.00	0.00
Ca	9.96	9.91	9.97	9.95	9.97	9.93	9.87	9.89	9.96	9.96	9.97	9.96
Na	0.00	0.00	0.00	0.00	0.00	0.00	0.00	0.00	0.00	0.00	0.00	0.00
K	0.00	0.00	0.00	0.00	0.00	0.00	0.00	0.00	0.00	0.00	0.00	0.00
Si	0.00	0.00	0.00	0.00	0.00	0.00	0.00	0.00	0.00	0.00	0.00	0.00
P	5.53	5.48	5.64	5.70	5.66	5.58	5.62	5.59	5.61	5.46	5.91	5.47
S	0.00	0.01	0.03	0.04	0.04	0.05	0.05	0.02	0.02	0.03	0.01	0.01
cations	15.53	15.48	15.67	15.74	15.70	15.63	15.66	15.61	15.63	15.49	15.91	15.48
F	1.96	1.92	1.16	1.19	1.28	1.21	1.95	2.01	1.19	2.00	1.89	1.84
Cl	0.08	0.18	0.02	0.03	0.03	0.03	0.05	0.04	0.06	0.03	0.05	0.15

A18: Average EMP data for apatite grains from representative lithologies.

Sample	CS70a	CS71a	CS79	CS85a	CS95a	CS101	CS104	CS107	CS115	CS122	CS124	CS142
n =	11	12	19	23	50	46	5	10	20	6	5	23
Lithology	fwb	fwb	sl	fwb	gn	fnor	grano	fwb	fwb	fwb	fwb	gn
b/m	b	b	b	b	b	m	m	m	m	m	m	m
SiO_2	0	0	0	0	0	0	0	0	0	0	0	0
FeO	0.13	0.09	0.2	0.31	0.12	0.21	0.13	0.19	0.17	0.38	0.13	0.12
MnO	0.04	0.06	0.08	0.07	0.08	0.04	0.06	0.05	0.06	0.06	0.06	0.04
MgO	0.05	0.04	0.06	0.07	0.07	0.09	0.05	0.09	0.06	0.04	0.03	0.04
SrO	0	0	0	0	0	0	0	0	0	0	0	0
CaO	54.58	54.3	54.48	54.32	54.94	54.86	54.84	53.98	53.6	54.73	55.01	55.62
Na_2O	0	0	0	0	0	0	0	0	0	0	0	0
K_2O	0	0	0	0	0	0	0	0	0	0	0	0
P_2O_5	37.61	37.77	41.4	41.02	40.81	41.24	40.93	40.87	41.28	41.63	41.44	41.81
SO_3	0.21	0.25	0.03	0.03	0.95	0.21	0.23	0.2	0.13	0.02	0	0.07
F	3.62	3.43	3.62	3.6	3.61	3.62	3.57	3.49	3.6	3.6	3.5	3.45
Cl	0.07	0.08	0.82	1.03	0.07	0.26	0.28	0.35	0.24	0.22	0.02	0.1
Subtotal	96.31	96.02	100.69	100.45	100.65	100.53	100.09	99.22	99.14	100.68	100.19	101.25
O=F, Cl	1.54	1.46	1.71	1.75	1.54	1.58	1.57	1.55	1.57	1.57	1.48	1.48
Total	94.77	94.56	98.98	98.7	99.11	98.95	98.52	97.67	97.57	99.11	98.71	99.77
Cations calculated on the basis of 2 OH and 212 (OH, O, F, Cl)												
Fe^{2+} p.f.u.	0.02	0.01	0.03	0.04	0.02	0.03	0.02	0.03	0.03	0.05	0.02	0.02
Mn	0.01	0.01	0.01	0.01	0.01	0.01	0.01	0.01	0.01	0.01	0.01	0.01
Mg	0.01	0.01	0.02	0.02	0.02	0.02	0.01	0.02	0.02	0.01	0.01	0.01
Sr	0.00	0.00	0.00	0.00	0.00	0.00	0.00	0.00	0.00	0.00	0.00	0.00
Ca	9.96	9.97	9.94	9.93	9.95	9.94	9.96	9.94	9.95	9.93	9.97	9.97
Na	0.00	0.00	0.00	0.00	0.00	0.00	0.00	0.00	0.00	0.00	0.00	0.00
K	0.00	0.00	0.00	0.00	0.00	0.00	0.00	0.00	0.00	0.00	0.00	0.00
Si	0.00	0.00	0.00	0.00	0.00	0.00	0.00	0.00	0.00	0.00	0.00	0.00
P	5.43	5.48	5.97	5.92	5.84	5.91	5.87	5.95	6.06	5.97	5.93	5.92
S	0.03	0.03	0.00	0.00	0.12	0.03	0.03	0.03	0.02	0.00	0.00	0.01
cations	15.45	15.51	15.97	15.93	15.96	15.93	15.90	15.97	16.08	15.97	15.93	15.93
F	1.95	1.86	1.95	1.94	1.93	1.94	1.91	1.90	1.97	1.93	1.87	1.83
Cl	0.02	0.02	0.24	0.30	0.02	0.08	0.08	0.10	0.07	0.06	0.01	0.03

A19: Average EMP data for apatite grains from representative lithologies.

Sample	CS3	CS5	CS18b	CS62a	CS70a	CS71a	CS79	CS85a	CS93a	CS101
n =	12	16	3	29	17	1	5	12	4	51
Lithology	qtgb	fnor	feb	fwb	fwb	fwb	sl	fwb	gn	fnor
b/m	b	b	b	b	b	b	b	b	b	m
SiO_2	36.74	38	39.25	39.14	38.58	36.65	37.77	37.98	39.75	39.55
TiO_2	4.21	2.6	2.57	4.02	2.49	2.78	3.69	2.97	1.94	3.11
Al_2O_3	12.4	12.49	12.7	12.11	12.21	12.24	12.61	12.93	12.17	12.5
Cr_2O_3	0	0.01	0	0.01	0.01	0	0.06	0.1	0	0.03
FeO	22.05	16.86	13.29	14.38	16.04	17.71	17.33	17.29	12.67	12.99
MnO	0.12	0.13	0.13	0.13	0.17	0.2	0.15	0.19	0.18	0.13
MgO	9.95	14.06	16.83	15.84	14.28	13.37	13.81	13.92	16.54	17.06
BaO	0	0	0	0	0	0	0	0	0	0
CaO	0.05	0.02	0.03	0.1	0.1	0.01	0.01	0.06	0.2	0.27
Na_2O	0.19	0.07	0.06	0.06	0.23	0.07	0.08	0.09	0.72	0.13
K_2O	8.57	9.08	8.74	9.14	8.8	9.31	8.78	8.96	8.68	8.76
F	0.15	0.12	0.51	0.16	0.48	0.4	0.06	0.16	0.84	0.3
Cl	0.35	0.32	0.08	0.09	0.06	0.02	0.21	0.3	0.16	0.06
H_2O	5.22	6.24	5.81	4.82	6.55	7.24	5.44	5.05	6.15	5.11
Subtotal	100	100	100	100	100	100	100	100	100	100
O = F, Cl	0.14	0.12	0.23	0.09	0.22	0.17	0.07	0.14	0.39	0.14
Total	99.86	99.88	99.77	99.91	99.78	99.83	99.93	99.86	99.61	99.86
Cations calculated on the basis of 24 (O, OH, F, Cl)										
Si	5.34	5.33	5.43	5.50	5.37	5.13	5.35	5.41	5.50	5.50
Al^{IV}	2.12	2.06	2.07	2.01	2.00	2.02	2.10	2.17	1.98	2.05
Al^{VI}	0.00	0.00	0.00	0.00	0.00	0.00	0.00	0.00	0.00	0.00
Ti	0.46	0.27	0.27	0.43	0.26	0.29	0.39	0.32	0.20	0.33
Fe^{2+}	2.68	1.98	1.54	1.69	1.87	2.07	2.05	2.06	1.47	1.51
Cr	0.00	0.00	0.00	0.00	0.00	0.00	0.01	0.01	0.00	0.00
Mn	0.02	0.02	0.02	0.02	0.02	0.02	0.02	0.02	0.02	0.02
Mg	2.16	2.94	3.47	3.32	2.97	2.79	2.91	2.96	3.41	3.54
Ba	0.00	0.00	0.00	0.00	0.00	0.00	0.00	0.00	0.00	0.00
Ca	0.01	0.00	0.00	0.02	0.02	0.00	0.00	0.01	0.03	0.04
Na	0.05	0.02	0.02	0.02	0.06	0.02	0.02	0.03	0.19	0.04
K	1.59	1.63	1.54	1.64	1.56	1.66	1.59	1.63	1.53	1.55
cations	14.42	14.26	14.36	14.63	14.13	14.02	14.44	14.61	14.33	14.57
F	0.14	0.11	0.45	0.14	0.42	0.35	0.05	0.14	0.74	0.26
Cl	0.17	0.15	0.04	0.04	0.03	0.01	0.10	0.15	0.08	0.03
OH	5.07	5.85	5.37	4.52	6.09	6.77	5.14	4.80	5.68	4.74
Fe #	0.55	0.40	0.31	0.34	0.39	0.43	0.41	0.41	0.30	0.30
Mg #	0.45	0.60	0.69	0.66	0.61	0.57	0.59	0.59	0.70	0.70

A20: Average EMP data for biotite grains from representative lithologies.

Sample	CS104	CS107	CS110	CS112	CS115	CS120	CS124	CS127	CS140	CS142
n =	7	31	20	4	7	3	5	7	27	15
Lithology	grano	fwb	mnor	sl	fwb	gn	fwb	fwb	sl	gn
b/m	m	m	m	m	m	m	m	m	m	m
SiO_2	38.7	39.57	40.04	39.99	37.67	37.89	37.76	37.79	40.18	39.22
TiO_2	3.14	3.48	2.06	3.56	3.66	3.27	2.02	3.44	1.79	3.08
Al_2O_3	11.97	12.47	11.31	10.97	12.51	12.24	12.38	13.29	12.37	12.49
Cr_2O_3	0.06	0.02	0.09	0.15	0.05	0.01	0.05	0.28	0.27	0.02
FeO	12.55	12.29	11.59	7.49	19.36	18.27	19.62	8.76	12.55	14.12
MnO	0.13	0.1	0.1	0.05	0.17	0.23	0.19	0.01	0.06	0.1
MgO	17.25	17.26	17.17	19.9	12.16	12.63	11.73	17.87	18.09	16.05
BaO	0	0	0	0	0	0	0	0	0	0
CaO	0.04	0.04	0.36	0.2	0.06	0.1	0.08	0.27	0.02	0.04
Na_2O	0.09	0.13	0.81	0.71	0.09	0.33	0.17	1.11	0.13	0.06
K_2O	9	9.04	8.13	8.41	8.68	9.05	8.84	8.06	8.95	9.25
F	0.33	0.31	0.19	0.23	0.29	0.66	0.61	0.61	0.13	0.43
Cl	0.07	0.08	0.29	0.14	0.12	0.1	0.11	0.19	0.31	0.06
H_2O	6.67	5.21	7.86	8.2	5.18	5.22	6.44	8.32	5.15	5.08
Subtotal	100	100	100	100	100	100	100	100	100	100
O = F, Cl	0.15	0.15	0.15	0.13	0.15	0.3	0.28	0.3	0.12	0.19
Total	99.85	99.85	99.85	99.87	99.85	99.7	99.72	99.7	99.88	99.81
Cations calculated on the basis of 24 (O, OH, F, Cl)										
Si	5.30	5.49	5.38	5.27	5.40	5.44	5.36	5.03	5.57	5.50
Al^{IV}	1.93	2.04	1.79	1.70	2.11	2.07	2.07	2.08	2.02	2.06
Al^{VI}	0.00	0.00	0.00	0.00	0.00	0.00	0.00	0.00	0.00	0.00
Ti	0.32	0.36	0.21	0.35	0.40	0.35	0.22	0.34	0.19	0.33
Fe^{2+}	1.44	1.43	1.30	0.83	2.32	2.19	2.33	0.98	1.46	1.66
Cr	0.01	0.00	0.01	0.02	0.01	0.00	0.01	0.03	0.03	0.00
Mn	0.02	0.01	0.01	0.01	0.02	0.03	0.02	0.00	0.01	0.01
Mg	3.52	3.57	3.44	3.91	2.60	2.70	2.48	3.55	3.74	3.36
Ba	0.00	0.00	0.00	0.00	0.00	0.00	0.00	0.00	0.00	0.00
Ca	0.01	0.01	0.05	0.03	0.01	0.02	0.01	0.04	0.00	0.01
Na	0.02	0.04	0.21	0.18	0.03	0.09	0.05	0.29	0.04	0.02
K	1.57	1.60	1.39	1.41	1.59	1.66	1.60	1.37	1.58	1.66
cations	14.15	14.53	13.79	13.71	14.47	14.55	14.15	13.70	14.64	14.59
F	0.29	0.27	0.16	0.19	0.26	0.60	0.55	0.51	0.11	0.38
Cl	0.03	0.04	0.13	0.06	0.06	0.05	0.05	0.09	0.15	0.03
OH	6.10	4.82	7.05	7.22	4.96	5.00	6.11	7.39	4.77	4.76
Fe #	0.29	0.29	0.27	0.17	0.47	0.45	0.48	0.22	0.28	0.33
Mg #	0.71	0.71	0.73	0.83	0.53	0.55	0.52	0.78	0.72	0.67

A21: Average EMP data for biotite grains from representative lithologies.

Sample	CS9	CS10b	CS13a	CS18b	CS19a	CS20	CS31a	CS34b
n =	4	7	11	1	2	1	2	8
Lithology	fnor	fwb	fwb	fwb	fwb	fwb	fwb	fwb
b/m	b	b	b	b	b	b	b	b
SiO_2	30.04	29.32	28.76	30.69	28.06	28.16	28.31	29.64
TiO_2	0.23	0.03	0.02	0.00	0.01	0.00	0.07	0.05
Al_2O_3	18.14	18.16	18.70	16.44	19.14	16.37	19.76	18.44
FeO	22.36	14.63	15.53	16.42	17.59	16.42	18.62	14.16
MnO	0.21	0.19	0.28	0.21	0.33	0.30	0.27	0.23
MgO	17.33	24.42	23.07	22.13	21.74	21.64	21.71	24.83
CaO	0.57	0.05	0.06	0.61	0.05	0.51	0.08	0.05
Na_2O	0.08	0.01	0.00	0.00	0.04	0.01	0.00	0.00
K_2O	0.00	0.00	0.00	0.04	0.00		0.00	0.00
H_2O	11.03	13.18	13.58	13.46	13.04	16.59	11.19	12.59
Total	100.00	100.00	100.00	100.00	100.00	100.00	100.00	100.00
Cation calculated on the basis of 24 (O, OH, F, Cl)								
Si	2.72	2.51	2.48	2.78	2.41	2.58	2.38	2.51
Al^{IV}	1.94	1.83	1.90	1.75	1.93	1.77	1.95	1.84
T sites	4.66	4.33	4.37	4.53	4.34	4.35	4.33	4.35
Al^{VI}	0.00	0.00	0.00	0.00	0.00	0.00	0.00	0.00
Ti	0.02	0.00	0.00	0.00	0.00	0.00	0.01	0.00
Fe^{3+}	0.00	0.00	0.00	0.00	0.00	0.00	0.00	0.00
Fe^{2+}	1.69	1.05	1.12	1.24	1.26	1.26	1.31	1.00
Mn	0.02	0.01	0.02	0.02	0.02	0.02	0.02	0.02
Mg	2.34	3.11	2.96	2.99	2.78	2.95	2.72	3.14
Ca	0.06	0.00	0.01	0.06	0.01	0.05	0.01	0.01
Na	0.02	0.00	0.00	0.00	0.01	0.00	0.00	0.00
K	0.00	0.00	0.00	0.00	0.00	0.00	0.00	0.00
cations	8.79	8.51	8.48	8.84	8.42	8.63	8.39	8.52
Cl	0.02	0.00	0.00	0.00	0.01	0.02	0.00	0.00
F	0.10	0.11	0.00	0.00	0.04	0.00	0.00	0.03
OH	6.67	7.52	7.81	8.14	7.47	10.14	6.27	7.12
O	0.00	0.00	0.00	0.00	0.00	0.00	0.00	0.00
Fe_FeMg	0.42	0.25	0.27	0.29	0.31	0.30	0.32	0.24
Mg_FeMg	0.58	0.75	0.73	0.71	0.69	0.70	0.68	0.76

A22: Average EMP data for chlorite grains from representative lithologies.

Sample	CS35	Cs37a	CS51a	CS60	CS71a	CS115	CS122	CS124
n =	3	24	2	9	6	1	3	3
Lithology	fwb	fnor	fwb	fwb	fwb	fwb	fwb	fwb
b/m	b	b	b	b	b	m	m	m
SiO_2	29.09	28.79	25.85	29.55	28.63	26.96	27.15	26.23
TiO_2	0.00	0.05	0.14	0.18	0.01	0.08	0.03	0.04
Al_2O_3	19.17	18.61	18.21	17.34	17.35	18.49	18.10	18.60
FeO	15.89	15.64	30.79	20.02	21.72	24.30	28.01	28.54
MnO	0.27	0.22	0.27	0.26	0.35	0.31	0.36	0.39
MgO	23.47	22.21	12.25	19.70	18.56	16.73	14.04	12.85
CaO	0.02	0.09	0.54	0.45	0.29	0.02	0.20	0.10
Na_2O	0.00	0.07	0.00	0.08	0.04	0.02	0.03	0.10
K_2O	0.00	0.00	0.00	0.00	0.06	0.08	0.04	0.03
H_2O	12.06	14.31	11.94	12.44	12.99	13.02	12.04	13.10
Total	100.00	100.00	100.00	100.00	100.00	100.00	100.00	100.00
Cation calculated on the basis of 24 (O, OH, F, Cl)								
Si	2.46	2.53	2.36	2.65	2.58	2.40	2.47	2.41
Al^{IV}	1.91	1.93	1.96	1.83	1.84	1.94	1.94	2.01
T sites	4.36	4.45	4.31	4.48	4.42	4.34	4.41	4.42
Al^{VI}	0.00	0.00	0.00	0.00	0.00	0.00	0.00	0.00
Ti	0.00	0.00	0.01	0.01	0.00	0.01	0.00	0.00
Fe^{3+}	0.00	0.00	0.00	0.00	0.00	0.00	0.00	0.00
Fe^{2+}	1.12	1.15	2.35	1.50	1.64	1.81	2.13	2.19
Mn	0.02	0.02	0.02	0.02	0.03	0.02	0.03	0.03
Mg	2.95	2.91	1.67	2.63	2.49	2.22	1.90	1.76
Ca	0.00	0.01	0.05	0.04	0.03	0.00	0.02	0.01
Na	0.00	0.01	0.00	0.01	0.01	0.00	0.01	0.02
K	0.00	0.00	0.00	0.00	0.01	0.01	0.01	0.00
cations	8.46	8.55	8.41	8.71	8.62	8.42	8.50	8.44
Cl	0.00	0.01	0.04	0.02	0.02	0.01	0.02	0.00
F	0.00	0.07	0.00	0.00	0.09	0.03	0.04	0.24
OH	6.80	8.39	7.27	7.45	7.82	7.74	7.31	8.04
O	0.00	0.00	0.00	0.00	0.00	0.00	0.00	0.00
Fe_FeMg	0.28	0.28	0.58	0.36	0.40	0.45	0.53	0.55
Mg_FeMg	0.72	0.72	0.42	0.64	0.60	0.55	0.47	0.45

A23: Average EMP data for chlorite grains from representative lithologies.

Sample	n=	Lithology	b/m	Cl (wt. %)	F (wt. %)	Total
CS3	20	fwb	b	0.038	0.000	96.84
CS5	13	fwb	b	0.006	0.000	94.61
CS12	24	fwb	b	0.031	0.000	94.78
CS18b	15	fwb	b	0.021	0.000	97.82
CS20	21	fwb	b	0.054	0.000	93.92
CS24	30	fwb	b	0.061	0.000	96.08
CS31a	8	fwb	b	0.031	0.000	97.26
CS37a	16	fwb	b	0.027	0.000	97.31
CS41b	25	fwb	b	0.028	0.000	96.55
CS60	24	fwb	b	0.033	0.242	93.08
CS62a	23	fwb	m	0.119	0.393	98.10
CS70a	20	fwb	m	0.054	0.216	92.67
CS71a	23	fwb	m	0.077	0.115	95.57
CS104	21	fwb	m	0.047	0.261	88.73
CS107	9	fnor	b	0.026	0.002	97.90
CS115	7	fnor	b	0.083	0.000	97.05
CS122	26	gn	m	0.087	0.479	97.87
CS124	6	qtgb	b	0.192	0.907	80.81
CS142	13	grano	m	0.083	0.213	95.37

A24: Average chlorine and fluorine in representative amphibole grains.

Sample	n=	Lithology	b/m	Cl (wt. %)	F (wt. %)	Total
CS12	2	fwb	b	0.056	2.180	97.36
CS18b	29	fwb	b	0.099	2.233	97.53
CS20	5	fwb	b	0.096	2.393	97.06
CS24	25	fwb	b	0.106	2.252	96.52
CS31a	14	fwb	b	0.162	3.699	100.89
CS41b	2	fwb	b	0.214	2.179	96.04
CS51a	21	fwb	b	0.086	3.680	95.17
CS60	26	fwb	b	0.162	3.581	100.71
CS62a	18	fwb	b	0.509	3.454	96.41
CS70	11	fwb	b	0.067	3.624	95.46
CS71a	12	fwb	b	0.076	3.433	95.65
CS85a	25	fwb	b	1.050	3.609	99.97
CS107	16	fwb	m	0.522	3.575	99.27
CS115	23	fwb	m	0.242	3.470	96.62
CS122	6	fwb	m	0.220	3.604	100.15
CS124	9	fwb	m	0.041	3.491	98.04
CS37a	31	fnor	b	0.144	3.541	95.45
CS101	52	fnor	m	0.280	3.626	100.13
CS79	19	sl	b	0.824	3.621	100.07
CS95a	50	gn	b	0.071	3.608	100.24
CS142	23	gn	m	0.100	3.448	100.66
CS3	93	qtgb	b	0.618	3.609	97.44
CS104	6	grano	m	0.253	3.182	88.47
CS2	33	apal	b	0.268	3.671	97.22

A25: Average chlorine and fluorine in representative apatite grains.

Sample	n=	Lithology	b/m	Cl (wt. %)	F (wt. %)	Total
CS18b	3	fwb	b	0.085	0.510	94.02
CS62a	8	fwb	b	0.079	0.162	95.16
CS70a	15	fwb	b	0.048	0.497	92.98
CS71a	2	fwb	b	0.029	0.410	92.37
CS85a	13	fwb	b	0.281	0.155	95.17
CS107	41	fwb	m	0.084	0.306	86.59
CS115	8	fwb	m	0.109	0.257	95.02
CS124	11	fwb	m	0.096	0.740	93.21
CS127	7	fwb	m	0.246	0.938	95.83
CS5	19	fnor	b	0.319	0.112	92.93
CS101	19	fnor	m	0.063	0.368	94.91
CS110	9	mnor	m	0.610	0.216	94.73
CS79	6	sl	b	0.246	0.168	94.63
CS140	28	sl	m	0.303	0.129	94.82
CS142	15	gn	m	0.062	0.426	94.75
CS3	37	qtgb	b	0.283	0.206	92.09
CS104	7	grano	m	0.072	0.328	93.21
CS2	11	apal	b	0.288	0.423	97.17

A26: Average chlorine and fluorine in representative biotite grains.

Sample	n=	Lithology	b/m	Cl (wt. %)	F (wt. %)	Total
CS10b	9	fwb	b	0.013	0.086	89.07
CS13a	11	fwb	b	0.004	0.002	87.65
CS19a	2	fwb	b	0.064	0.040	87.86
CS31a	2	fwb	b	0.005	0.000	88.95
CS34b	8	fwb	b	0.001	0.025	87.51
CS35	2	fwb	b	0.008	0.000	96.71
CS60	9	fwb	b	0.059	0.000	88.99
CS9	4	fnor	b	0.605	0.102	90.10
CS37a	23	fnor	b	0.061	0.072	87.08
CS110	3	mnor	m	0.041	0.296	99.35

A27: Average chlorine and fluorine in representative titanite grains.